

A Strip Theory Approximation for Wave Forces on Submerged Vehicles in Finite Depth Water

By Jan A. Rybka

B.S., Naval Architecture and Marine Engineering
United States Coast Guard Academy (2001)

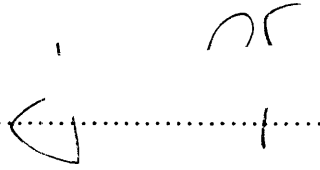
Submitted to the Department of Ocean Engineering and the
Department of Mechanical Engineering in partial fulfillment of the
requirements for the degrees of
Master of Science in Naval Architecture and Marine Engineering
And
Master of Science in Mechanical Engineering
At the

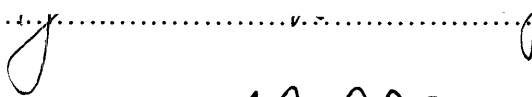
MASSACHUSETTS INSTITUTE OF TECHNOLOGY

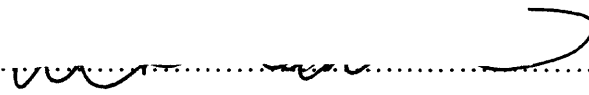
June 2005

© Jan Rybka, 2005. All rights reserved.

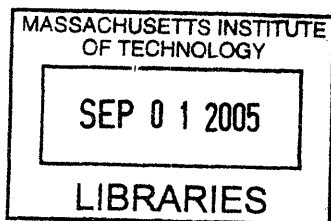
The author hereby grants MIT permission to reproduce and publicly
distribute paper and electronic copies of this thesis in whole or part.

Author..... 
Department of Ocean Engineering
17 MAY 2005

Certified by..... 
Jerome Milgram
Professor of Naval Architecture
Thesis Supervisor

Accepted by..... 
Michael S. Triantafyllou
Chairman, Department Committee of Graduate Students
Department of Ocean Engineering

Accepted by.....
Lallit Anand
Chairman, Department Committee on Graduate Studies
Department of Mechanical Engineering



ARCHIVES

A Strip Theory Approximation for Wave Forces on Submerged Vehicles in Finite Depth Water

By Jan Rybka

Submitted to the Department of Ocean Engineering
On May 17, 2005, in partial fulfillment of
the requirements for the degrees of
Master of Science in Naval Architecture and Marine Engineering
And
Master of Science in Mechanical Engineering

Abstract

Autonomous Underwater Vehicles (AUV's) are becoming of increasing use in shallow waters for oceanographic data collection, coastal mapping, and military operations such as mine surveillance along enemy coastlines. Currently the control of AUV's in shallow water is very limited, largely due to a lack of knowledge of vessel forces in shallow water, especially in the presence of surface wave effects. The limitations of current control systems do not afford enough confidence to operate the vehicles in very close proximity to shore or in large waves because the control in the horizontal plane is not adequately reliable enough to prevent bottoming and free surface broaching.

Current control system parameters are altered through trial and error to enable reasonable vehicle behavior in shallow water but the control of the vehicle is limited because a thorough understanding of wave forces on these vehicles is non existent. The development of a good analytical tool which adequately models wave forces and moments on an AUV in shallow water waves will enable the development of control systems which will be better able to maneuver the vehicle in shallower water and larger waves than the conditions in which AUV's are currently used.

The purpose of this thesis is to further develop, verify, and apply a Strip Theory based analytical tool, which has been developed by Prof. Jerry Milgram. The developed code models dynamic wave forces on a small submarine in shallow submergence and finite depth water through the use of a Strip Theory summation of cross section forces calculated through Green's theorem in a two dimensional panel method code. For this thesis a study of three dimensional flow effects on the control fins is conducted through the use of WAMIT, a three-dimensional panel method code for marine structures. The code is tested for data convergence to determine the sizing of both the Greens theorem solution domain and the panel sizing for the solution. To validate the accuracy and reliability of the Strip Theory Code in question, its results are compared to WAMIT output for identical test conditions. Also, existing experimental data for the REMUS AUV is used as a comparison and validation for the code. The resulting code correctly models sway, heave, pitch, and yaw forces and moments with reasonable accuracy and it can be used in future work to develop more reliable control systems and operating limitations for AUV's.

Thesis Supervisor: Jerome Milgram
Title: Professor of Ocean Engineering, MIT

Acknowledgements

I would like to thank my thesis advisor, Professor Milgram, for giving me the opportunity to work on this project with him. His guidance, direction, and chiefly his patience have enabled my understanding and completion of this work. This thesis is completed mostly through his hard work and countless hours dealing with the code in question and the bugs it has contained. Additionally, the numerous and demanding hours spent in meetings together were of inestimable benefit to me and my understanding of this difficult material. Thanks again Jerry.

Also I would like to thank the Coast Guard for not only allowing, but supporting me through my MIT re-education. And finally, I would of course like to thank my family and friends for the love and support they have shown me during my time in this program.

Biographical Note

Jan Rybka is a Lieutenant Junior Grade in the United States Coast Guard. He graduated from the United States Coast Guard Academy in May 2001 with a Bachelor of Science Degree in Naval Architecture and Marine Engineering. Upon graduation, he was assigned to the U.S. Coast Guard Cutter POLAR SEA, home-ported in Seattle WA, where he served as the Damage Control Assistant and Auxiliary Division Officer. He is receiving two Master of Science degrees in Ocean Engineering and Mechanical Engineering.

Contents

A Strip Theory Approximation for Wave Forces on Submerged Vehicles in Finite Depth Water	1
Abstract	2
Acknowledgements.....	3
Biographical Note	4
Contents	5
List of Figures	6
List of Tables	8
Chapter 1: Introduction	9
1.1 Motivation.....	9
1.2 Purpose.....	9
Chapter 2: Strip Theory Implementation	11
2.1 Theory	11
2.2 MATLAB Code	11
2.3 The REMUS Autonomous Underwater Vehicle.....	13
Chapter 3: Prior Work.....	15
3.1 Experimental Work.....	15
3.2 Experimental Results	16
3.3 Numerical Approximation in Sabra's Thesis.....	17
3.4 Recalculated WAMIT Data	18
Chapter 4: Un-modeled Three Dimensional Fin Effects	21
4.1 Added Mass versus Aspect Ratio, Case A.....	21
4.2 Added Mass versus Aspect Ratio, Case B	26
Chapter 5: Convergence Study	29
5.1 Domain Shape	29
5.2 Wavelength Influences on Domain Width.....	30
5.3 Panel Sizing Study	32
5.3 Domain Sizing Conclusion	34
Chapter 6: Strip Theory to WAMIT Comparison.....	35
Chapter 7: Strip Theory to Experimental Comparison	46
Chapter 8: Conclusions	59
8.1 Summary and Conclusions	59
8.2 Future Work.....	60
Appendix A: Development of the Strip Theory.....	61
Appendix B: MATLAB form of the Diffraction Strip Theory Code.....	75
Bibliography	84

List of Figures

Figure 1 REMUS Coordinate System.....	13
Figure 2 Dimensioned Profile Drawing of the REMUS AUV	13
Figure 3: Zero Speed Diffraction Heave Data Comparison.....	18
Figure 4 Zero Speed Diffraction Heave Data Comparison.....	19
Figure 5 WAMIT vs Experiment Moment Comparison for Beta 090.....	20
Figure 6 WAMIT vs Experiment Heave Phase Comparison.....	20
Figure 7 REMUS Tail Fin Dimensions	22
Figure 8 WAMIT Model of REMUS.....	23
Figure 9 REMUS Model with 3 Times Aspect Ratio	24
Figure 10 Aspect Ratio vs Added Mass, Test 1, Case A	25
Figure 11 Aspect Ratio vs Added Mass, Test 2, Case A	25
Figure 12 Aspect Ratio vs Added Mass, Test 1, Case B	27
Figure 13 Aspect Ratio vs Added Mass, Test 2, Case B	27
Figure 14 Two Dimensional Domain Diagram	29
Figure 15 Convergence Study, 10 m Wavelength	31
Figure 16 Convergence Study, 6.0 m Wavelength	31
Figure 17 Convergence Study, 20 m Wavelength	32
Figure 18 Panel Sizing Study.....	33
Figure 19 WAMIT v STC F2 , 135 Beta.....	36
Figure 20 WAMIT v STC F2 Phase, 135 Beta.....	36
Figure 21 WAMIT v STC F2 Data, 045 Beta.....	37
Figure 22 WAMIT v STC F2 Data, 090 Beta.....	37
Figure 23 WAMIT v STC F3 , 180 Beta.....	38
Figure 24 WAMIT v STC F3 Phase, 180 Beta.....	38
Figure 25 WAMIT v STC F3 Data, 000 Beta.....	39
Figure 26 WAMIT v STC F3 Data, 045 Beta.....	39
Figure 27 WAMIT v STC F3, 090 Beta	39
Figure 28 WAMIT v STC F3 Data, 135 Beta.....	40
Figure 29 WAMIT v STC F5 , 000 Beta.....	40
Figure 30 WAMIT v STC F5 Phase, 000 Beta	41
Figure 31 WAMIT v STC F5 , 090 Beta.....	41
Figure 32 WAMIT v STC F5 Phase, 090 Beta.....	42
Figure 33 WAMIT v STC F5 Data, 180 Beta.....	42
Figure 34 WAMIT v STC F5 Data, 135 Beta.....	43
Figure 35 WAMIT v STC F5 Data, 045 Beta.....	43
Figure 36 WAMIT v STC F6 , 090 Beta.....	44
Figure 37 WAMIT v STC F6 Phase, 090 Beta.....	44
Figure 38 WAMIT v STC F6 Data, 045 Beta.....	45
Figure 39 WAMIT v STC F6 Data, 135 Beta.....	45
Figure 40 Experiment v STC F2 Data, 045 Beta	46
Figure 41 Experiment v STC F2 Data, 090 Beta	46
Figure 42 Experiment v STC, F2 Data, 135 Beta.....	47
Figure 43 Experiment v STC F3 Data, 000 Beta.....	47

Figure 44 Experiment v STC F3 Data, 045 Beta.....	48
Figure 45 Experiment v STC F3 Data, 090 Beta.....	48
Figure 46 Experiment v STC F3 Data, 135 Beta.....	48
Figure 47 Experiment v STC F3 Data, 180 Beta.....	49
Figure 48 Experimental v STC, F3 with Speed, 000 Beta.....	49
Figure 49 Experiment v STC F3 Phase with Speed, 000 Beta.....	50
Figure 50 Experiment v STC, F3 with Speed, 180 Beta.....	50
Figure 51 Experiment v STC F3 Phase with Speed, 180 Beta.....	51
Figure 52 Experiment v STC F5 Data, 000 Beta.....	51
Figure 53 Experiment v STC F5 Data, 045 Beta.....	52
Figure 54 Experiment v STC, F5 Data, 135 Beta.....	52
Figure 55 Experiment v STC F5 Data, 180 Beta.....	52
Figure 56 Experimental v STC, F5 , 090 Beta.....	53
Figure 57 Experiment v STC, F5 Phase, 090 Beta.....	53
Figure 58 Experiment v STC, F5 with Speed, 000 Beta.....	54
Figure 59 Experiment v STC F5 Phase with Speed, 000 Beta.....	54
Figure 60 Experimental v STC, F5 with Speed, 180 Beta.....	55
Figure 61 Experiment v STC F5 Phase with Speed, 180 Beta.....	55
Figure 62 Experiment v STC F6 Data, 045 Beta.....	56
Figure 63 Experiment v STC F6 Data, 135 Beta.....	56
Figure 64 Experimental v STC, F6 , 090 Beta.....	57
Figure 65 Experiment v STC F6 Phase, 090 Beta.....	57
Figure 66 Coordinate and Motion Definitions.....	63
Figure 67 Cross Section of an Underwater Vehicle in a Two-Dimensional Computation Domain, Viewed from Forward, Looking aft.....	66
Figure 68 Experiment v Theory for Amplitude of Heave Force with Theoretical Section Pressure base on Encounter Frequency, ω , Equation (A-33).....	69
Figure 69 Experiment v Theory for Amplitude of Heave Force with Theoretical Section Pressure based on Fixed Frame Frequency, ω_0 , Equation (A-34).....	70
Figure 70 Experiment v Theory for Amplitude of Pitch Moment with Theoretical Section Pressure based on Fixed Frame Frequency, ω , Equation (A-33).....	70
Figure 71 Experiment v Theory for Amplitude of Pitch Moment with Theoretical Section Pressure based on Fixed Frame Frequency, ω_0 , Equation (A-34).....	71
Figure 72 Vertical Profile of the Tail Section of the REMUS AUV.....	72

List of Tables

Table 1 Diffraction STC MATLAB m Files..... 11
Table 2 Main Dimensions For REMUS AUV 14
Table 3 Naval Academy Experiment Parameter Range 15
Table 4 Model Fin Data for Case A..... 24
Table 5 Model Fin Data for Case B 26
Table 6 Extra Test Parameters For WAMIT to Strip Theory Comparison..... 35

Chapter 1: Introduction

1.1 Motivation

Autonomous Underwater Vehicles (AUV's) and small submarines have become of increasing importance to the maritime industry. They are used extensively for mapping, oceanographic data collection, and they have increasing use in military applications such as mine sweeping. Traditionally AUV's have been used in deep water applications but they are quickly becoming of use in shallow water where a large amount of oceanographic problems are poorly understood and where mine clearance is of importance. To date, no one has approached the problem of modeling forces on a moving submerged vessel in shallow water waves. Until a force model is developed, each new AUV design will require extensive costly testing to develop controllers which can operate these vessels in shallow water.

The completion of a good modeling program has several important uses. As mentioned above it will be extremely useful in the development of a dynamic control system. Additionally, an accurate model will enable AUV designers to determine maneuvering characteristics for vessels at early stages of the design process without model testing. This will greatly reduce design cost and time and can result in the production of highly controllable vehicles.

Besides being able to maneuver in shallow water, the control system that is possible from the analytical tool in question will enable the development of AUV's which can dock with a mother ship in shallow water and which will not breach the surface when operating near the surface in wave conditions. The ability to dock with a submerged rig from a mother ship greatly reduces the time of data collection for an AUV because the vessels do not need to be loaded onboard each time they need a battery charged or to transmit data.

AUV's are generally positively buoyant to ensure that mechanical failures result in a vehicle floating to the surface rather than sinking to the bottom. Unfortunately this means that in maneuvering, the vessel requires forward pitch to maintain depth. When operating in shallow water, if the vehicle broaches the surface it can not push itself back below without manual assistance from someone on the surface. A vehicle which is controlled adequately to avoid surface broaching means the vessel can operate unobserved in shallow water without the need of surface personnel who would otherwise need to be on hand to resubmerge a broached AUV, which is dangerous and costly in shallow waters.

1.2 Purpose

The purpose of this thesis is to further develop, verify, and apply a strip theory based analytical tool, developed by Prof. Jerry Milgram, which models dynamic wave forces on a small submarine in shallow submergence and finite depth water. The numerical model which has been painstakingly developed by Prof Milgram must be tested to determine its accuracy and to help debug the program in question.

A study of the required domain and panel sizing for the convergence of the two dimensional panel method codes output was conducted to ensure that the extracted data is error free. Also an analysis of three dimensional fin effects was conducted to determine if a correction factor for the flow around the leading and trailing edges of the control fins was needed for the full solution of the code.

To validate the accuracy of the code numerous numerical experiments were conducted for comparison with previously conducted experiments for the REMUS AUV. Additionally, the code will be compared to the results of another numerical hydrodynamic model called WAMIT to determine the Strip Theory Codes accuracy.

Chapter 2: Strip Theory Implementation

2.1 Theory

The code presented in this thesis is a strip theory program developed by Prof. Jerome Milgram and is largely based on the strip theory presented in “Ship Motions and Sea Loads” by Salvesen, Tuck, and Faltinsen, which is referred to throughout this thesis as STF [2]. The program is designed to solve both the radiation and diffraction problems for a submerged body to determine hydrodynamic coefficients and for force and moment data in sway, heave, pitch, and yaw. Surge and roll have been excluded because they are not of consequence in the maneuvering and general hydrodynamics of a vehicle. The basic theory outlined in SFT has been adjusted to model a submerged body in finite depth water and the code uses a two-dimensional panel method implementation of Greens Theorem to determine the sectional forces. The code is expanded to include fin lift forces and moments which are not developed in a strip theory code.

Since the code was developed by Prof. Milgram, he has written a synopsis of the theory on which his code is derived, included in this thesis as Appendix A. This synopsis contains a full explanation of the uses of strip theory, along with the solution method for the velocity potential using Green’s theorem, and a full description of the fin lift effects included in the code. MATLAB was used as the main programming language because of its ease of use and familiarity. A version of the strip theory code and its subroutines is included in this thesis as Appendix B. This MATLAB code, contains modifications to Professor Milgram’s code made by the author to facilitate obtaining results presented in this thesis. For simplicity the code and its use as a solver will be referred to as Strip Theory Code (STC) throughout this thesis.

2.2 MATLAB Code

The actual programming of the STC is divided into two main codes, one of which solves the diffraction problem for the vehicle, the other of which solves the radiation problem. Table 1 below lists the subroutines of the STC for the diffraction problem with a brief description of each subroutines function. The subroutines essentially perform the same function for the radiation problem however they are altered to determine the radiation potential.

Diffraction Problem m Files	
DiffPblm.m	Base File; Imports data, Integrates Stripwise Components, Prints Data
strippart.m	Solves Greens thm, Determines 2D Sectional Forces and Coefficients
matrix.m	Creates Matrix Components for Solution of Green’s Theorem
setpans.m	Determines Panel Geometry for 2D Sections
inflcofauv.m	Determines g and dgdn by running localize.m and rank2d.m
localize.m	Determines Local Coordinates for 2D Sections
rank2d.m	Determines Green Function (g) and dgdn for 2D Sections
wnf.m	Solves Dispersion relation for wavenumber (not always needed)
remallL.dat	Geometric Input File
finremus.dat	Fin Data Input File
casename.in	Run Setup File

Table 1 Diffraction STC MATLAB m Files

Both the diffraction and the radiation versions of the STC require 3 separate input files to run and to process the subroutines called. The required inputs are a geometry file which describes each section of the vehicle body, a fin input file which provides numerical data for the fin orientation and dimensioning, and a run setup file which sets the experimental conditions for each test case.

The geometry file is very simple in format. The first line is a number indicating the number of sections there are to describe the vehicle. The next line is the start of the first section and each subsequent section is listed in order, one after the other. For each section the first line has two numbers, the first of which is the number of panels in the section, the second of which is the x position of the section. Every subsequent line is the y and z coordinates for the panel vertices of the section.

The fin input file is also a simple numeric listing. The first line indicates the number of fins for the body. Each line after that states four numbers, which indicate, the x position of the $\frac{1}{4}$ chord, the planform area of the fin, the orientation of the fin in the y-z plane (in degrees), and lift coefficient per unit angle of attack (in radians).

The run setup file can be of many formats depending on how the program is set up. The input file format for the version of the code located in Appendix B is described here. The STC is set up so that it can run multiple cases from a single input file, the first line of the input file should contain only the number of data runs intended for that input file. Each data run being conducted from that input file is then represented by a single line of data in the input file containing the following six pieces of information: Run Number, Heading (Beta), Speed (U), Submergence(s), Depth (h), wave height (in cm), and Wavelength (λ).

The diffraction solver, and the radiation solver have different output formats, but both return data to the user in the form of several output files, the base name of which is specified by the user through an input function in running the STC. The diffraction program outputs force and moment data into two output files, one for the horizontal plane motions, the other for the vertical plane motions. The radiation program outputs added mass and damping coefficients along with force values into eight output files. The data in each file is appropriately labeled and is intuitive to the user.

The notation for the degrees of freedom in the STC is the standard numeric appointment where 2 is Sway, 3 is Heave, 5 is Pitch, and 6 is Yaw.

2.3 The REMUS Autonomous Underwater Vehicle

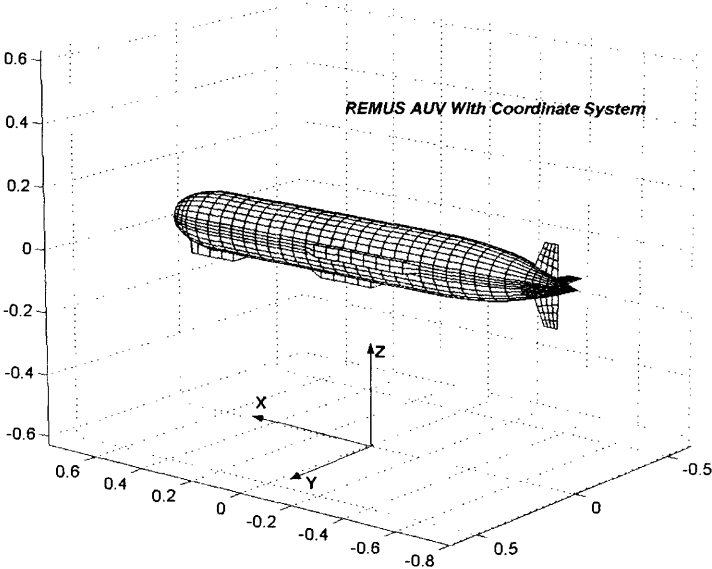


Figure 1 REMUS Coordinate System

The REMUS AUV was used as the test vehicle for the experimentation and validation of Prof. Milgram’s strip theory code. It was used primarily because a large amount of experimental data was previously collected for the vehicle in 2000 and the data provides a good validation for the accuracy of the code. Additionally, REMUS is a good test model because it is a commonly used AUV, with a slender body, which is required in strip theory. As a majority of the data presented in this thesis is fully dimensional, it is important the reader is familiar with the dimensions of the vehicle. Figure 1 below is a dimensioned drawing of the vehicle which, taken from the thesis of Greg Sabra [7]. Table 1 provides overall dimensions for the vehicle body by section. It should be noted that for the calculation of vehicle damping forces it is assumed that the body is neutrally buoyant, or that its weight is equal to its displacement. The tail fin dimensions are located in chapter 4 of this thesis, along with a discussion of lift generation.

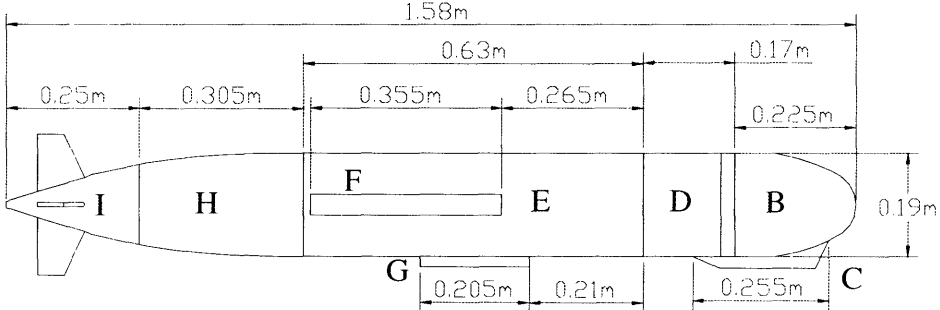


Figure 2 Dimensioned Profile Drawing of the REMUS AUV

Vehicle Section	Length (X)	Width (Y)	Height (Z)
Total Vehicle	1.58 m	0.23 m	0.21 m
Nose Section	0.225 m	0.19 m	0.19 m
Forward Transducer	0.255 m	Varies	Varies
Transducer Ring	0.17 m	0.19 m	0.19 m
Parallel Mid-body	0.63 m	0.19 m	0.19 m
Side Transducer	0.355 m	0.02 m	0.04 m
Ballast	0.205 m	0.04 m	0.02 m
Tail Section	0.305 m	0.19 m	0.19 m
Fin Section	0.25 m	0.15 m	0.15 m
Submerged Volume	0.0376 m ³		

Table 2 Main Dimensions For REMUS AUV

Chapter 3: Prior Work

Experimental work was done for determining the wave forces on AUV's in finite depth water was approached in two separate thesis by Greg Sabra and Erik Oller in 2003 [7] [8]. Each approached the problem through experiment, using a model of the REMUS AUV.

3.1 Experimental Work

The diffraction problem was approached through Sabra's thesis and was based on experiments done at the US Naval Academy Marine Hydromechanics laboratories tow tank with a full scale model of the REMUS AUV. The experiments were done to determine the diffraction forces on the vehicle in the presence of a single wave. The experiments provided force and moment data including magnitude and phase for sway, heave, pitch, and yaw. Surge and roll were not considered. Data runs were conducted for a wide range of wave angles with the vehicle at zero speed; however, due to the limited tank size the vehicle was restricted to head and stern seas (beta 180 and 000) for data runs with the vehicle moving. The following table provides the ranges over which the Naval Academy tow tank experiments were conducted.

Experiment Parameter Range	
Depth (h)	1.52 m
Submergence (s)	0.285 - 0.857 m
Base Frequency (ω)	2.972 - 8.822 rad/s
Wavelength (λ)	0.792 - 6.34 m
Wave Amplitude (a)	5.449 - 0.630 m
Speed (u)	0 - 2.06 m/s
Heading (beta)	0, 45, 90, 135, 180 deg

Table 3 Naval Academy Experiment Parameter Range

Unfortunately due to the size of the vehicle and the limitations of wave sizing available in the tank, the average loads measured were very small. The loads were so small that on average they were approximately one percent of the rated load for the load cell used. Additionally the load cell used was waterproofed with o-ring seals which allow for compression in oscillation; delaying the frequency measurements in terms of force phase.

In addition to the difficulty in determining phase values due to the high signal to noise ratio there were some confusions in vehicle orientation in the tank. There are very few indications within the thesis on whether or not the vehicle was oriented in the positive or negative x direction for data runs at oblique angles. In comparing the experimental phase data with numerical results it is apparent that for certain cases the vehicle is oriented in the opposite direction, accounting for a 180 degree phase shift for some of the data runs.

The radiation problem was approached through Ollers' thesis with experiments conducted on a 0.4334 scale model of the REMUS vehicle in the MIT Marine Instrumentation and Computation Laboratories tow tank. Unlike in the experiments documented in Sabra's work, these experiments were focused on determining the radiation forces of the vehicle without the presence of a wave. A small amount of valuable data was collected through this work and was reduced to values for added mass and damping coefficients for the vehicle.

Unfortunately, due to delays in the development of the software and data acquisition systems the amount of data collected was very limited and consequently it is not as reliable as the data found in Sabra's work. For this reason the bulk of the comparative data provided in this thesis will be in comparison to the experimental data collected through Sabra's thesis.

3.2 Experimental Results

Several important findings came out of the experimental work done by both Sabra and Oller. In general there has not been a large amount of tow tank data collected for AUV's in the presence of waves and it was important for both theses to pay attention to the differences in the hydrodynamics between submerged and surface vehicles.

One of the primary differences is the determination that fin lift effects are very important in AUV hydrodynamics in comparison to their importance in surface ships. This means that the amount of force created by the fins is much larger in AUV's than in surface ships and have much larger effects on the vessels motions and maneuverability. This is largely because fins represent a much larger area of the vehicle for AUV's. While the vehicles has forward speed, the orbital velocities present due to wave motion and the transverse velocities caused vehicle motions create flow angles of attack developing lift forces which effect both damping and added mass terms. The linearized analytical equations describing these forces along with more data and information concerning fin effects are presented in a later section of this thesis.

Another interesting determination from the experimental research previously conducted is that the radiative forces developed by and AUV are much more significant than those developed by a surface ship. This is because in a surface ship the motion of the vessel is counteracted, or damped, by the movement of the free surface, which has a very large restoring force acting to damp the ships motions. In a submerged body the movement of the free surface is negligible with the vessels motion and there is no restoring force generated so the small amount of radiative force caused by the vessels motion plays a much larger role proportionately in the damping of the submerged vehicle. This is easily seen in the case of heave motions, as a surface vessel is heaved, the free surface moves out of balance with the equilibrium waterline of the vessel and gravity acts as a damper to counteract the vehicle motions. In a submerged body, heave motion is not counteracted by a similar force because there is no equilibrium waterline. Consequently the largest portion of damping in a submerged body is created by the wave radiation occurring as the body is oscillated due to exciting forces.

The goal of both sets of experiments was to develop a full set of data which could correctly predict the control variables so the REMUS AUV could be maneuvered in shallow water. Although the data collected was reasonably accurate, it was limited in scope due to the tank sizing limitations listed above, and due to time and data collections restrictions. Consequently, the data is not significant to develop hydrodynamic models and maneuvering control systems which are adequately reliable for use. The development of an analytical tool as presented in this thesis will adequately provide the data for the AUV's hydrodynamic mode and maneuvering control system. Additionally, the experiments done by both Oller and Sabra provide excellent comparative data to determine the accuracy of the analytical tool.

3.3 Numerical Approximation in Sabra's Thesis

Sabra's thesis contains a section on numerical and computational testing, which includes data calculated from solutions to the problem using two separate numerical models, SWAN2 and WAMIT. As part of his thesis both companies were contracted to model the REMUS AUV in identical situations as those conducted in his experimental work. Neither SWAN2 nor WAMIT are designed to correctly model this problem but are nonetheless useful.

SWAN2 is a 3-dimensional panel method code, which is very accurate at modeling the steady or unsteady free surface potential flow around a stationary or moving ship in finite depth. Although the program was not initially designed to determine the flow around submerged bodies it was modified by one of the developers of the code to model this problem.

Sabra concluded that the data collected from SWAN2 for the experimental cases with forward speed were reasonably close to experimental values for force magnitudes but the moment values in pitch and yaw were very disappointing. Additionally there appeared to be errors in the experimental values for force and moment phases, which made comparison and validation of SWAN2 difficult.

In addition to using SWAN2, WAMIT, which is another 3-dimensional panel method code, was used to numerically model the experiments. WAMIT is used to model the potential flow around submerged structures and its results have been validated and found very satisfactory on multiple equations (ref...). In order to validate the experimental results of Sabra's thesis, Chang-Ho Lee of WAMIT Inc. was contracted to run the code for conditions identical to the experimental test conditions at zero speed. As the code is designed for marine structures it can not be used to model vehicle motions and is only valid for the zero speed cases.

Because WAMIT is used extensively in this thesis as a comparison and validation of the Strip Theory code in question a brief description of WAMIT's properties follows. As stated in the WAMIT v5.4 users manual, the code "is a three-dimensional panel program developed for the linear analysis of the interaction of surface waves with offshore structures" [6]. As mentioned previously it is designed for the modeling of marine structures, which can be mounted on the sea bottom, submerged, or located on the free surface. The program works for finite or infinite depth values and can be used to analyze singular or multiple interacting bodies. The code is executed through two main programs POTEN and FORCE. The first of which solves the three-dimensional velocity potential around the input body, the latter of which determines the desired hydrodynamic parameters. The flow is assumed to be ideal, and the free surface boundary conditions are linearized. The radiation and diffraction velocity potentials are obtained by using Greens's theorem with the free-surface source potential as the Green function. In evaluation, the source strengths are evaluated using the source distribution method, which uses the same source potential.

Sabra concluded that WAMIT was reasonably accurate in predicting both forces and moments for the zero speed test cases of the Naval Academy tow tanks experiments. As with the SWAN2 test cases, there were problems in dealing with the phase data due to the errors mentioned previously in the experiment. Sabra's conclusion that WAMIT was a good numerical model for the vehicle in the test cases was largely based on the output following the same trends as the experimental data when compared to certain non-dimensional variables. A direct comparison of the WAMIT data provided by Chang-Ho Lee and the experimental force and moment magnitudes shows that the WAMIT data consistently underestimates the magnitudes, as shown below in Figure 3. Following the completion of Sabra's thesis it was determined that the data given to Chang-Ho Lee wasn't clearly defined. He was given submergence values from the

free surface to the center of the vehicles cylinder body but he assumed that the submergence given was to the top of the vehicles cylinder body. Consequently the data presented in Sabra's thesis was for submergence values that are 0.095m too deep, resulting in force measurements that are on average to small.

The plot format shown in Figure 3 is used extensively in this thesis to compare numerical data values which are supposed to be equivalent or close to equivalent. The data sets to be compared are put on opposing axes which means that if the values are equivalent then they would lie directly on the line $y = x$. For the most part this thesis will compare a lot of data to see if it is equivalent and no non-dimensionalization would make it easier to see data equivalency than this format of plot.

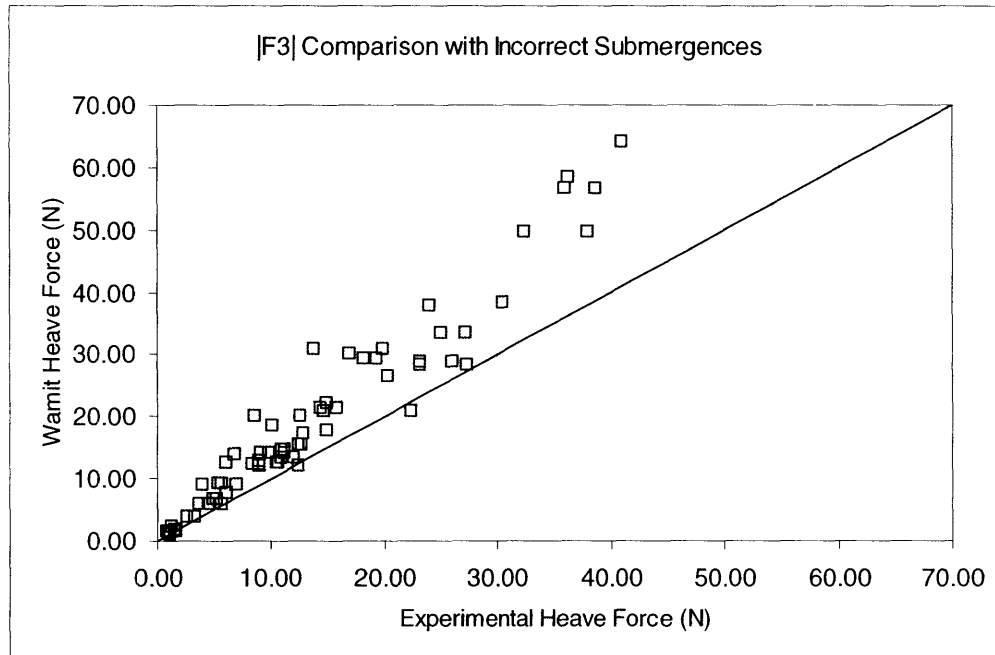


Figure 3: Zero Speed Diffraction Heave Data Comparison

3.4 Recalculated WAMIT Data

Because the WAMIT data contained in the Sabra thesis is done for incorrect submergences it was recalculated as part of the work for this thesis. For the majority of the test cases the data with correct submergences matches the experimental data quite closely. A plot of the heave magnitude data is displayed in Figure 4 below.

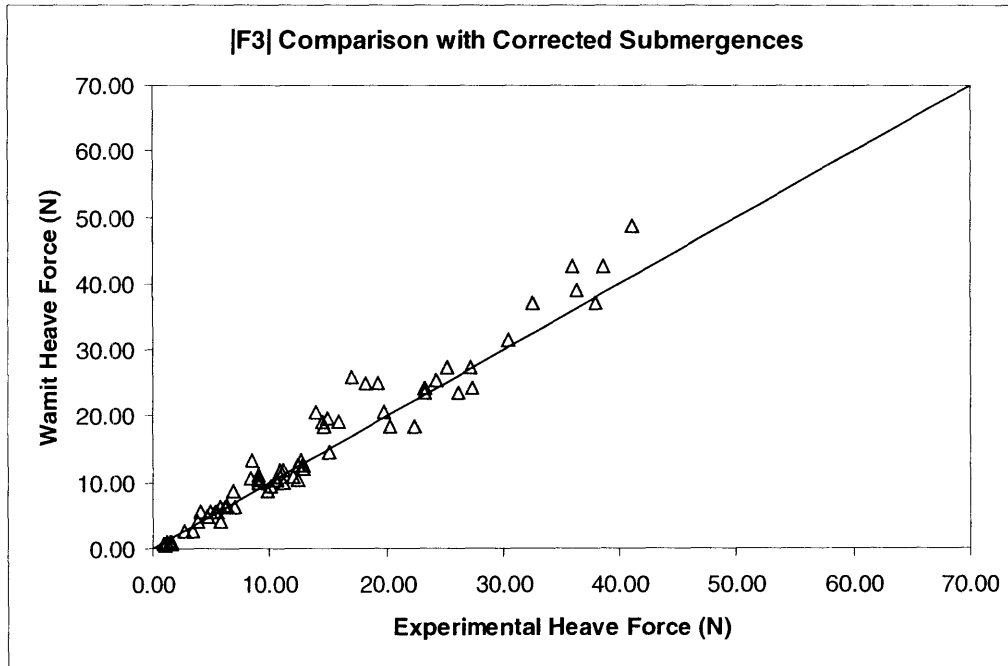


Figure 4 Zero Speed Diffraction Heave Data Comparison

It is apparent that the recalculated data is much closer to the experimental data from Sabra's thesis and Figure 4 is typical of the sway, pitch and yaw data with one exception. The test cases with a beam sea, meaning a beta value of 090, give pitch and yaw data where the experimental data values are much lower than the corresponding WAMIT data. Figure 5 is a plot of both the yaw and pitch moment data in beam seas. This trend is quite possibly explained the small value for the total moment in this case. As mentioned previously the force and moment range for the load cell used in the Naval Academy experiments is much larger than the moments encountered in the experiments. In the case of beam seas the yaw and pitch moments are quite small and consequently the error in the data collection could account for the deviation of the experimental data from the WAMIT output. Additionally, the phase data does not produce very matching results.

As shown in Figure 6 the experimental phase data does not match the WAMIT phase data in the same manner as the magnitude data. Still, despite the large number of outliers there is a substantial amount of data wherein the WAMIT and experimental phase data does match. As discussed earlier there were some problems in determining phase values from the experimental data and this is evident in the phase comparison.

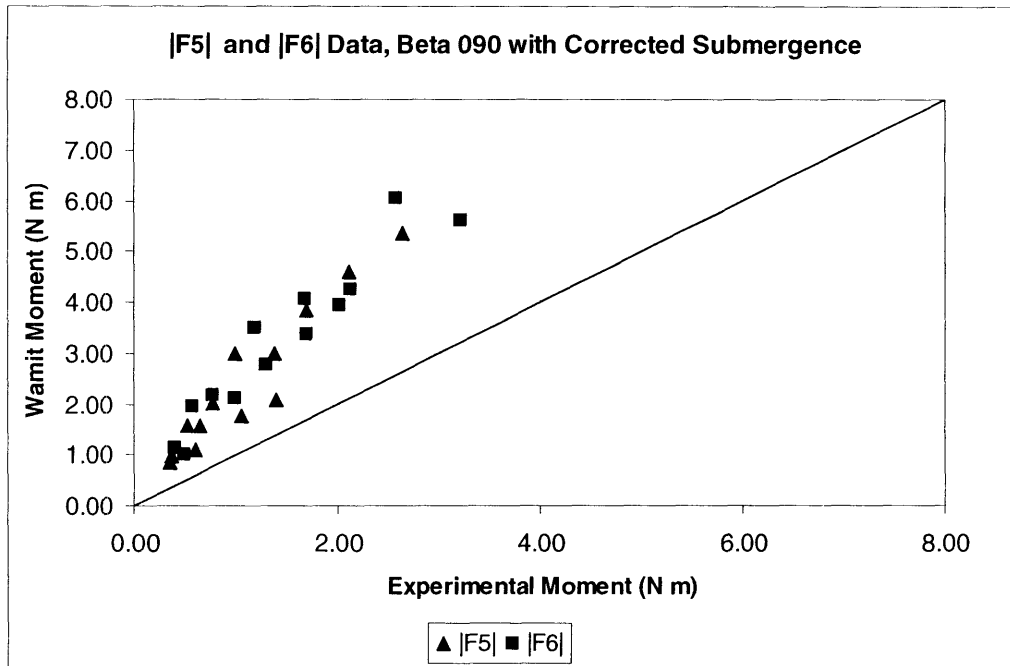


Figure 5 WAMIT vs Experiment Moment Comparison for Beta 090

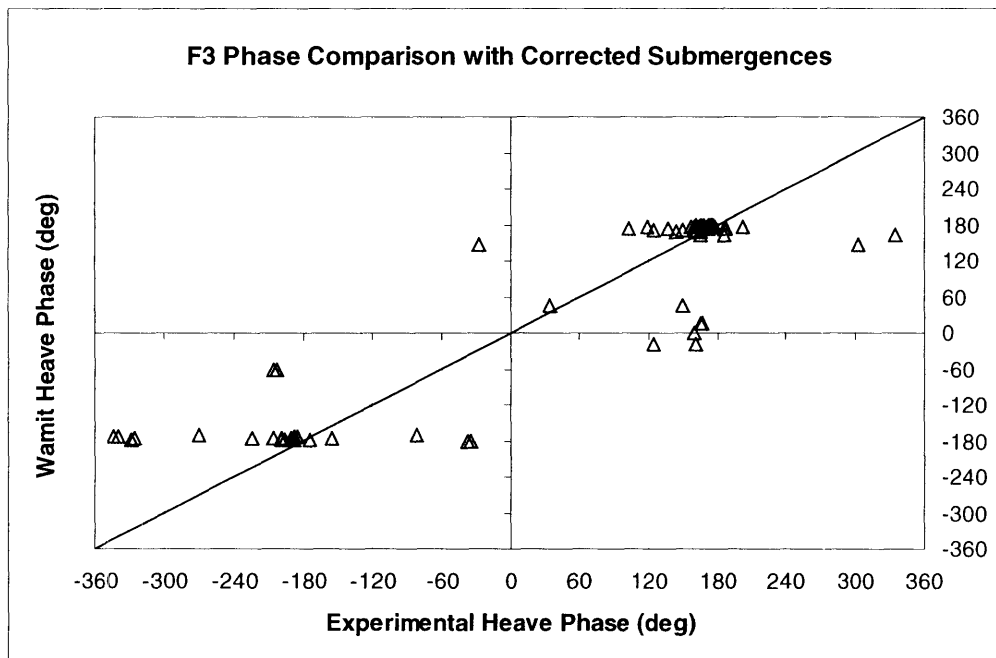


Figure 6 WAMIT vs Experiment Heave Phase Comparison

Regardless of the moment differences for beam sea cases, the recalculated WAMIT data's similitude to the experimental results of Sabra's thesis provides substantial proof that the magnitude of force and moment data for both the experimental from the Naval Academy's tow tank and the WAMIT data are both reasonably valid as they display similar values.

Chapter 4: Un-modeled Three Dimensional Fin Effects

As mentioned previously, the forces caused by the fins of an AUV comprise a large portion of the hydrodynamic force on the body due to the relative size of the fins. Additionally the fins contribute a majority of the vehicles damping force because the vehicle is so far away from the free surface. As such, it is extremely important that the fins are modeled correctly for the strip theory code in question.

Fin lift, caused by circulation around the fin, is a very well understood force and is modeled very simply. Professor Milgram's theory write-up in Appendix A contains a large section on how fin lift force is accounted for in the STC. The derivation of the equations is based on empirical equations presented in Sighard Hoerner's book "Fluid-Dynamic Lift" [9] and requires fin data such as span, aspect ratio, and plan form area, and coefficient of lift, which are inputted to the code through the fin input file as discussed in chapter 2.

4.1 Added Mass versus Aspect Ratio, Case A

In addition to fin lift forces, the fins play a role in the development of added mass for the vehicle. This hydrodynamic input is taken into account in the solution to the radiation strip theory problem but only in terms of each two dimensional slice of the body. Because the determination of added mass is only determined for the two dimensional section, the flow that goes around the leading and trailing edges of the fins is not considered in the strip theory solution. This could potentially be a large source of error in the strip theory consideration of the flow around the body, especially for a very slender fin which would allow a large portion of the flow to escape around the leading and trailing edges rather than go around the edge of the span.

Aspect Ratio, the ratio of span to chord, is in essence a measure of slenderness for a fin or airfoil. For low aspect ratio fins, very little of the flow around the fin would be around the leading and trailing edges in comparison to a high aspect ratio fin. Consequently, by modeling the full three-dimensional flow for a body with fins that have the same plan form area over a range of aspect ratios one could determine the effects of the amount of flow around the leading and trailing edges of the fin on added mass for the body.

As proven earlier, WAMIT is an adequate approximation for the three dimensional flow around an AUV with no forward speed. A study of aspect ratio versus added mass is accomplished by developing multiple three-dimensional models of the REMUS AUV where the tail fins each have the same plan form area but each has a different aspect ratio. Aspect ratio is often defined as:

$$AR = \frac{\overline{Span}^2}{Area} \quad (4.1)$$

$$Area = \overline{Span} \times \overline{Chord} \quad (4.2)$$

Note that for the above equations a bar above a value indicates the average of that quantity. With concern to added mass the portion of the fin which is of consequence is the area protruding from the main cylinder body. For this reason average span is the height from the center of the fin to the tip and average chord is the average of the root chord and the tip chord. The dimensioned

drawing below, taken from Sabra [7], gives the plan form view of the tail fins for the REMUS AUV.

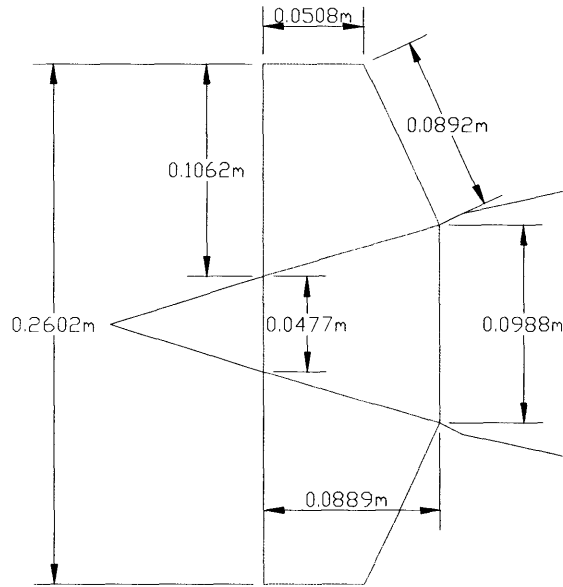


Figure 7 REMUS Tail Fin Dimensions

For this case the fin aspect ratio is developed as such:

$$Span_{Lead} = 0.0806m$$

$$Span_{Trail} = 0.1062m$$

$$\overline{Span} = 0.0924m$$

$$Chord_{Root} = 0.0889m$$

$$Chord_{Tip} = 0.0508m$$

$$\overline{Chord} = 0.0698m$$

$$AR = 1.324$$

$$Area_{Fin} = 0.00646m^2$$

The geometric model of the REMUS AUV for WAMIT was provided from the data contained as part of Sabra's thesis. The model is a three dimensional discretization of the half of the body into 676 quadrilateral panels as shown graphically in Figure 8. The input for WAMIT only requires half the body to be defined if the body is port starboard symmetric. The input is simply a listing of control points for each panel distinctly and in order to develop different fins for the body it was necessary to create new control points for the associated fins manually. New models could have been developed through the use of AutoShip or other similar hull design software but was unnecessary and costly.

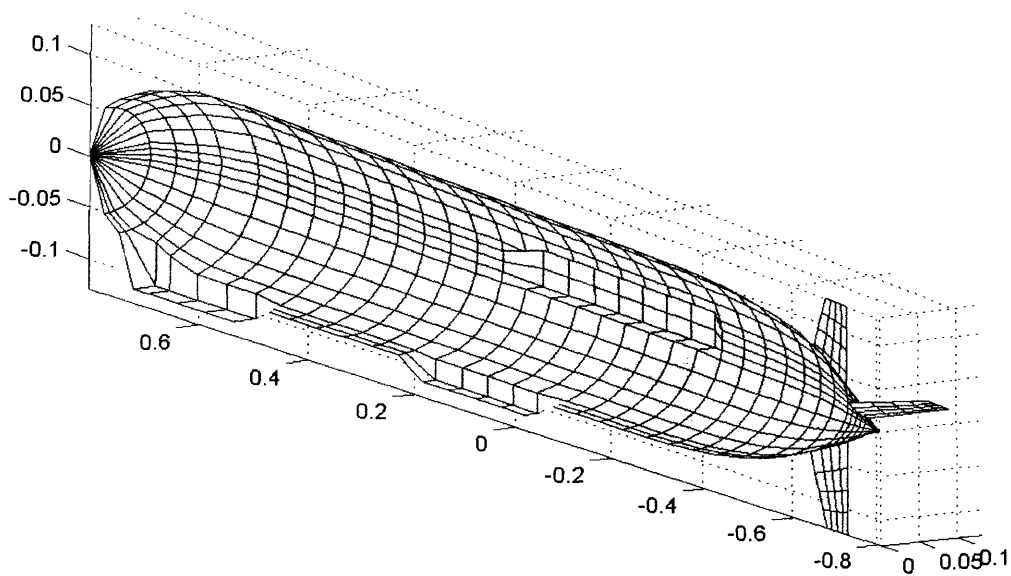


Figure 8 WAMIT Model of REMUS

An Excel algorithm was developed to stretch the panels on the fins to reach desired aspect ratios while maintaining the same plan form area. This task was simplified because all four of the tail fins for the REMUS vehicle are identical in shape. The original model of the vehicle has fins which have thickness along the root edge which connects to the cylinder body of the vehicle. To develop fins of different aspect ratios it was necessary to change the length of the root chord along the vehicle body. In order to simplify this, the model fins were changed so that at the intersection of the fin with the body there was no thickness. Only the row of control points along the cylinder body has no thickness, which means the rest of the fin does have thickness and this modification created no noticeable variation in the results provided by WAMIT. Figure 9 below shows the panel layout for the fins, which is the same four by four panel arrangement for all the models created for the aspect ratio study. Additional panels were not added as that would complicate the development of the models unnecessarily. However, by not increasing the number of panels the aspect ratio of the panels themselves changes rather drastically as large distortions in fin aspect ratio are achieved. This distortion in panel shape provides a potential source of error in the numerical solution by distorting the fin spacing.

In changing the root chord length the control points along the body are moved fore or aft to maintain continuity and reasonably shape panels. To determine the new control point locations along the body a cubic spline interpolation was used in MATLAB to nearly identical cylinder bodies in each model.

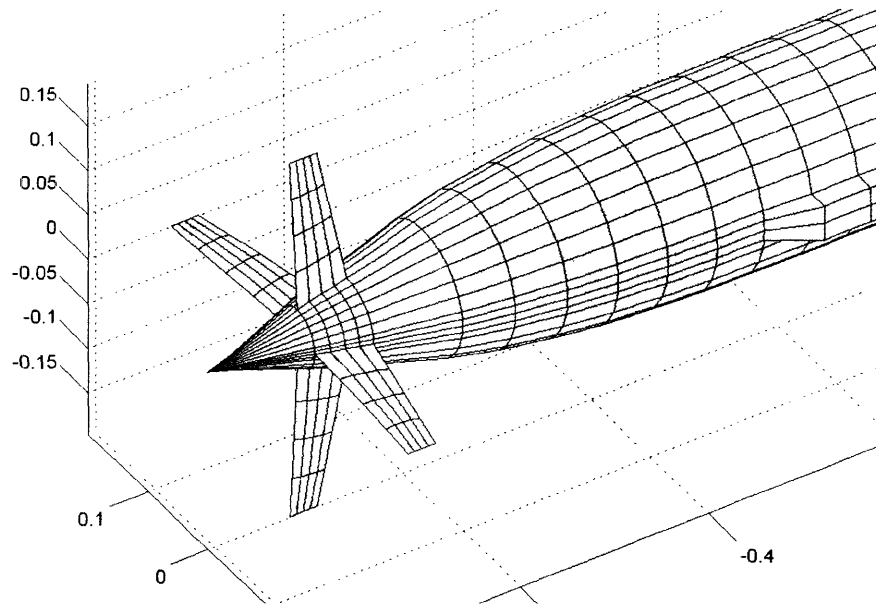


Figure 9 REMUS Model with 3 Times Aspect Ratio

For purposes of this study 9 different REMUS models were made for input to WAMIT with aspect ratio's ranging from one quarter to 6 times the original aspect ratio. Table 4 below shows the important fin data for each model.

AR Multiple	Aspect Ratio	Planform Area	Avg Span
0.25	0.3318	0.00646	0.04624
0.50	0.6621	0.00646	0.06540
0.75	0.9929	0.00646	0.08010
1	1.3241	0.00646	0.09249
1.5	1.9862	0.00646	0.11328
2	2.6482	0.00646	0.13080
2.5	3.3103	0.00646	0.14624
3	3.9724	0.00646	0.16020
4	5.2965	0.00646	0.18498
6	7.9447	0.00646	0.22655

Table 4 Model Fin Data for Case A

Each model was run through WAMIT for 2 different test conditions and the added mass values were compared to see if the change in aspect ratio affected their values. As can be seen in Figures 10 and 11 below, there is a negligible change in added mass as the aspect ratio changes for both test cases, the parameters of which are labeled on top of each plot. Additionally, with the distortion of the quadrilateral panels on the fin over these aspect ratios the small change in added mass is not satisfactory to show a dominant trend. For this reason the test has been reevaluated with a different formulation of aspect ratio.

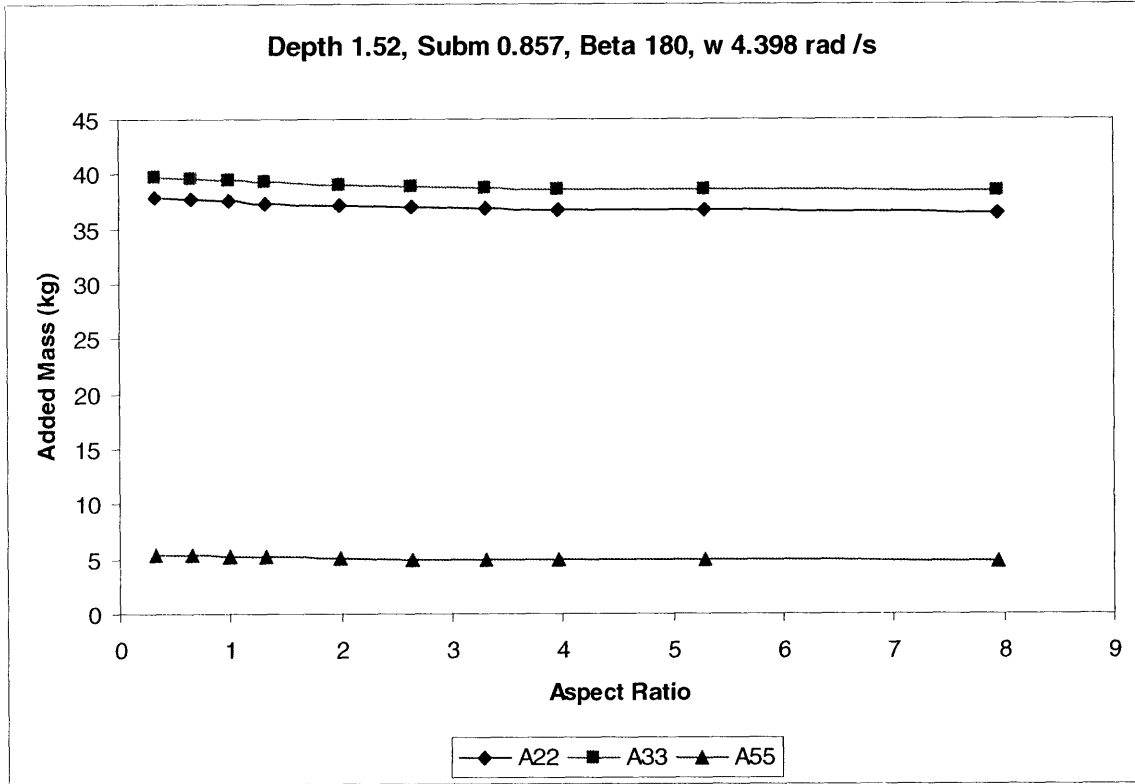


Figure 10 Aspect Ratio vs Added Mass, Test 1, Case A

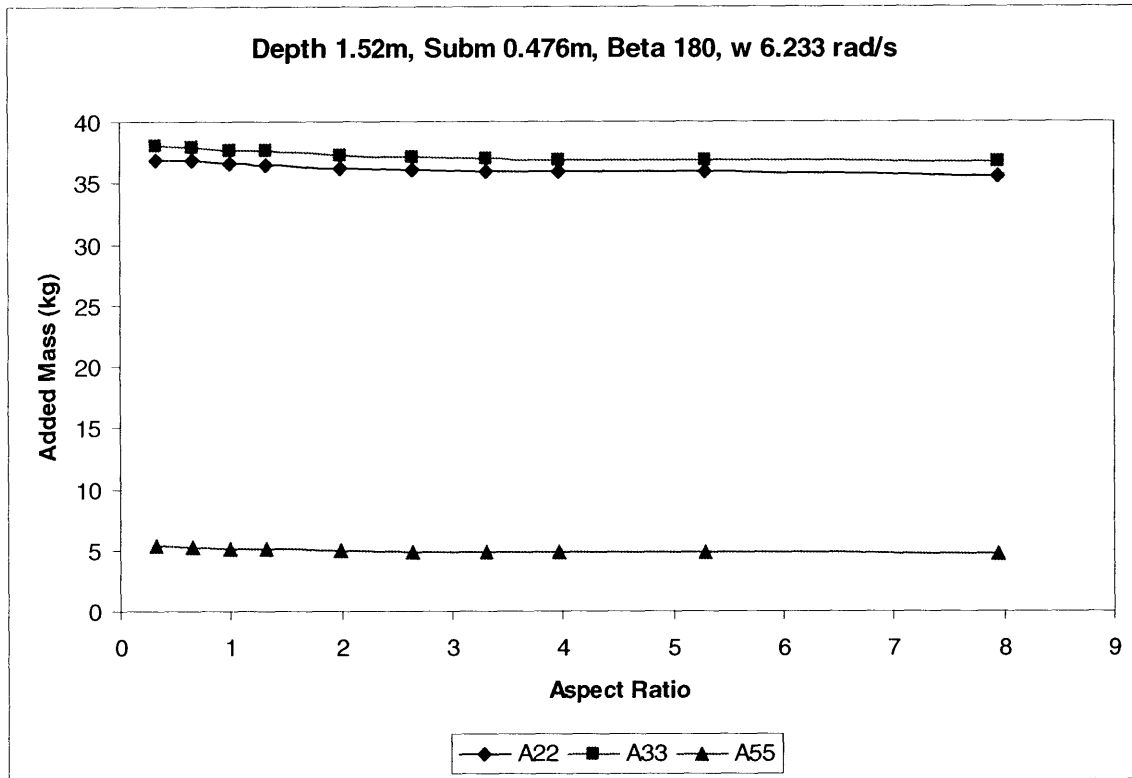


Figure 11 Aspect Ratio vs Added Mass, Test 2, Case A

4.2 Added Mass versus Aspect Ratio, Case B

In cases where fin lift is considered the aspect ratio is often calculated using a different area than that used in Case A above. For this reason, the experiment above will be recreated using this other approach to aspect ratio to be certain that there is no discernible trend between aspect ratio and added mass.

Another approach at defining fin area in situations of lift generation is to include the cylinder body or fuselage to the fin area calculation. Because there is a large amount of lift generation at the root of the fin, the cylinder body to which the fin is attached is often considered to be a part of the fin itself. Meaning that in the case of the tail fins on REMUS, the tail fins on either side of the body can be considered to be the same fin, with a span running from one tip to the other and with the fin planform area including not only the area of the fins but also the projected area of the cylinder body in between. For the case of the standard REMUS vehicle the area is as such:

$$D_{center} = 0.0988 m \qquad \qquad \qquad Span = 0.2602 m$$

$$Chord_{Root} = 0.0889 m \qquad \qquad \qquad Chord_{Tip} = 0.0508 m$$

$$Area = D_C \cdot C_R + \frac{C_R + C_T}{2} \cdot (Span - D_C) \qquad (4.3)$$

$$Area = 0.02006 m^2 \qquad \qquad \qquad AR = 3.3753$$

For this test case fewer models were developed since the question had been examined in detail previously. Table 5 below gives fin dimensions for the models which were developed. Again, another Excel algorithm was developed to create the new models for input to WAMIT. The models were run for the same test cases as in case A and the data is presented in Figures 12 and 13.

AR Multiple	Aspect Ratio	Planform Area	Avg Span
0.25	0.8438	0.020059	0.13010
0.50	1.6877	0.020059	0.18399
1	3.3753	0.020059	0.26020
3	10.1259	0.020059	0.45068
5	16.8764	0.020059	0.58182
6	20.2516	0.020059	0.63736

Table 5 Model Fin Data for Case B

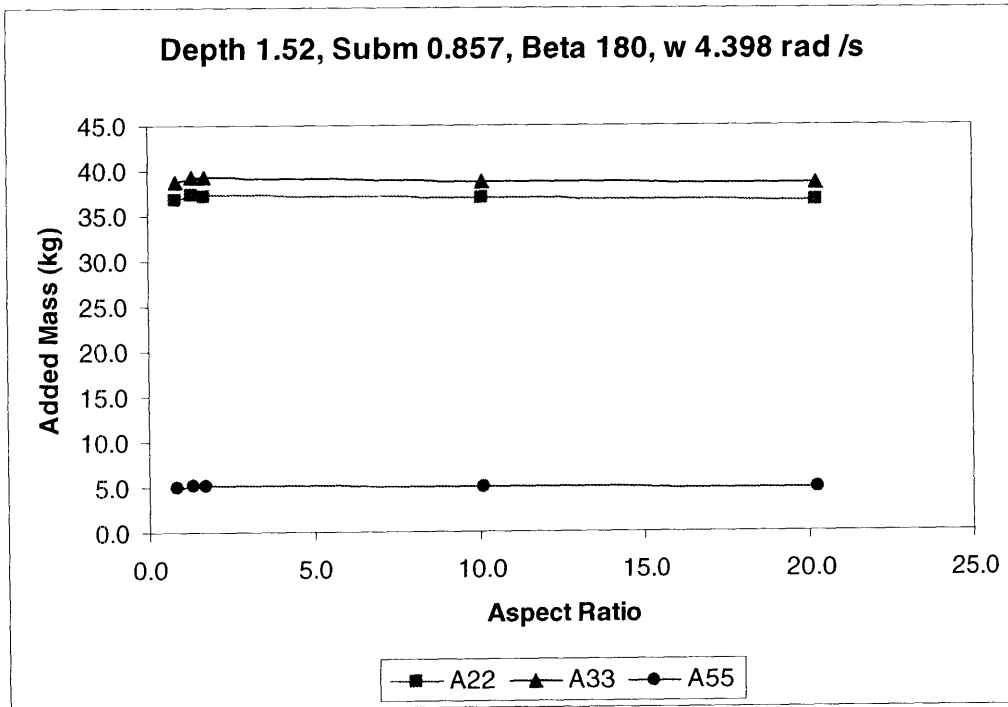


Figure 12 Aspect Ratio vs Added Mass, Test 1, Case B

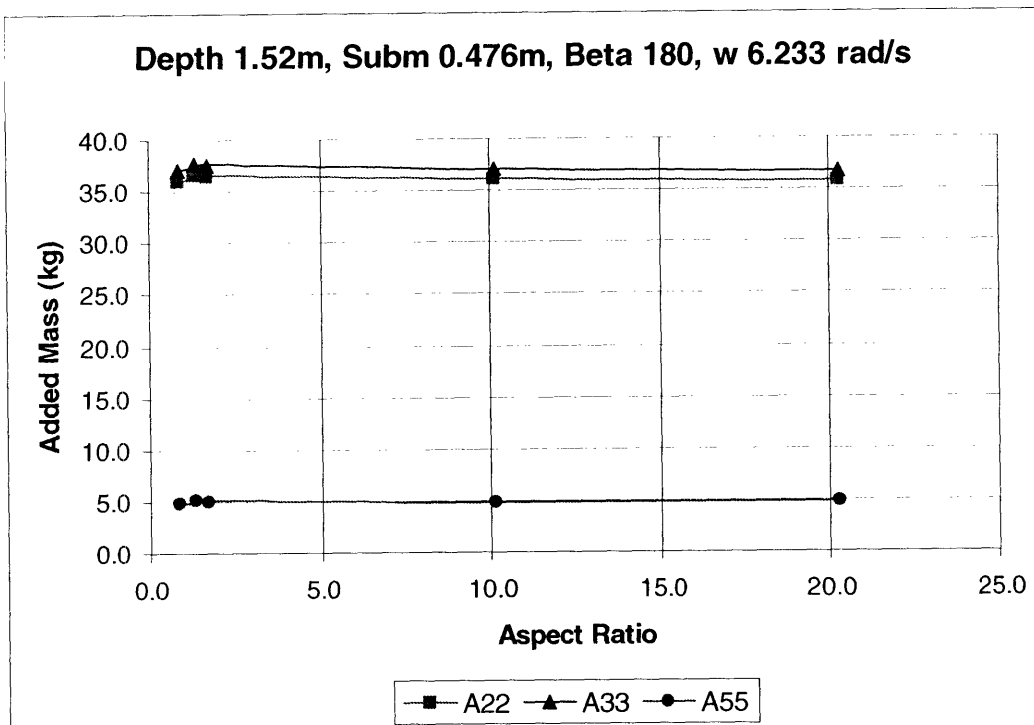


Figure 13 Aspect Ratio vs Added Mass, Test 2, Case B

Again, the added mass values show negligible change for differing aspect ratios. This conclusion yields the additional conclusion that the three dimensional flow effects around the leading and trailing edges of a fin are negligible in concern to added mass. Meaning that the added mass is predominantly a function of projected area which can be correctly modeled using two dimensional strips of the vehicle and no correction factor or large source of error is present for the added mass of the fins by using a strip theory approximation.

Chapter 5: Convergence Study

The two dimension force calculations of the STC are accomplished through the use of a panel method in two dimensions. Because the calculation is for finite depth water and shallow vehicle submergences the body and all the edges of the domain in which the section is located must be part of the panel method solution. This means that the domain must be paneled as well as the body and consequently it is important to evaluate the influence of domain sizing and panel sizing on the STC solution.

5.1 Domain Shape

The domain to be considered is essentially the rectangular box shown in Figure 14 below. The two dimension slice of the vehicle is located at $y = 0$ and submerged to a centerline depth as specified in the programs input. The size of the domain is determined by the depth of the water, h , for which the user wishes to solve for the vehicle forces and by a width of the domain which is arbitrarily specified by the user through the variable hw . The correct width of the domain which allows for the most accurate solution to the STC is generally determined by the vehicles beam, as will be proven in this section. Additionally the number of panels along the domain is arbitrarily chosen by the user and again, the purpose of this chapter is to determine the correct sizing of the panels for the most accurate possible solution to the STC.

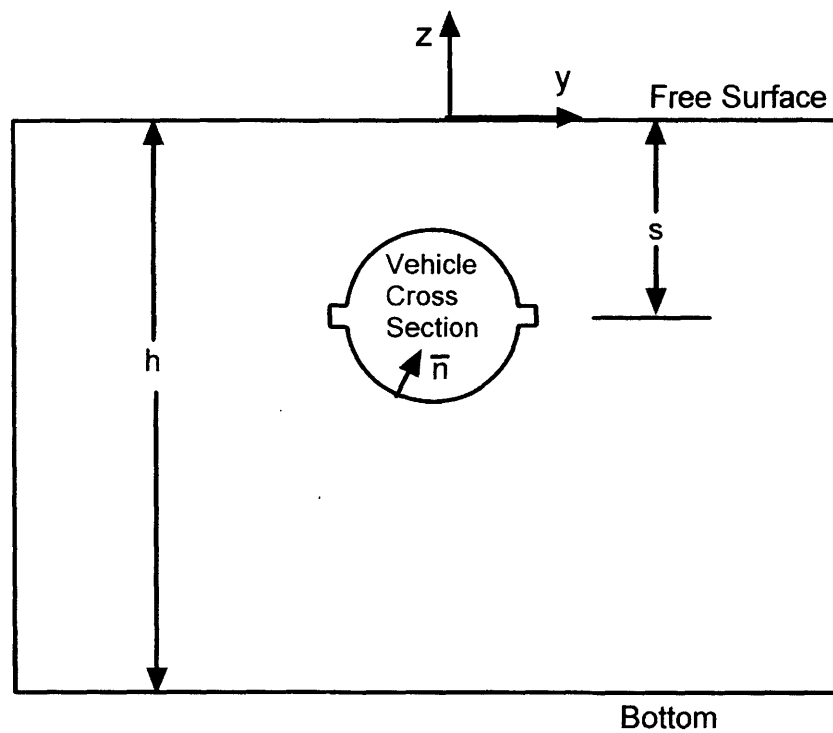


Figure 14 Two Dimensional Domain Diagram

The free surface and the bottom of the domain have a total number of panels equal to the variable nph which can be specified by the user. Because the area of both the free surface and the bottom directly above and below the vehicle experience the most change in velocity potential due to wave radiation and diffraction from the vehicle there is a cluster of 12 small panels which are centered directly above and below the body. The length of these small panels is also an input to the program, specified by the variable dhs , and their length does not have a large impact on the STC solution as long as they are reasonably small. As a general rule, the 12 panels should span approximately a vehicle diameter and a half. The length of the remaining panels is equal to the following equation

$$hp_size = \frac{2 \cdot hw - 12 \cdot dhs}{nph - 12} \quad (5.1)$$

The number of panels along the vertical walls of the domain is also specified by the user and are noted as the variable npv . These panels are evenly spaced over the water depth h , so their length is equal to

$$vp_size = \frac{h}{npv} \quad (5.2)$$

The vehicle section, including fins, is approximated by a number of input points which constitute the geometry of the body in the input file, which is specified by the program user. The code connects each pair of adjacent input points as a straight line panel with a control point located at the center of the panel. The solution to Green's theorem is calculated to determine the velocity potential at the panel centroid.

5.2 Wavelength Influences on Domain Width

In contemplating the size of the domain needed to accurately run the STC one would first guess that the width of the domain would be largely dependent on the wavelength for the test case in question. It is logical that the domain should have a width on order of the wavelength but in general this is not the case.

Figure 15 below shows the variation in the STC heave force output as the domain half width changes. For all three figures in this section, the nph was changed for each half width run of the code to ensure that each horizontal panel outside of the 12 small panels adjacent to the body is approximately 25 cm long. Also, all three figures in this section are for head seas.

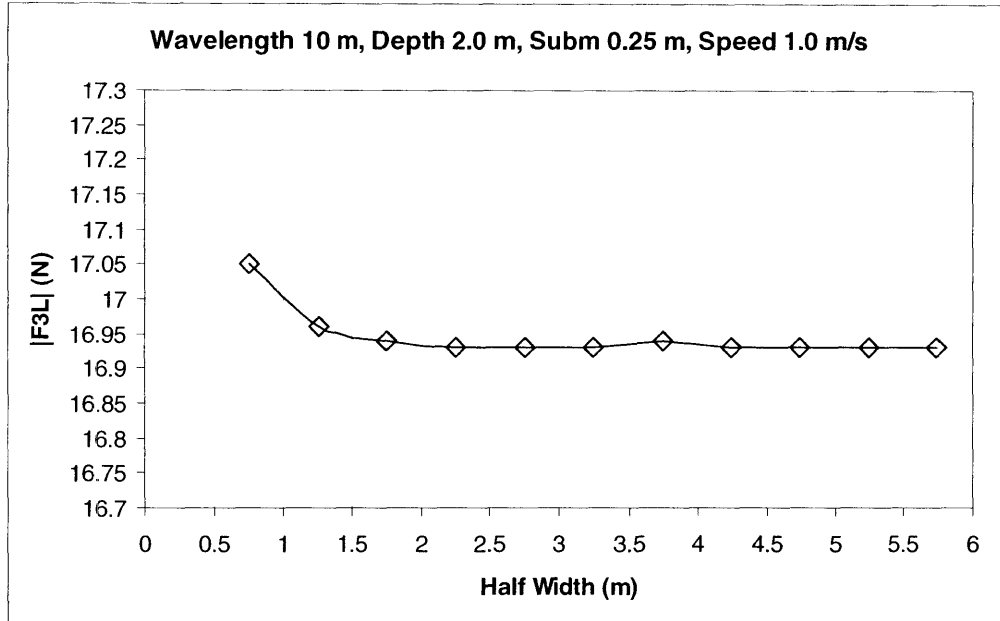


Figure 15 Convergence Study, 10 m Wavelength

It is apparent from visual inspection that the solution to the STC converges at approximately 16.93 N for this case at half widths above 2.25m.

Figure 16 below shows similar data as Figure 15 above but in this case the wavelength was decreased to 6 m and the submergence was doubled. Additionally, two separate sets of data are presented, one with 1 m/s speed, the other with 2 m/s of forward speed.

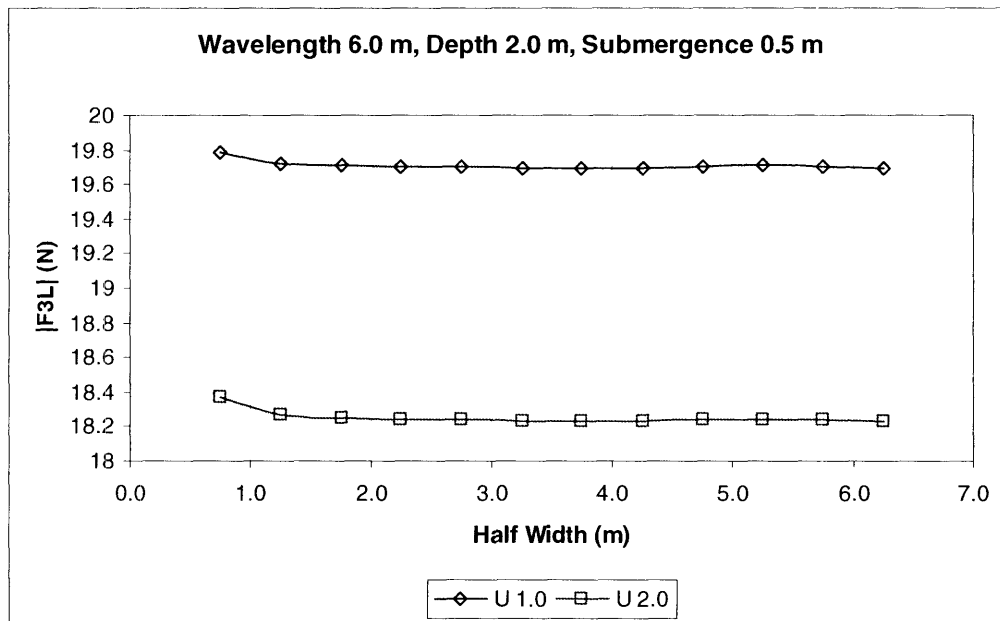


Figure 16 Convergence Study, 6.0 m Wavelength

As in Figure 15, the solution converges for both speeds at a half width above 2m. It is important to note that in this case the variation in the solution is not as great as in the case above where the vehicle was closer to the free surface. It is logical that the codes convergence has some dependence on submergence because a body close to the free surface will create larger and more influential waves along that free surface. The domain need necessarily be larger for a case of smaller submergence in order to allow room for the diffraction potential to be modeled appropriately along the free surface.

Figure 17 below is a similar plot to Figure 15 except the wavelength is now 20m and the vehicle submergence is now 1m. In this case there is no noticeable variation in the magnitude of the heave force as the domain half width varies.

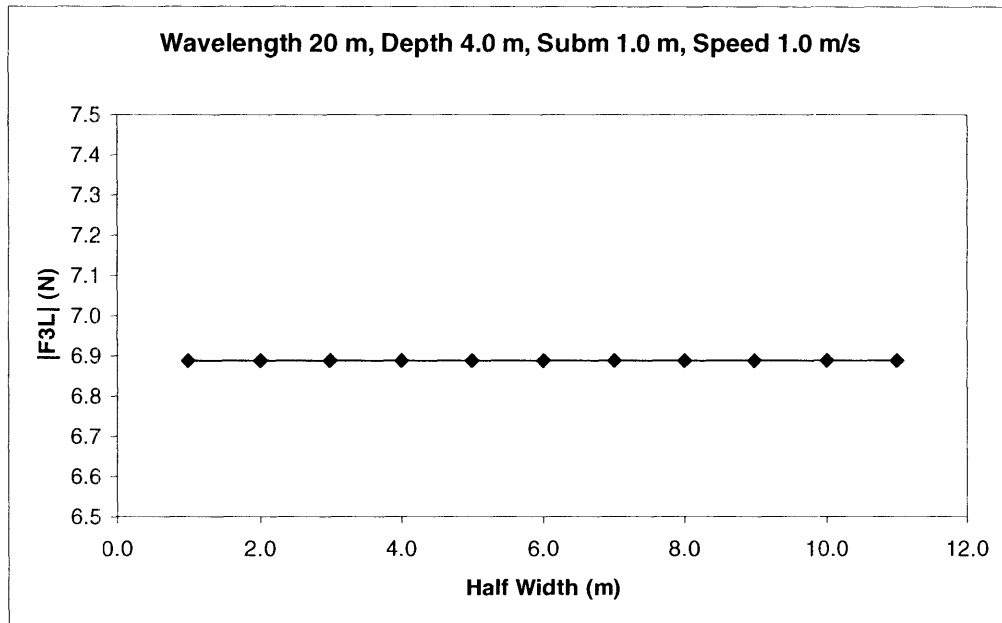


Figure 17 Convergence Study, 20 m Wavelength

The three studies shown above indicate that the convergence of the STC solution over domain half width is not dependent on test case wavelength or depth but dependent on vehicle geometry as this the only other length dimension specification in the problem. Additionally speed has no effect on this convergence. For the REMUS AUV the domain size should be approximately 5m in width to correctly model the vehicles forces. It is best to use close to the smallest domain width necessary for a stable solution because then the number of panels required is also reduced which has a great impact on the computation time necessary to fully calculate the code.

5.3 Panel Sizing Study

The number of panels required along the domain to obtain a reliable and solid solution is not an easily determined problem as it changes for most test conditions. For the majority of test cases where an AUV would be operating the submergence is deep enough that the size of the panels does not play a very significant role in the STC solution because the velocity potential along the surfaces does not change very dramatically over distance. Similar to the determination of the

panel sizing for the small panels adjacent to the body, it is best if enough panels are used to keep them relatively small, on the order of 0.2m long seems to be adequate.

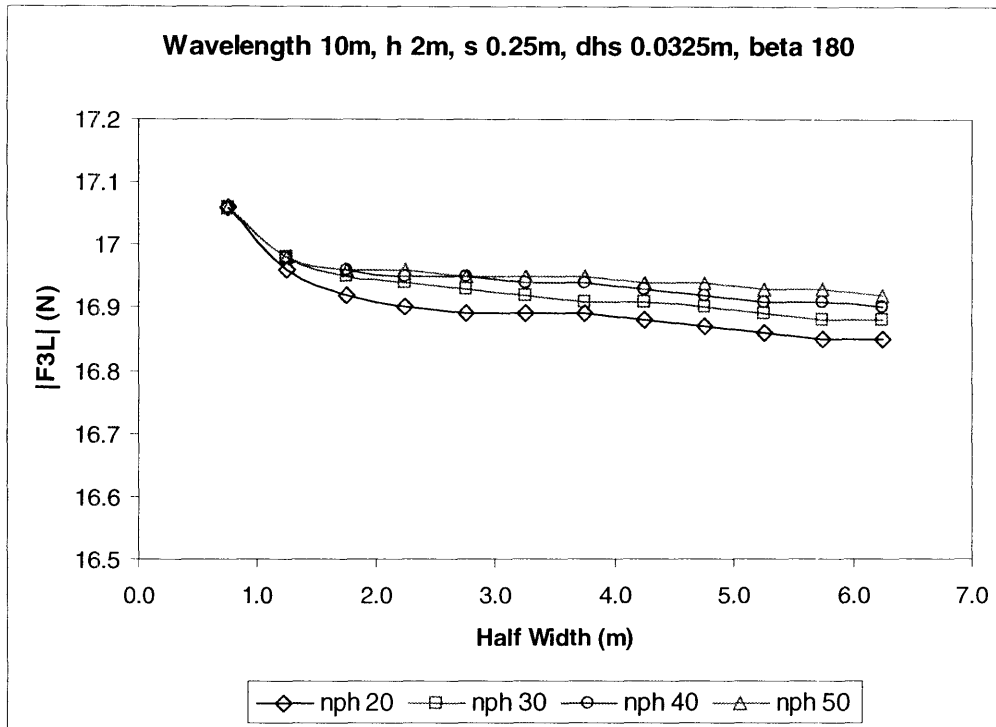


Figure 18 Panel Sizing Study

Figure 18 shows heave magnitude output for varying domain half width for four separate cases each of which has a different number of horizontal panels. The case with 20 horizontal panels produces an unreliable solution to the problem because once the domain is large enough to converge on the solution the panels are too large to adequately describe the variation in the potential solution.

The case with 30 panels displays an adequate solution at a half width of 2.25m, which corresponds to a panel size of 0.228m. For larger half widths this case begins to produce increasingly poor data due to the increase in panel size. The case with 40 panels displays an adequate solution at half widths varying from 2.25 to 3.75m, which correspond to panels of 0.145 to 0.254m. Similarly, the case with 50 panels provides a stable solution for a wider range of half widths which correspond to panels ranging from 0.82 to 2.66m.

Other tests were run for shorter waves and for deeper submergences however the data did not show that panel size showed appreciable influence on the solution and a plot of that data is not of consequence. Similarly, consequential data for the sizing of the number of vertical panels was not found.

As a mentioned earlier the correct panel sizing to obtain reliable solution is not, as one might think, a simple matter but is dependent on several test cases which were not fully understood. The research conducted shows that on average the panels should be plentiful enough to ensure that they are no larger than 25cm for reasonable data run conditions.

5.3 Domain Sizing Conclusion

As is evident from the previous two sections a complete understanding of the domain and panel size requirements is not available from the research conducted. In order to fully determine the requirements for the width of the domain it would be important to run similar convergence tests for vehicles of different dimensions than the REMUS AUV. Additionally, the conclusion as to the sizing of the panels for the domain boundaries is not a precise solution and to obtain a better solution it would be important to test the code for different vehicles, as for the domain width. Unfortunately due to time constraints in the completion of this thesis further testing with other vehicle geometries was not possible.

Regardless, it has been proven that the STC output is very reliable for the REMUS AUV with domain half widths above 2.25m and panels which are no longer than 25cm. This provides an adequate base to test the validity of the code on the REMUS vehicle.

Chapter 6: Strip Theory to WAMIT Comparison

The goal in writing this strip theory code was to develop an adequate model for force and moments on a submerged vehicle which requires simple input geometries. It is important to compare the results to a known and established program's results as this provides an excellent baseline for the accuracy of the code. WAMIT is a well known code that has been established and proven to be accurate for stationary objects; thusly it is an excellent comparative tool.

The plots below show data comparisons for the REMUS AUV of WAMIT output versus STC output for the experiment cases run in Sabra's thesis. Table 2 above shows the range of data input for the experimental test cases. Additionally WAMIT and STC data was collected for test parameters which could not be tested in the tow tank, the parameters for which are displayed in table 6 below. Of course, as WAMIT does not allow for forward speed, there is no data for test runs where the vehicle has forward speed in this section.

WAMIT vs Strip Theory Parameter Range	
Depth (h)	1.52 & 5 m
Submergence (s)	0.476 - 2.0 m
Base Frequency (ω)	1.266 - 3.511 rad/s
Wavelength (λ)	5.0 - 30.0 m
Wave Amplitude (a)	5.0 m
Speed (u)	0 m/s
Heading (beta)	45, 90, 135, 180 deg

Table 6 Extra Test Parameters For WAMIT to Strip Theory Comparison

Data for sway, heave, pitch, and yaw is broken into individual wave headings to help show the broad accuracy of the STC. In general the WAMIT output closely matches the experimental data for all four degrees of freedom considered. As this is the case, a large scale plot of magnitude and phase data is presented for a singular wave heading for sway, heave, pitch and yaw with additional smaller plots of the remaining data to condense the size of this report.

The sway data is presented in Figures 19 through 22 and the STC provides output which closely mimics the output of WAMIT. It is important to note that the phase data matches quite closely for WAMIT and STC output. This correlation reinforces the findings in Sabra's thesis that the experimental data does not present reliable values for phase data.

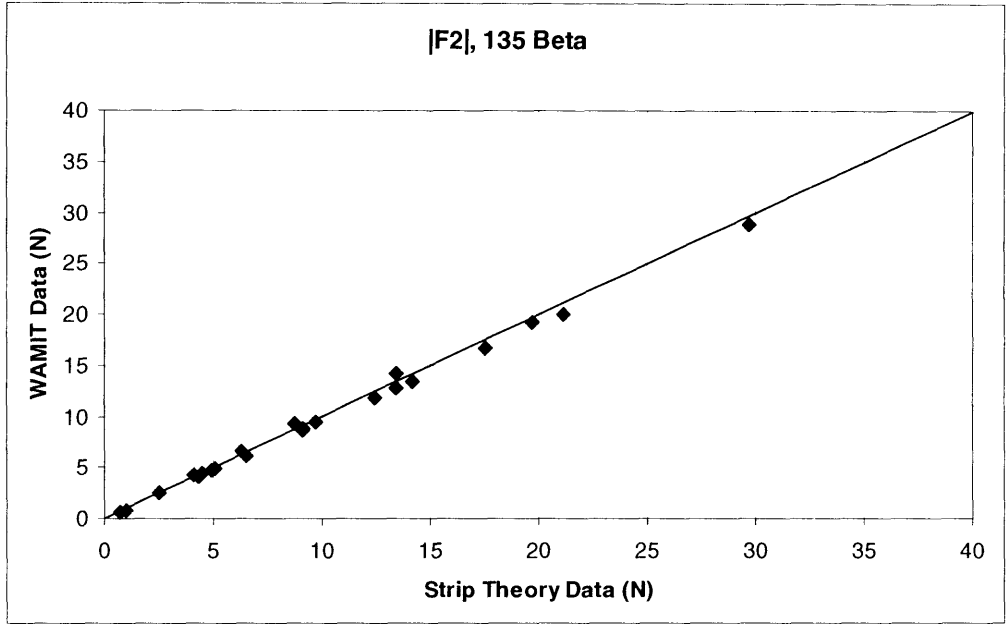


Figure 19 WAMIT v STC |F2|, 135 Beta

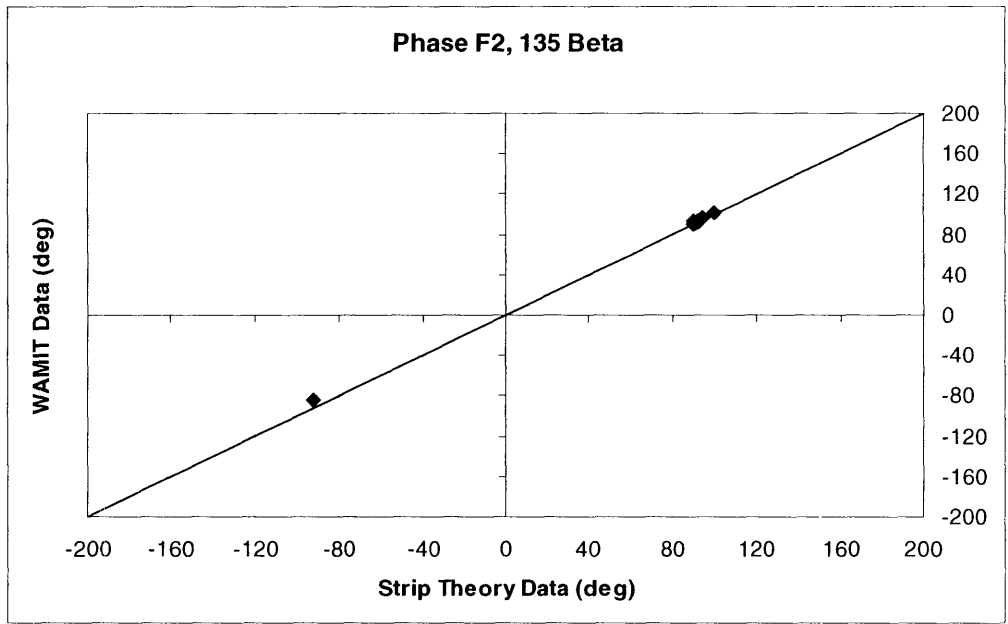


Figure 20 WAMIT v STC F2 Phase, 135 Beta

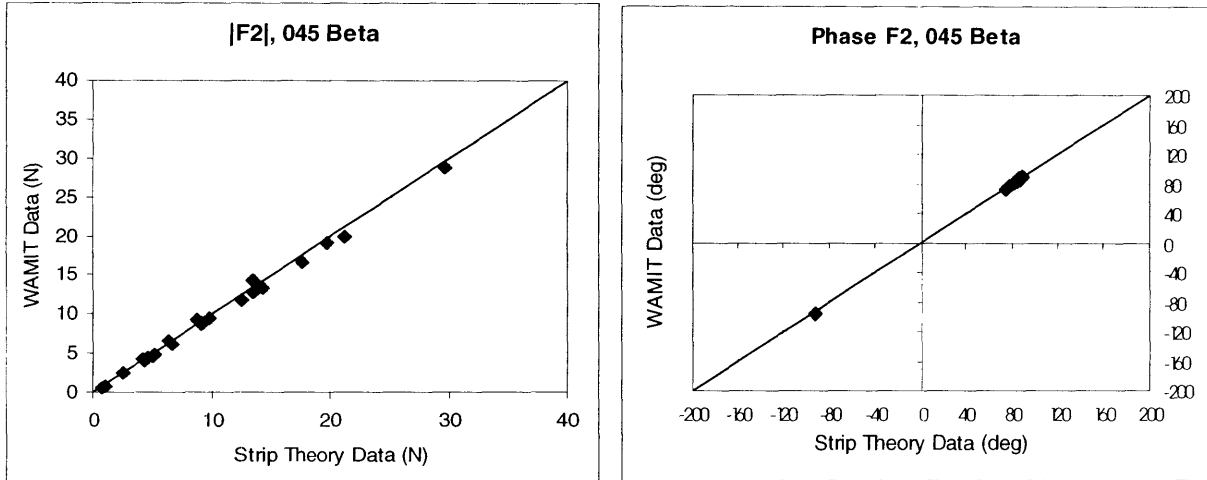


Figure 21 WAMIT v STC F2 Data, 045 Beta

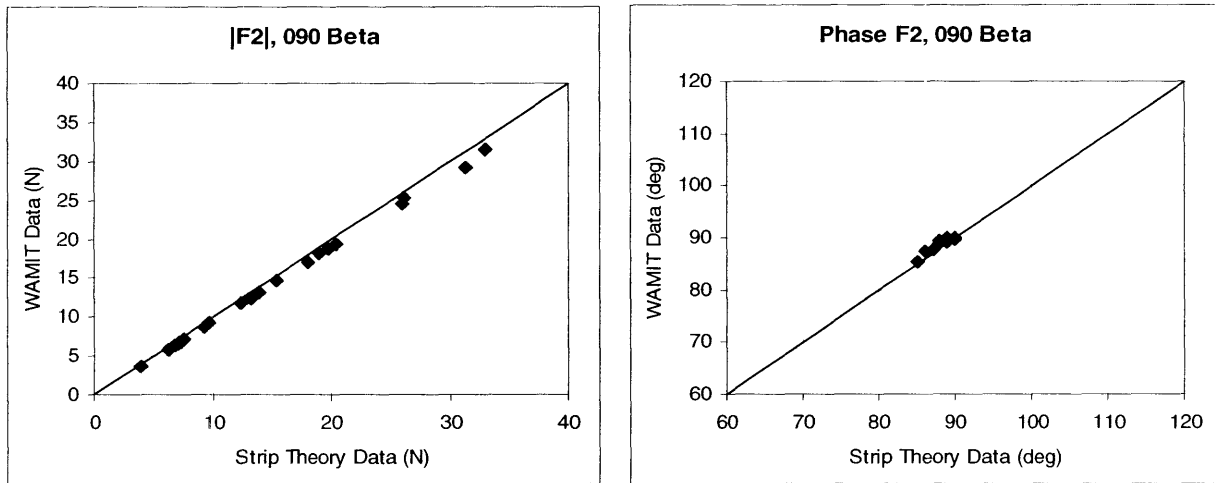


Figure 22 WAMIT v STC F2 Data, 090 Beta

The heave data is presented in Figures 23 through 28. As is the case in the sway force, the STC results closely mimic the results of WAMIT.

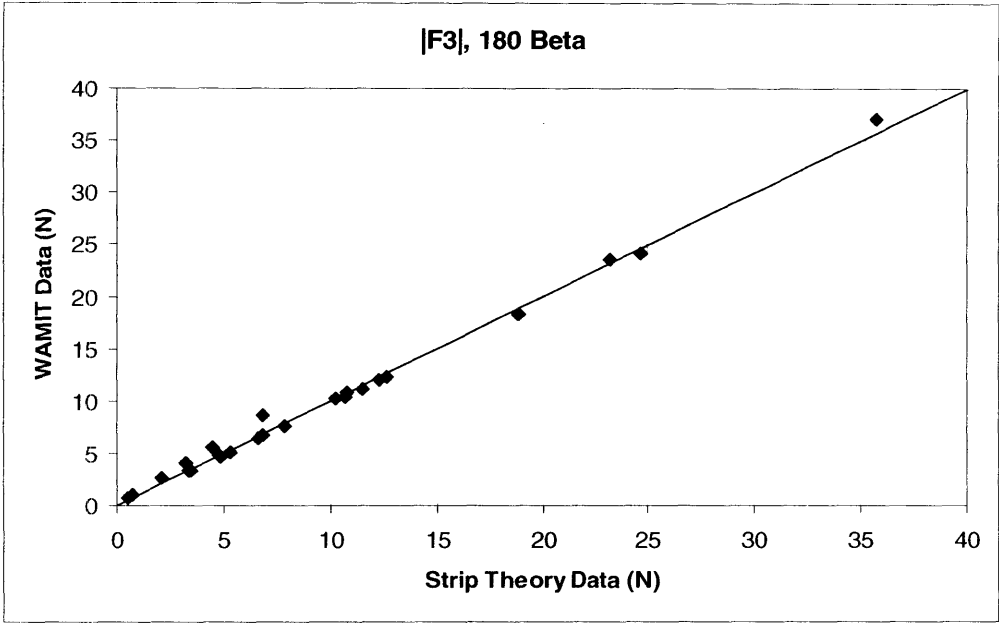


Figure 23 WAMIT v STC |F3|, 180 Beta

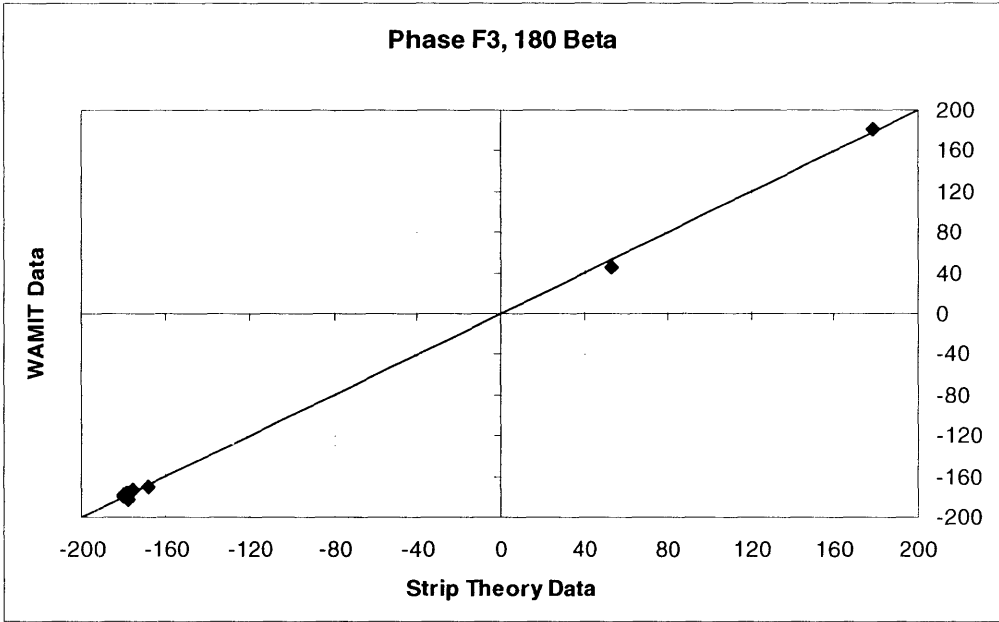


Figure 24 WAMIT v STC F3 Phase, 180 Beta

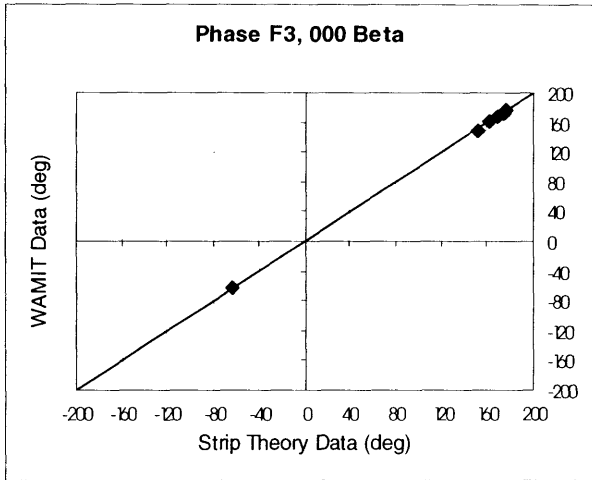
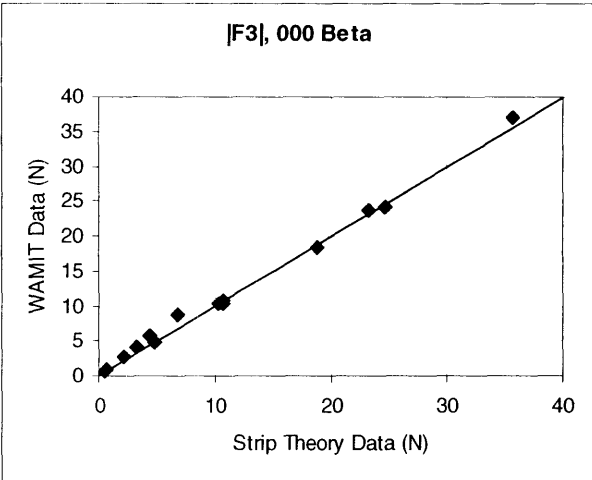


Figure 25 WAMIT v STC F3 Data, 000 Beta

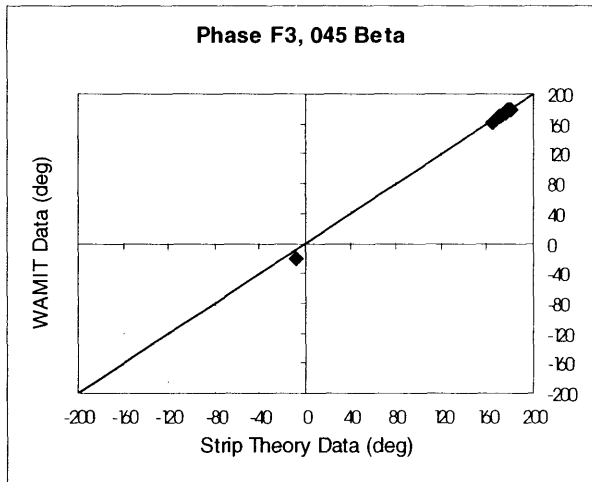
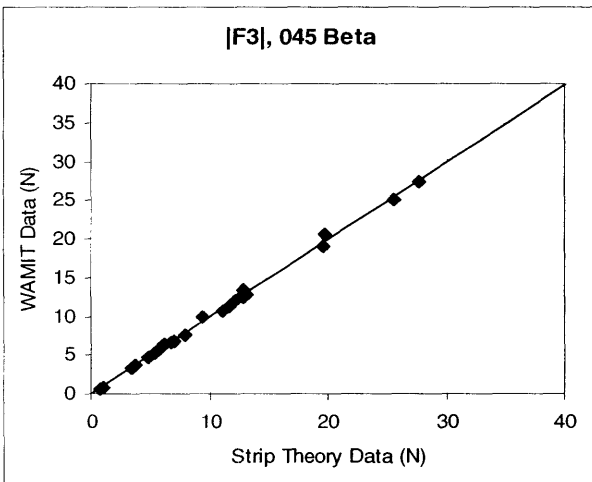


Figure 26 WAMIT v STC F3 Data, 045 Beta

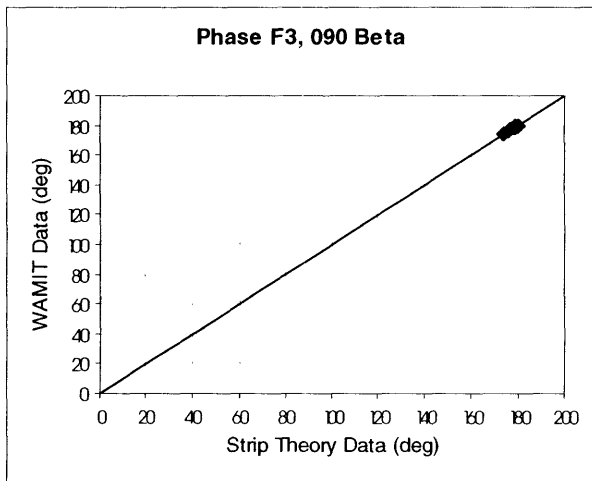
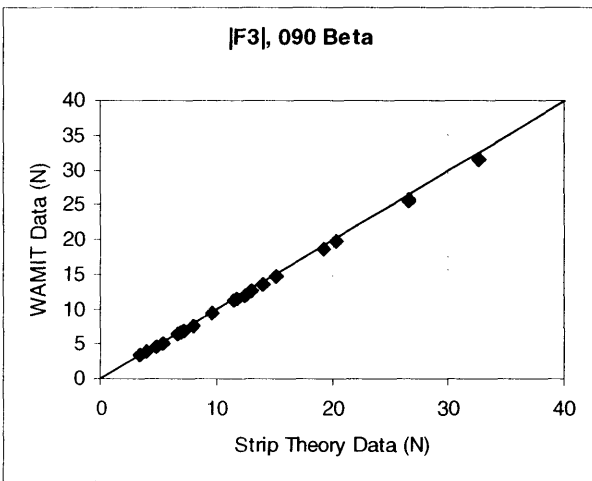


Figure 27 WAMIT v STC F3, 090 Beta

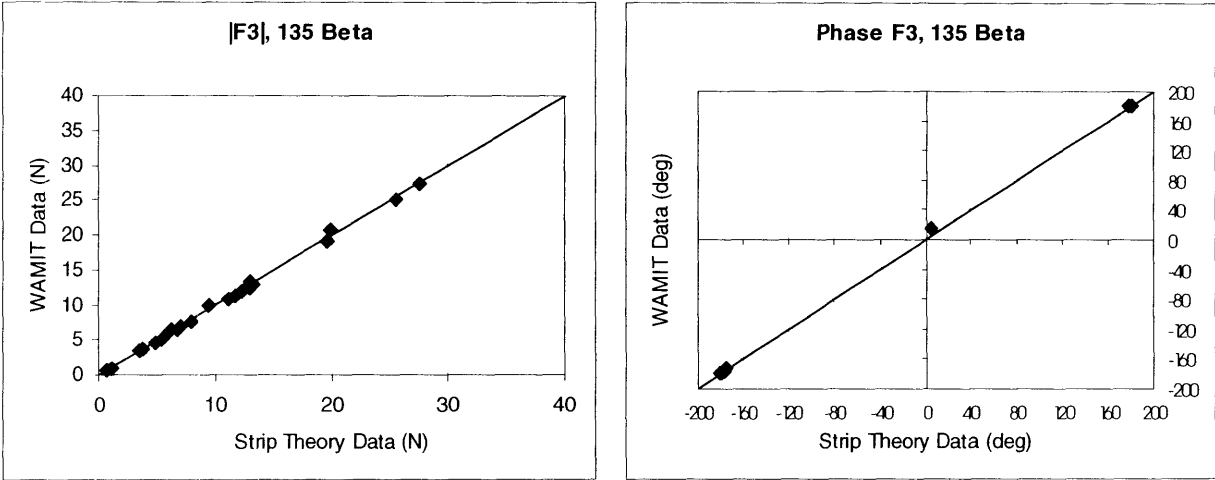


Figure 28 WAMIT v STC F3 Data, 135 Beta

In general, the relation between WAMIT and STC force data is more closely related than for moment data. Pitch data is presented in Figures 29 through 35. Even though the Moment data does not correlate as closely as the force data, the trend still shows that the STC provides reasonably close results to the WAMIT output and the difference is certainly within the margin of error for WAMIT.

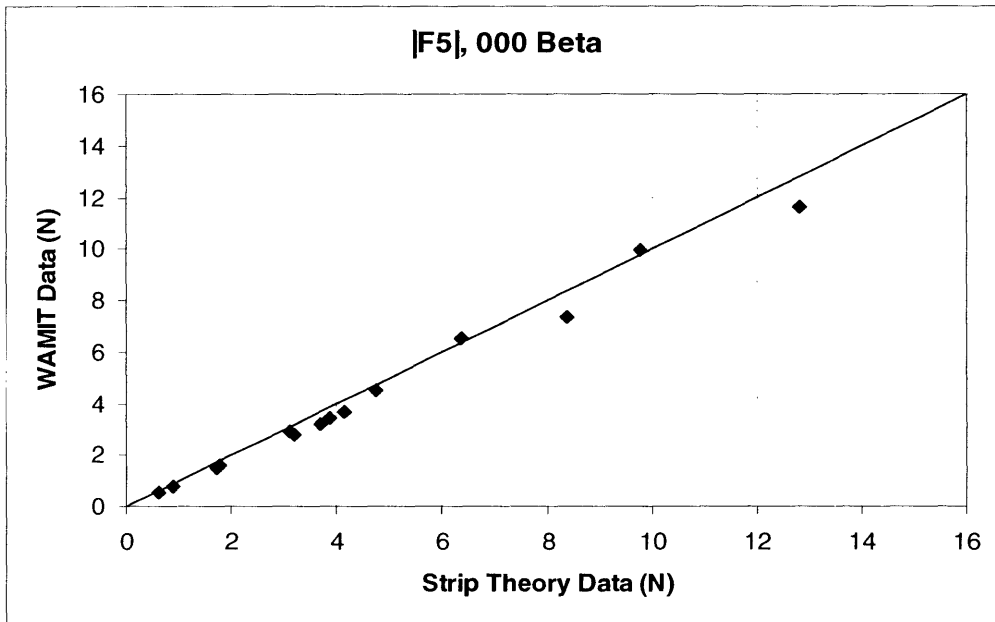


Figure 29 WAMIT v STC |F5|, 000 Beta

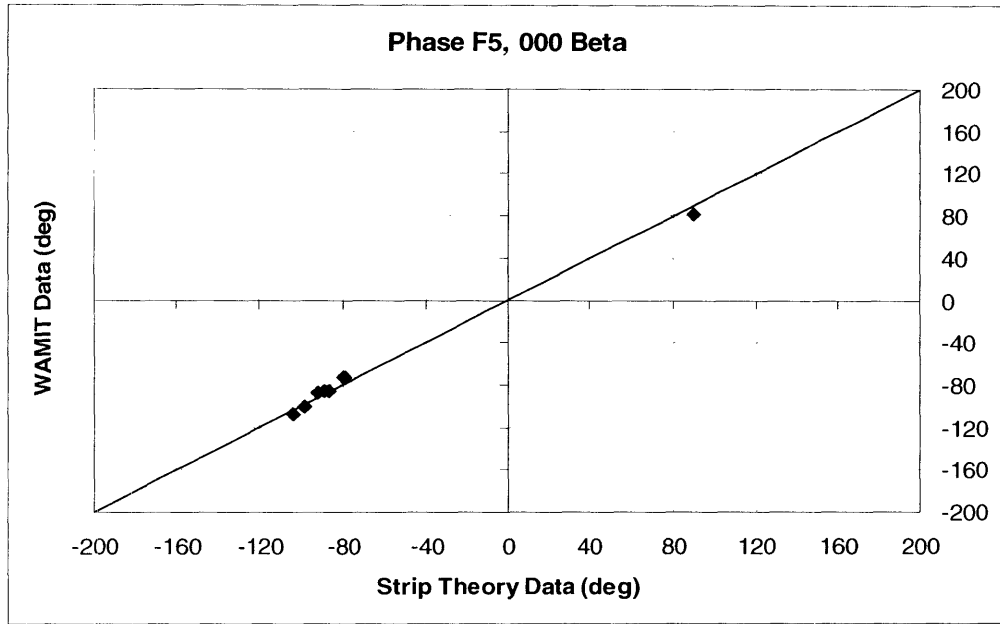


Figure 30 WAMIT v STC F5 Phase, 000 Beta

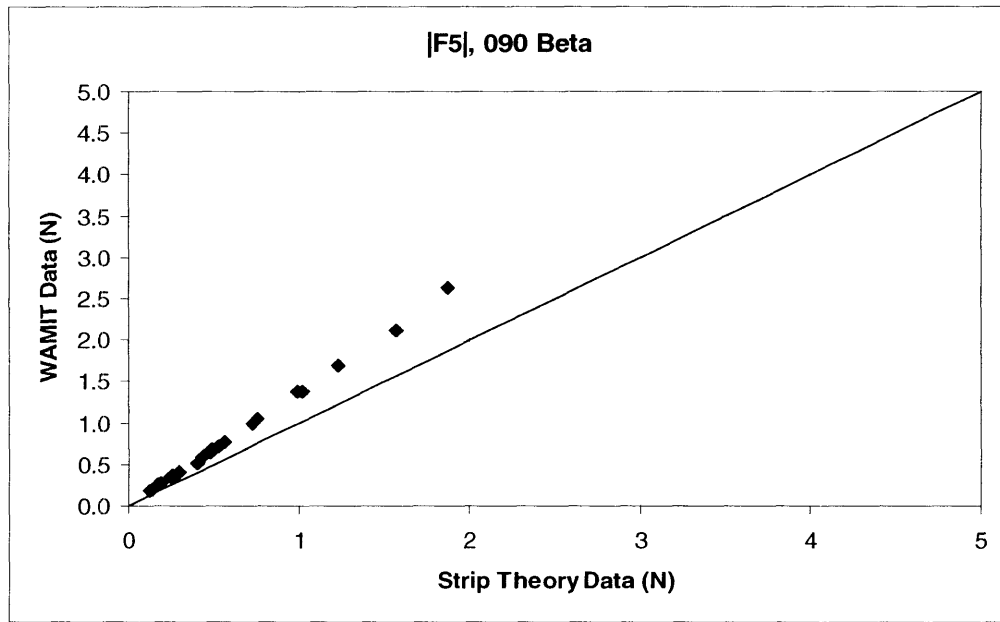


Figure 31 WAMIT v STC |F5|, 090 Beta

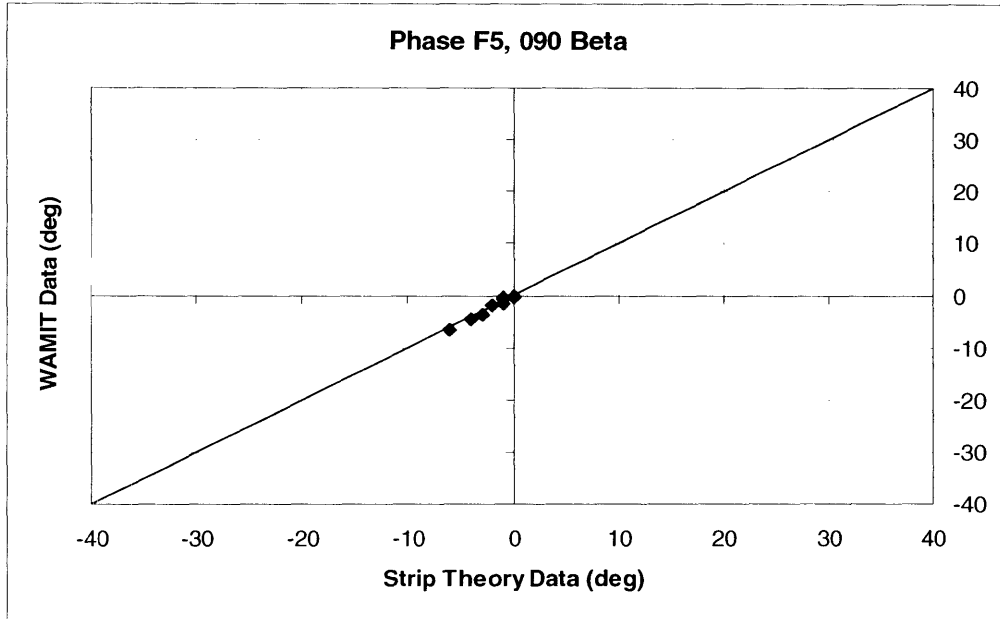


Figure 32 WAMIT v STC F5 Phase, 090 Beta

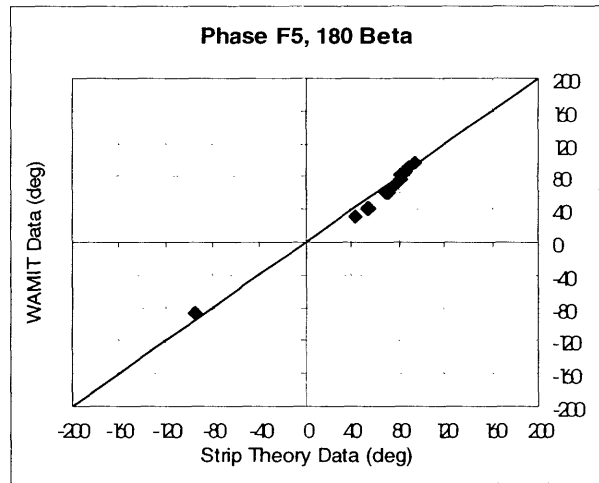
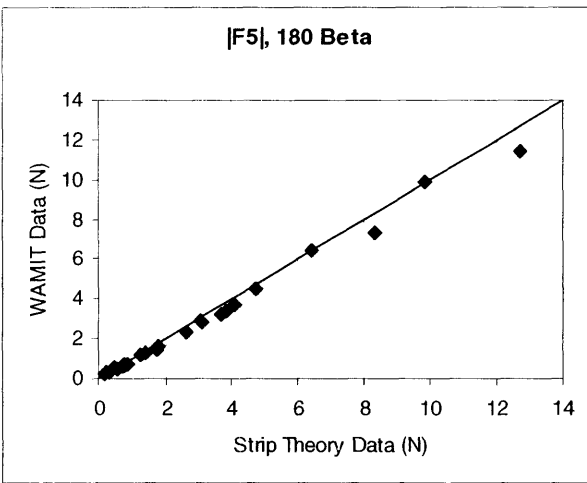


Figure 33 WAMIT v STC F5 Data, 180 Beta

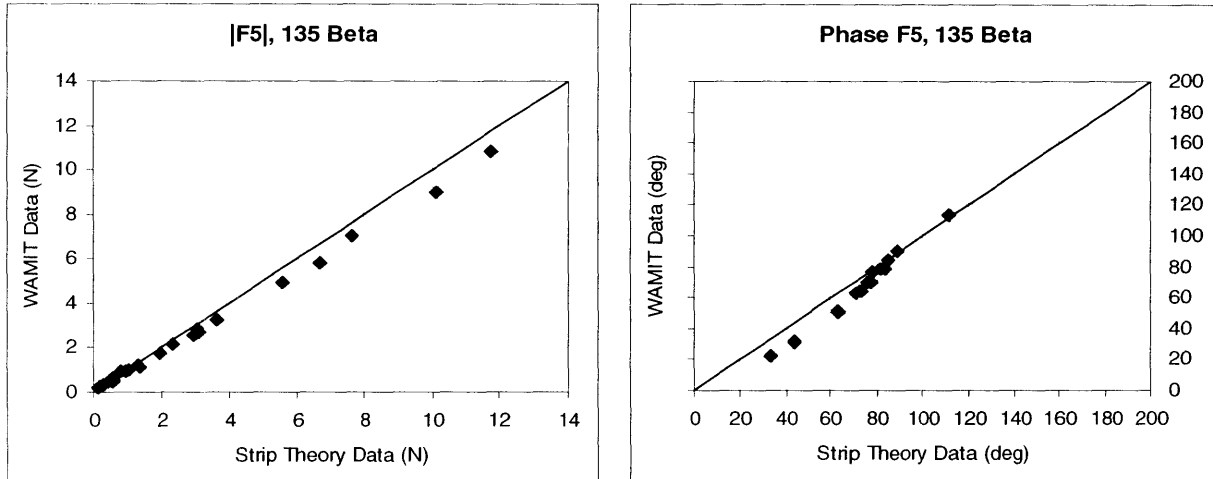


Figure 34 WAMIT v STC F5 Data, 135 Beta

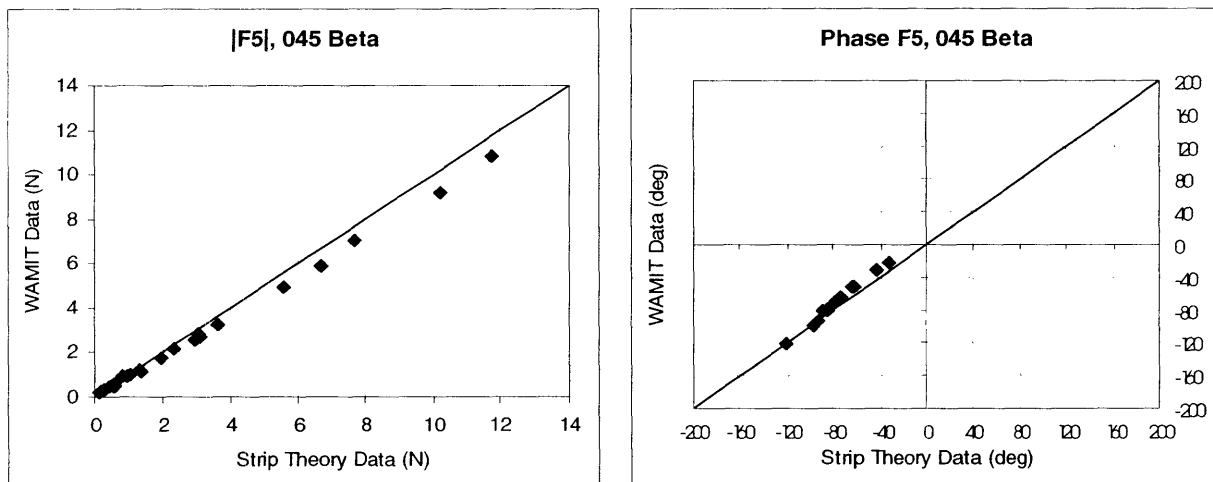


Figure 35 WAMIT v STC F5 Data, 045 Beta

The Yaw data is presented in Figures 36 through 39.

As is the case in the WAMIT to experimental data comparison shown in chapter 3, the data is disconnected in the cases of moment magnitude (pitch and yaw) for the beam sea case. This is shown in Figures 31, 32, 36, and 37. As in the experiment to WAMIT comparison the WAMIT data values are much higher in magnitude than the compared quantity of the STC data. The heave data comparison is noticeably worse than for the yaw data but the difference in values is still noticeable in both cases for the beam sea case. Note that, the phase data corresponds quite well regardless of the correspondence of the magnitude data.

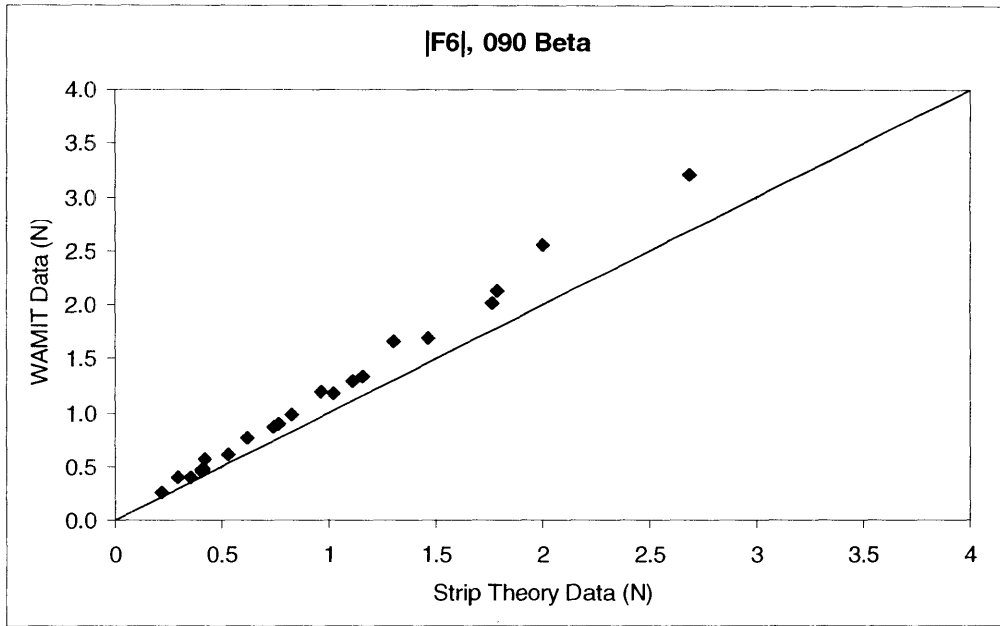


Figure 36 WAMIT v STC |F6|, 090 Beta

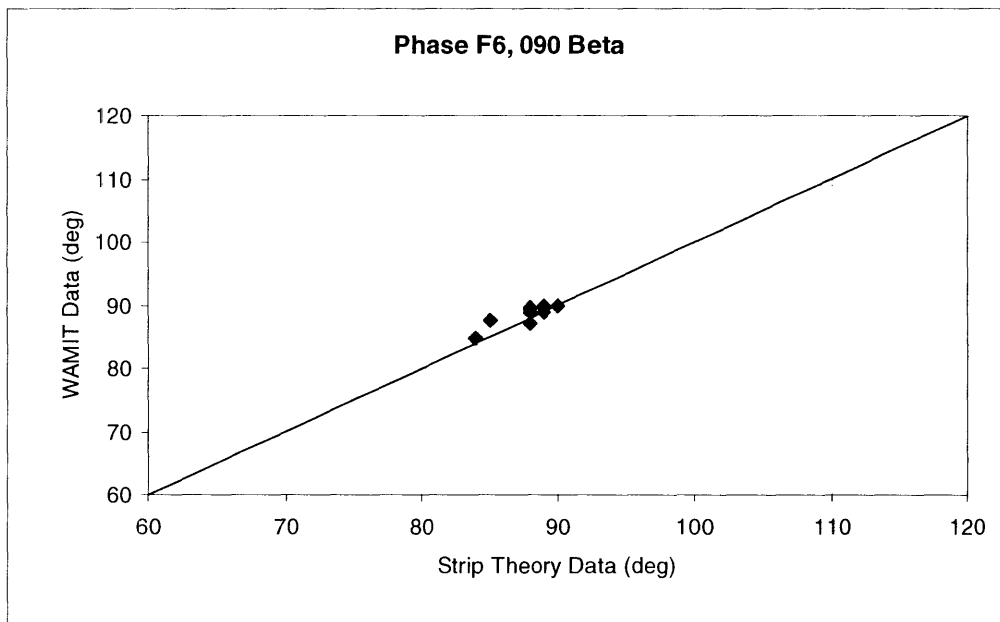


Figure 37 WAMIT v STC F6 Phase, 090 Beta

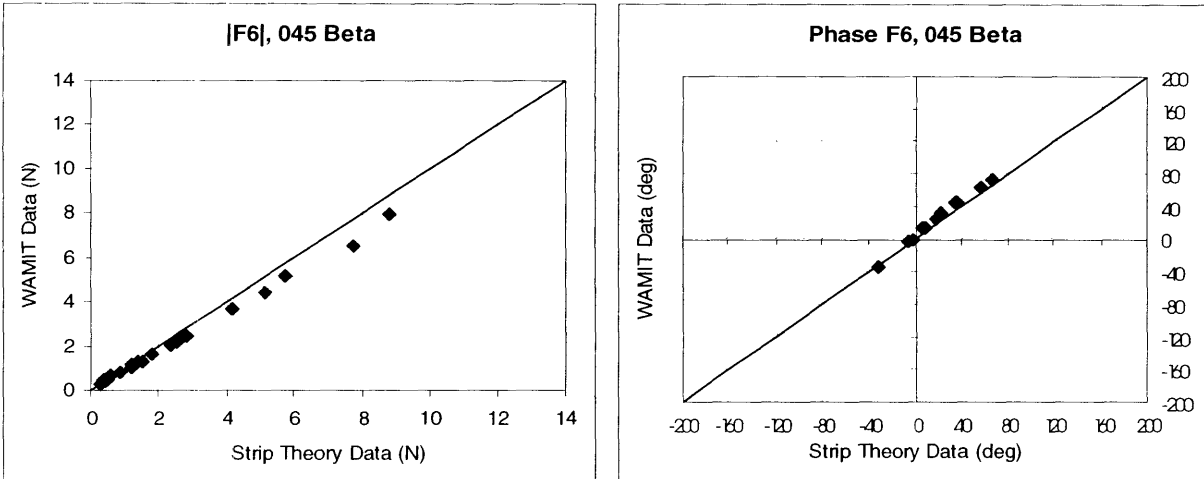


Figure 38 WAMIT v STC F6 Data, 045 Beta

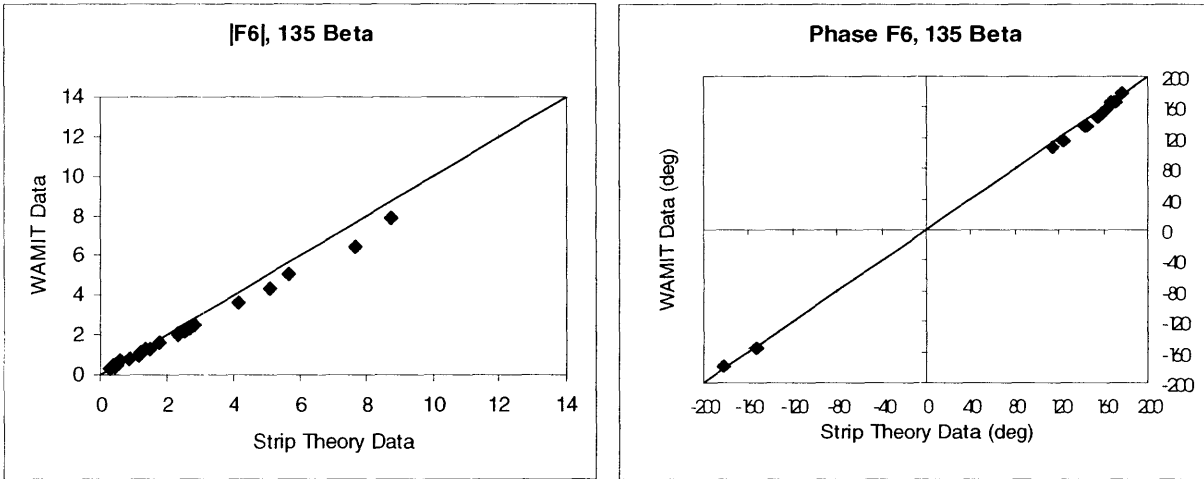


Figure 39 WAMIT v STC F6 Data, 135 Beta

In general the WAMIT comparison with the output for the Strip Theory Code is very promising. The data correlates very well and with less than a 5% difference on average for force data and approximately 10% difference for moment data. Also, as the moment data is generally small in magnitude the percent difference does not very accurately describe the small difference between the two programs outputs. Also the phase data comparison is very good with no major data outliers.

These results prove the accuracy of the STC in comparison to a very well known and proven numeric hydrodynamic model even though the comparison can only be done for test cases where the vehicle is not moving. It is also important to note the difference in the level of complexity between the two codes. WAMIT requires a full three dimensional solution to the problem which is not only computationally expensive but the input for the code is very complicated as the vehicle must be discretized into three dimensional panels for the entire body. On the other hand, the Strip Theory code gives reliable output with a very simple input of cross sectional geometry.

Chapter 7: Strip Theory to Experimental Comparison

The comparison of the Strip Theory Codes results to actual experimental data is of crucial importance in the validation of the code. This chapter presents a comparison of diffraction, or excitation forces on the REMUS AUV for the experimental conditions which were conducted at the Naval Academy's tow tank. As noted previously the phase data validity from those experiments is questionable and differences between the experimental data and the STC data is easily explained by the poor quality of the experimental data.

The Sway data is presented in Figures 40 through 42, and in general the STC seems to model the sway forces quite accurately. Recall that due to the limitations of the tow tank in which the experiments were conducted, sway and yaw data could only be collected for zero speed data runs.

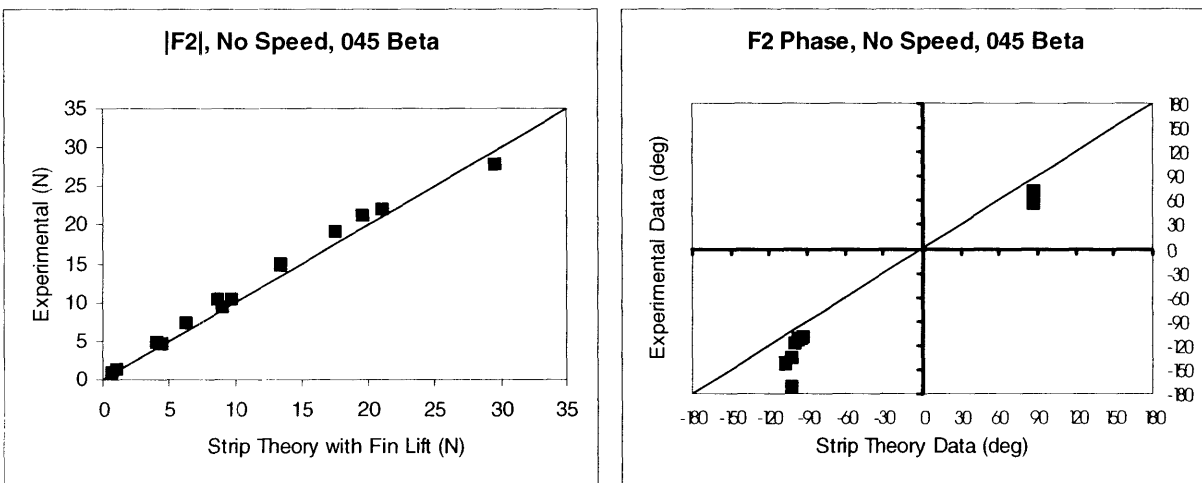


Figure 40 Experiment v STC F2 Data, 045 Beta

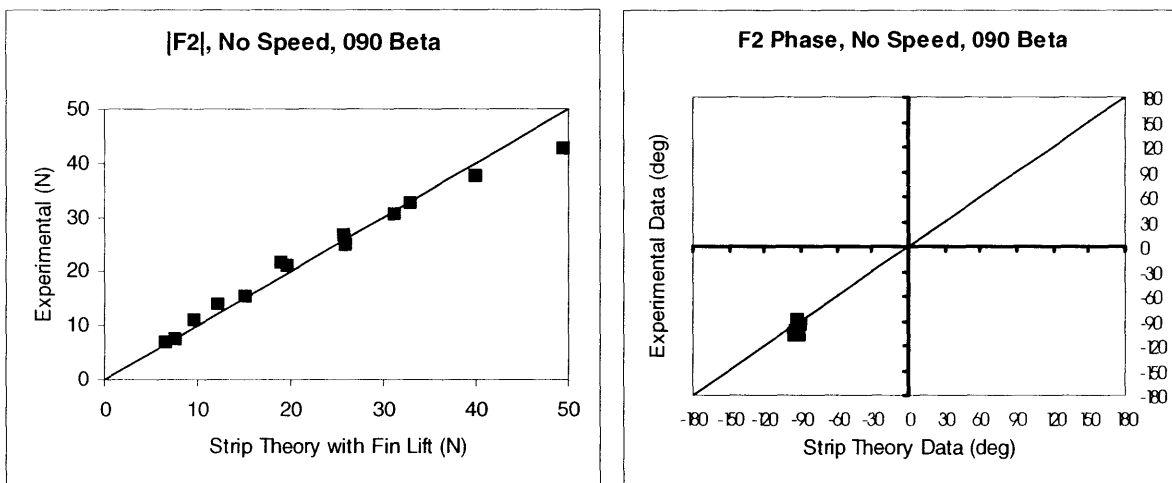


Figure 41 Experiment v STC F2 Data, 090 Beta

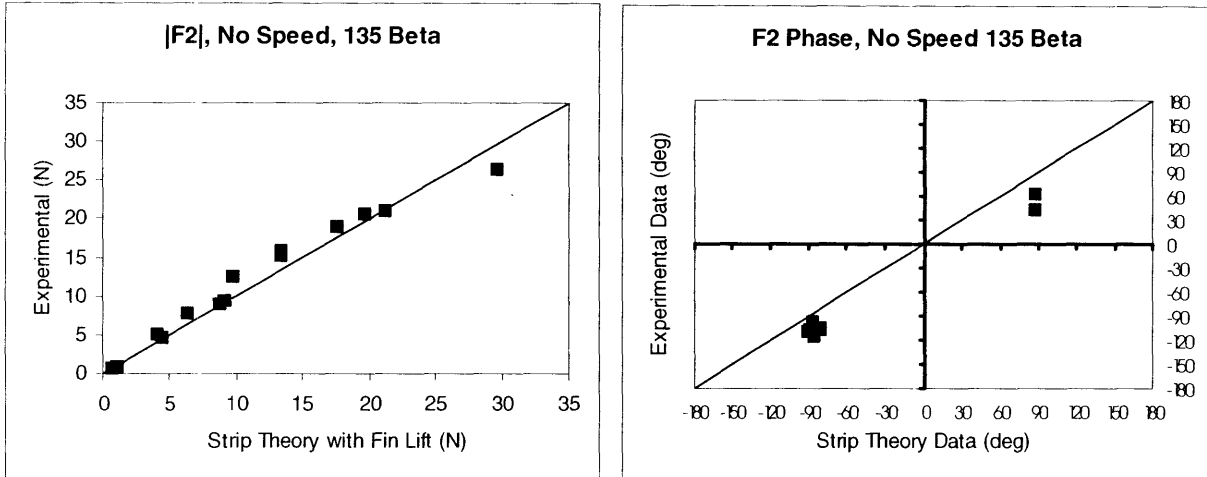


Figure 42 Experiment v STC, F2 Data, 135 Beta

The heave force comparison is displayed in Figures 43 through 51. The comparison is much more in depth than the sway comparison because there were a much larger number of experiments conducted for which the heave force was of consequence. As in sway data comparison, the zero speed heave force data is quite closely matched for force magnitude calculations. The general trend for each heading angle shows a solid connection between the experimental data and the STC output.

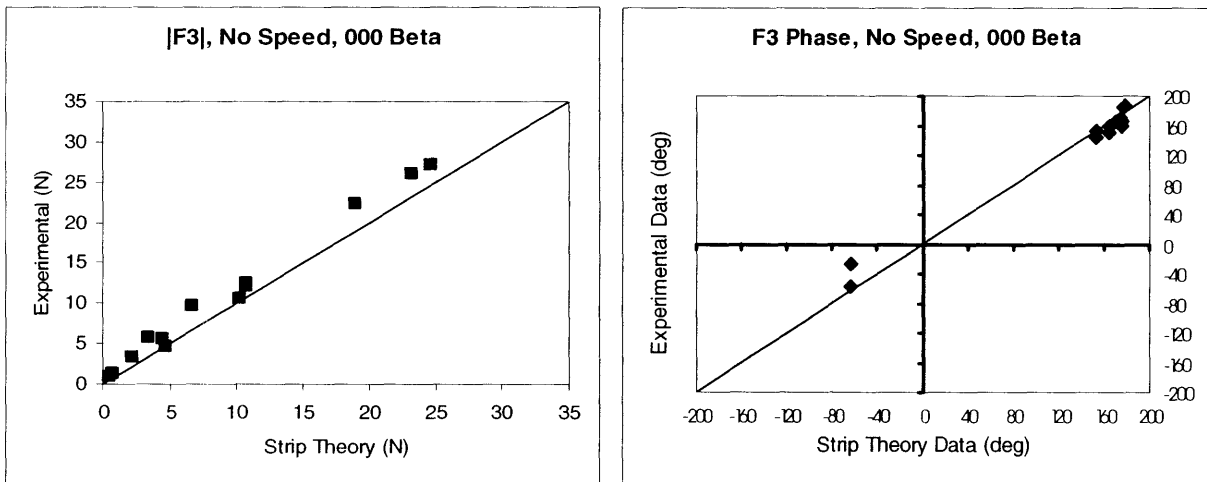


Figure 43 Experiment v STC F3 Data, 000 Beta

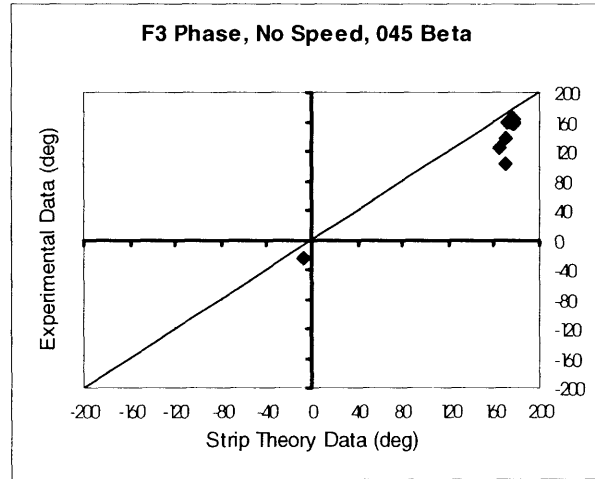
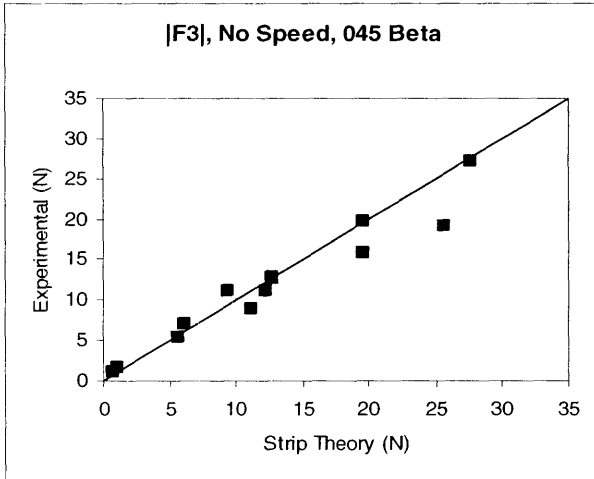


Figure 44 Experiment v STC F3 Data, 045 Beta

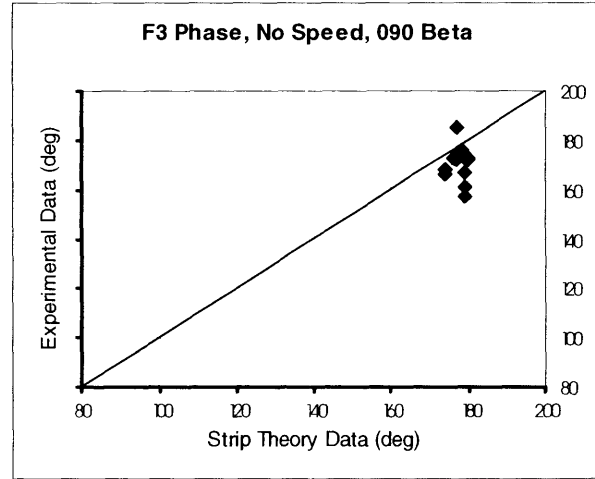
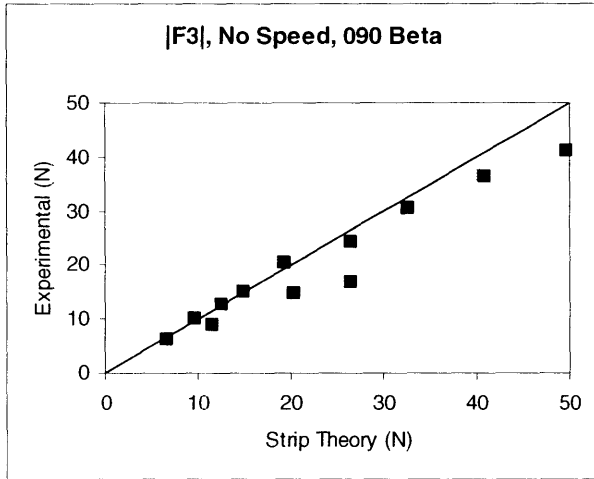


Figure 45 Experiment v STC F3 Data, 090 Beta

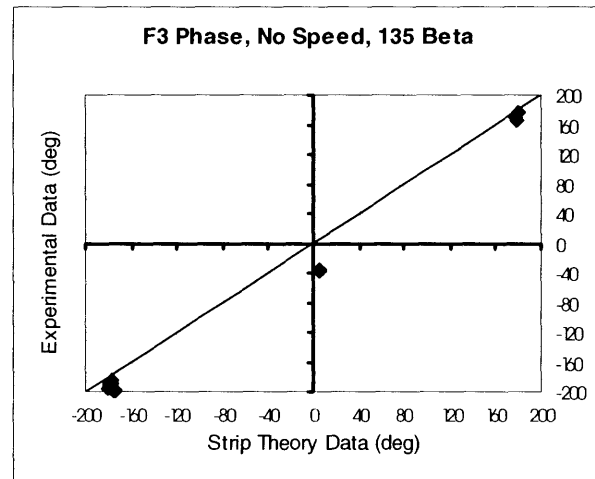
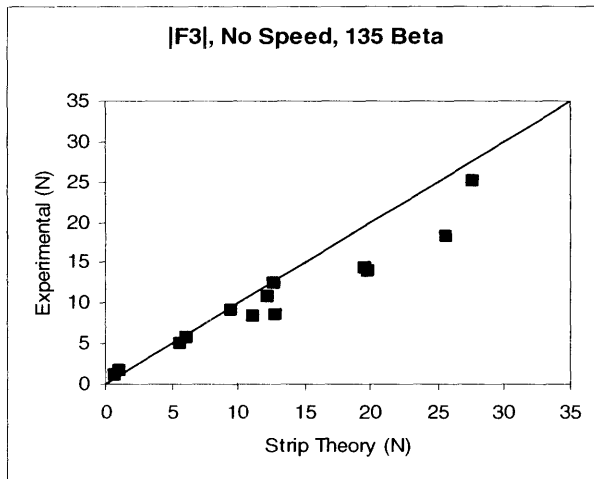


Figure 46 Experiment v STC F3 Data, 135 Beta

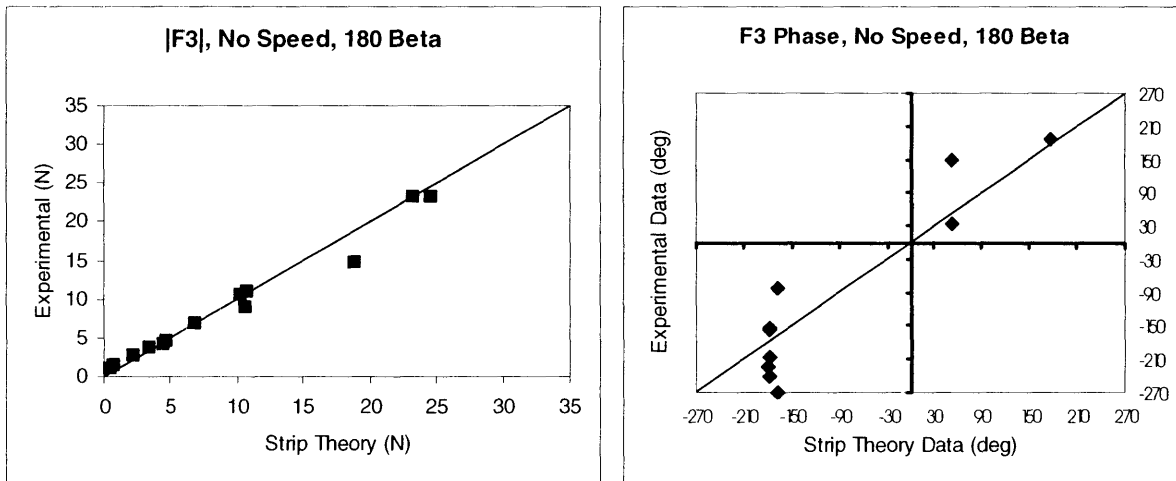


Figure 47 Experiment v STC F3 Data, 180 Beta

The plots of data with vehicle speed are presented in a larger format because they display the STC results both with and without fin lift effects. With the exception of two outliers in the data is closely matched and in nearly every case the addition of fin lift effects improves the data accuracy. Unfortunately the phase data is not as conclusive for the experiment cases with forward speed as the magnitude data is. Regardless, given the close comparison of WAMIT to STC data and the unreliable nature of the phase data from experiment the comparison is reasonable.

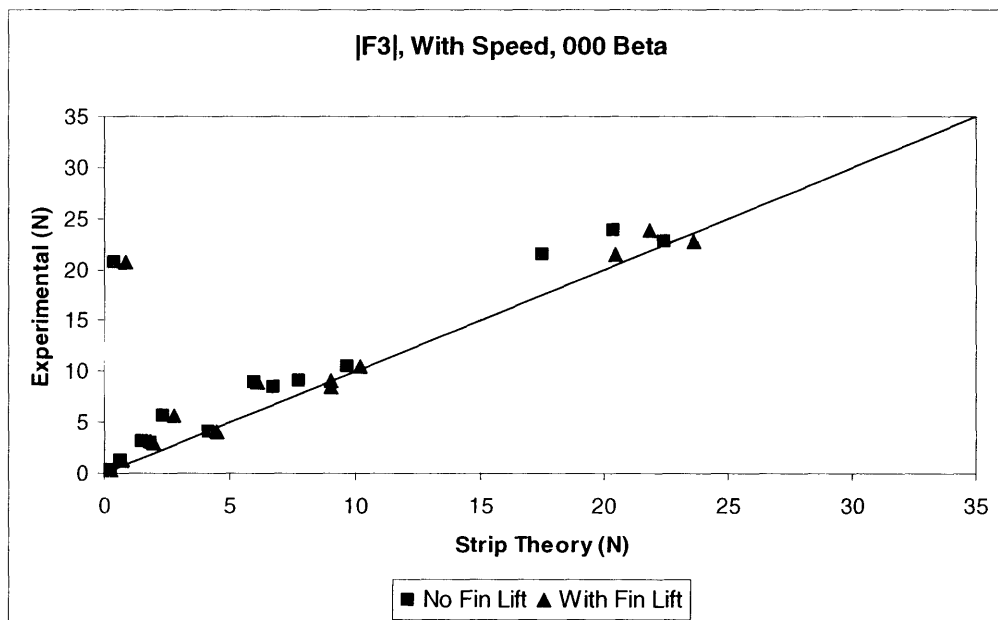


Figure 48 Experimental v STC, |F3] with Speed, 000 Beta

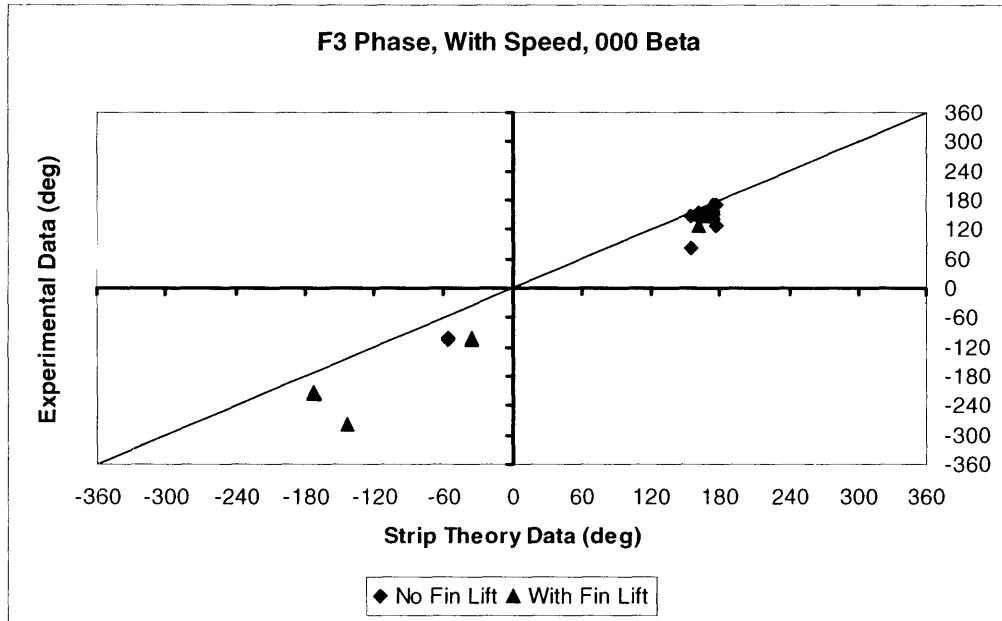


Figure 49 Experiment v STC F3 Phase with Speed, 000 Beta

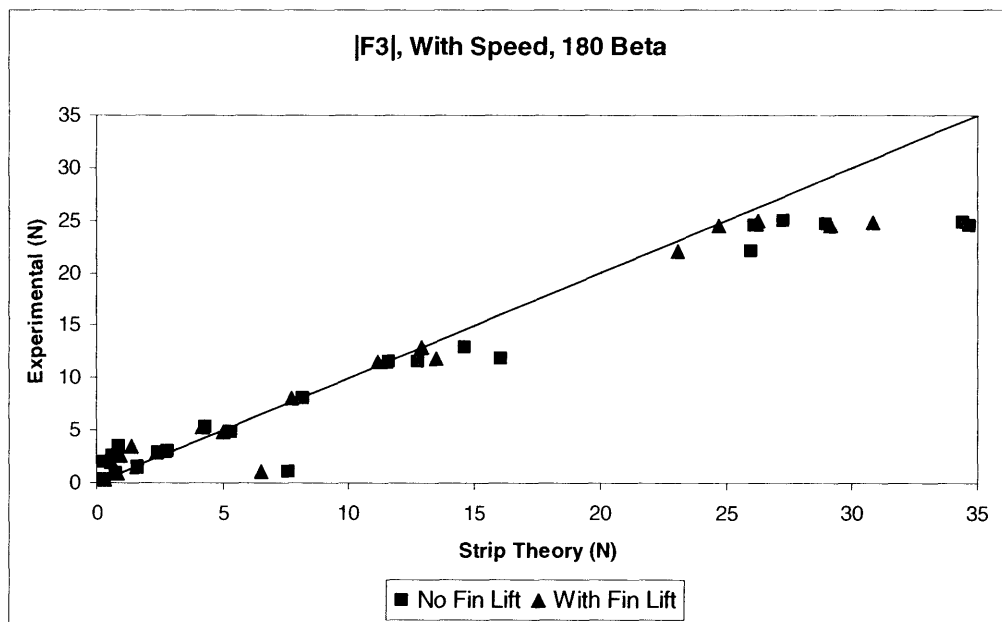


Figure 50 Experiment v STC, |F3| with Speed, 180 Beta

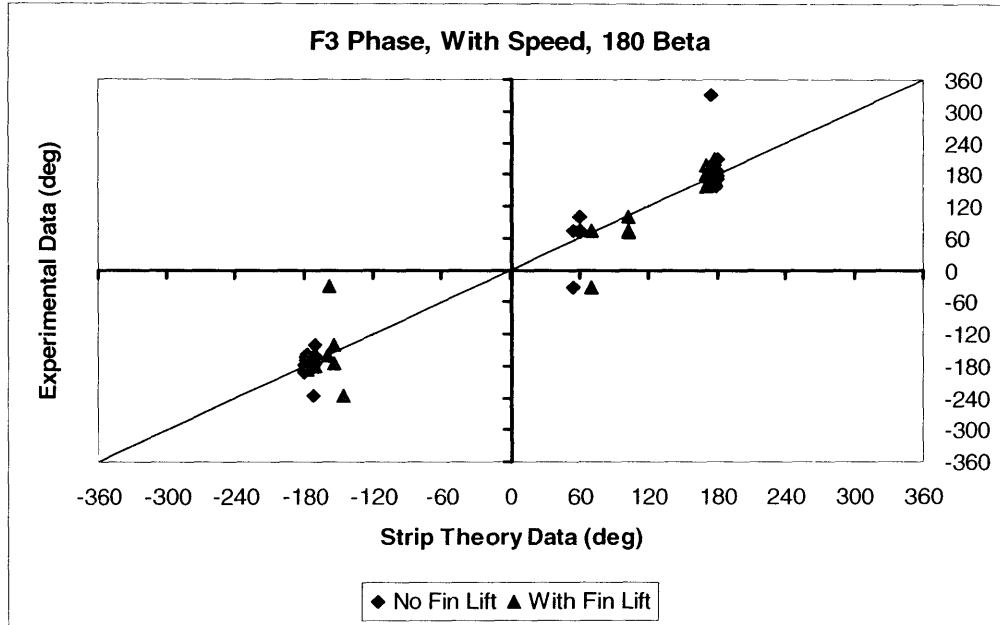


Figure 51 Experiment v STC F3 Phase with Speed, 180 Beta

The Pitch data comparison is presented in Figures 52 through 61. Unlike in the WAMIT to STC comparison the moment data comparison is not appreciably worse than the force data comparison. This helps reinforce that the STC is a reasonably accurate code in modeling practice.

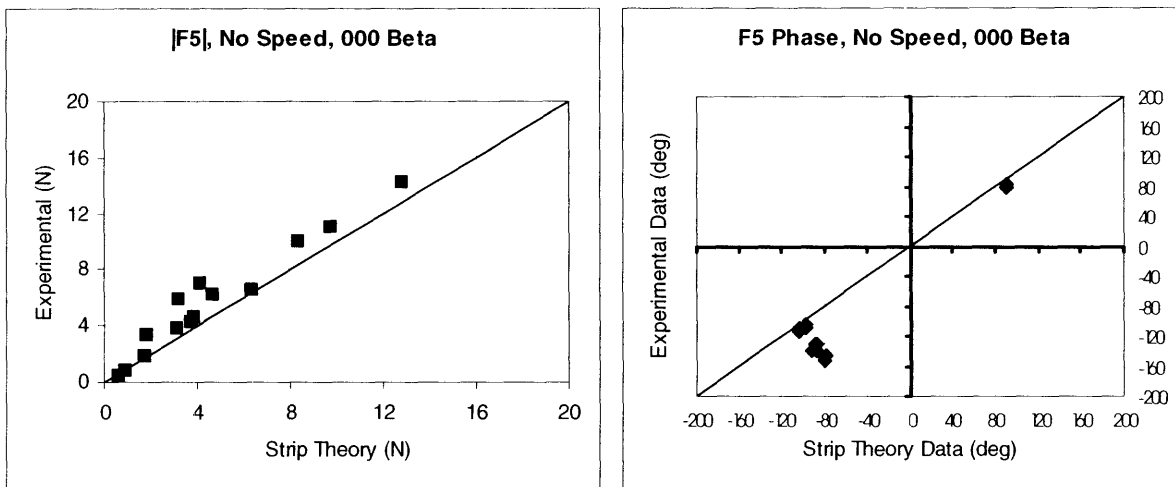


Figure 52 Experiment v STC F5 Data, 000 Beta

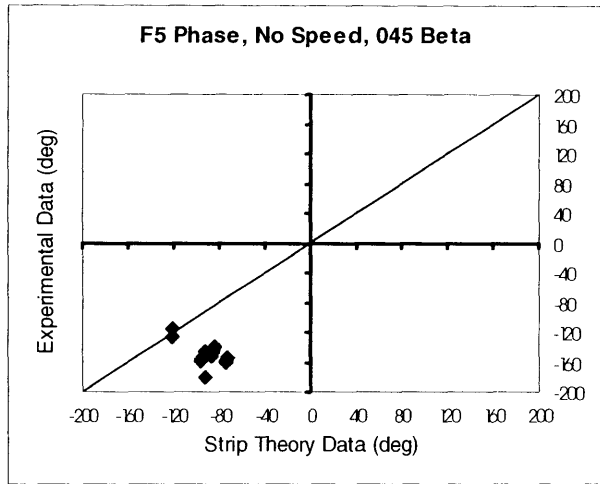
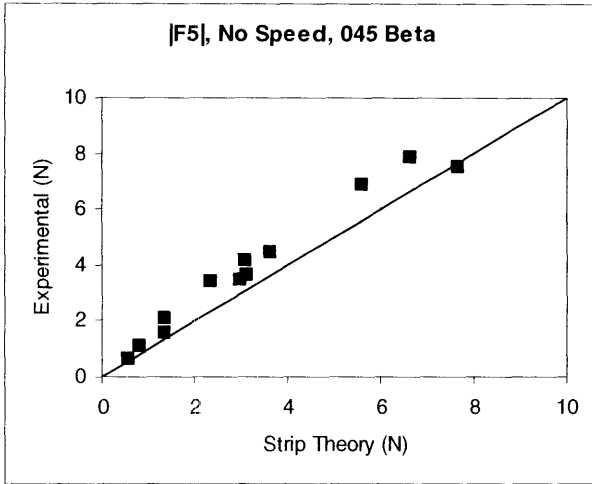


Figure 53 Experiment v STC F5 Data, 045 Beta

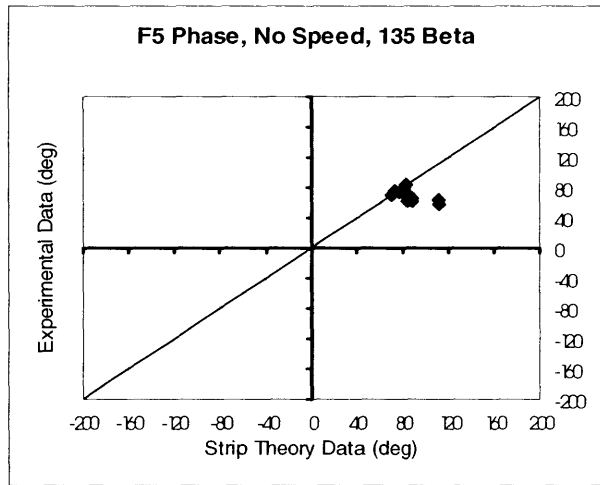
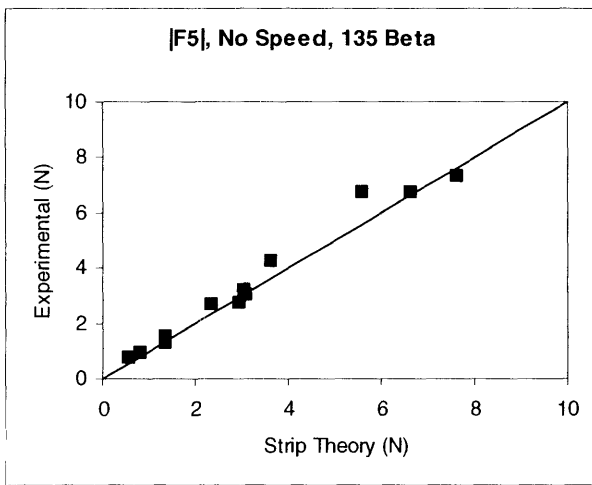


Figure 54 Experiment v STC, F5 Data, 135 Beta

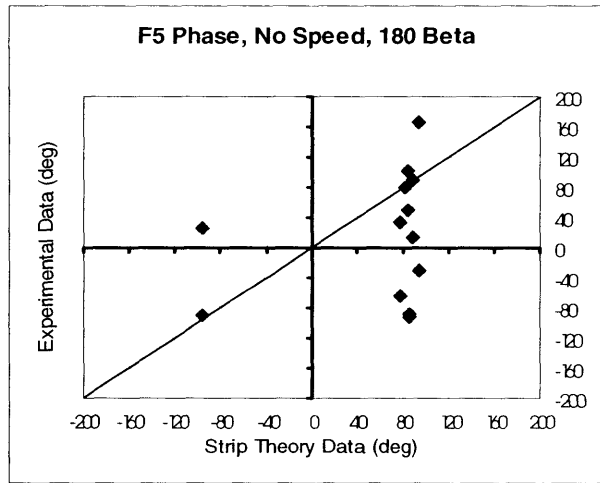
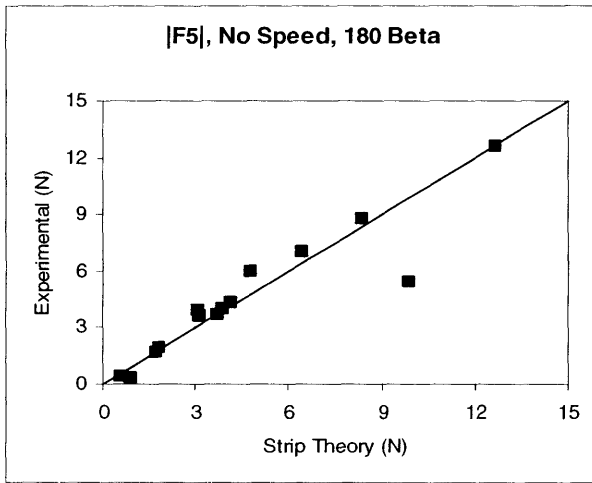


Figure 55 Experiment v STC F5 Data, 180 Beta

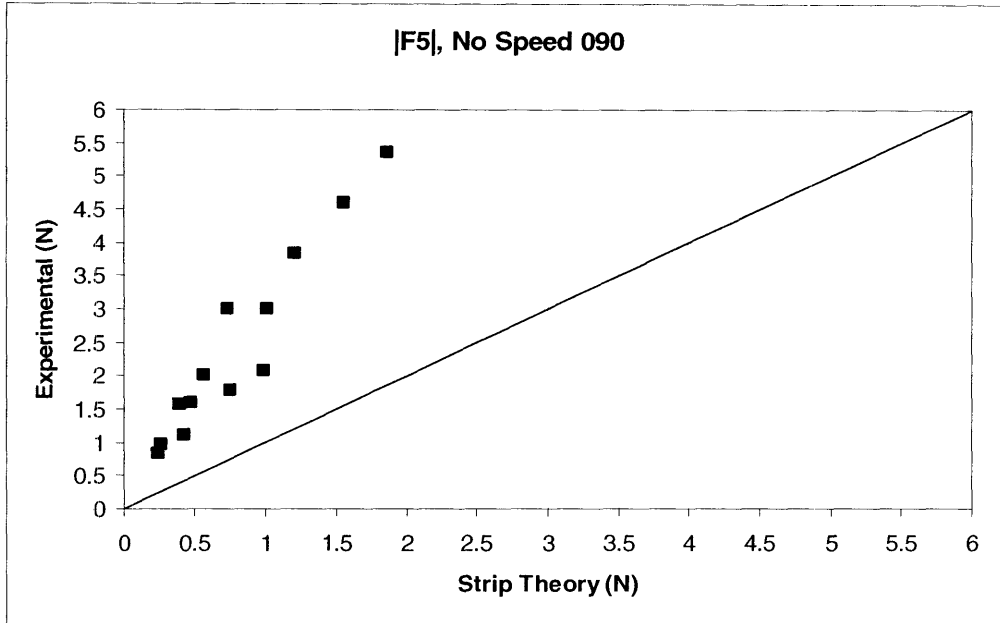


Figure 56 Experimental v STC, |F5|, 090 Beta

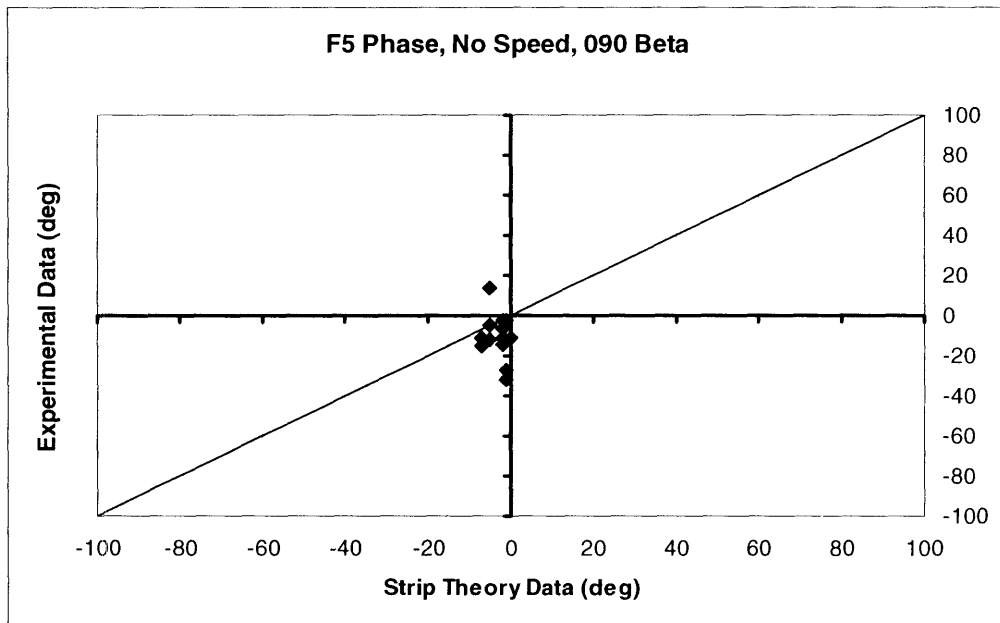


Figure 57 Experiment v STC, F5 Phase, 090 Beta

As shown in Figures 56, and 57 above and in Figures 64 and 65 below, there is a continuing problem in modeling moment data for data runs with beam seas. In this case the experimental data is considerably lower in magnitude than the STC data. As noted before, in cases of beam seas the pitch and moment data is quite small in magnitude for the REMUS AUV and consequently the actual scale of the data comparison is not that large but represents a large percent difference. This magnitude of the difference argument explains the error in representing moments for beam sea conditions to a small extent but does not fully explain the phenomenon.

From all three comparisons it is shown that WAMIT underestimates the moment data in comparison to both experiment and STC data while the STC moment data is larger than that of experiment and WAMIT. With all three data sets showing inconsistent differences in the moment data it is not possible to even suggest which data set is the closest to the true excitation moment on the body.

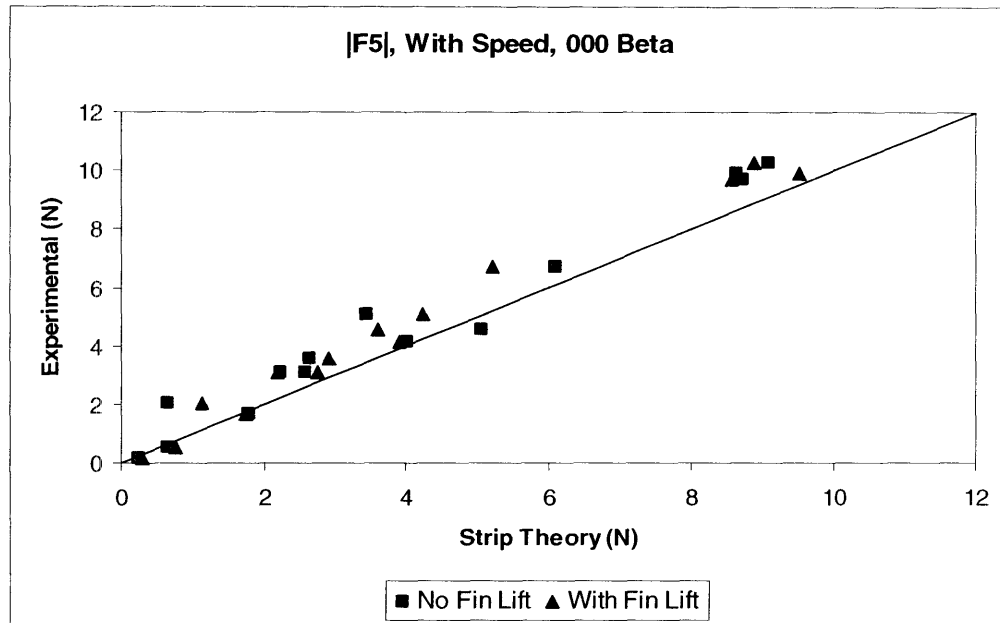


Figure 58 Experiment v STC, |F5| with Speed, 000 Beta

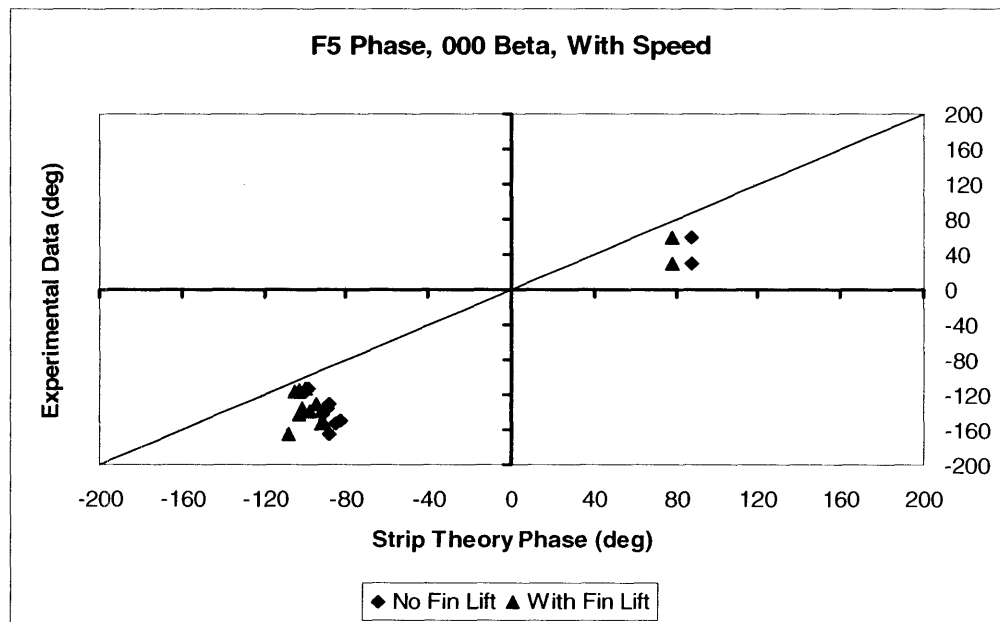


Figure 59 Experiment v STC F5 Phase with Speed, 000 Beta

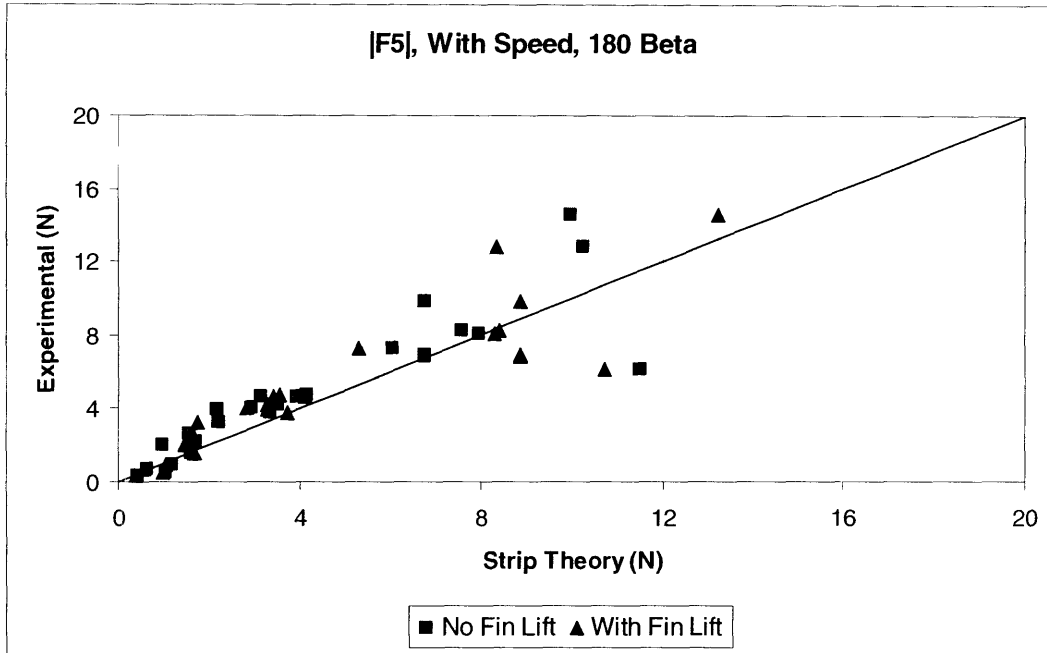


Figure 60 Experimental v STC, |F5] with Speed, 180 Beta

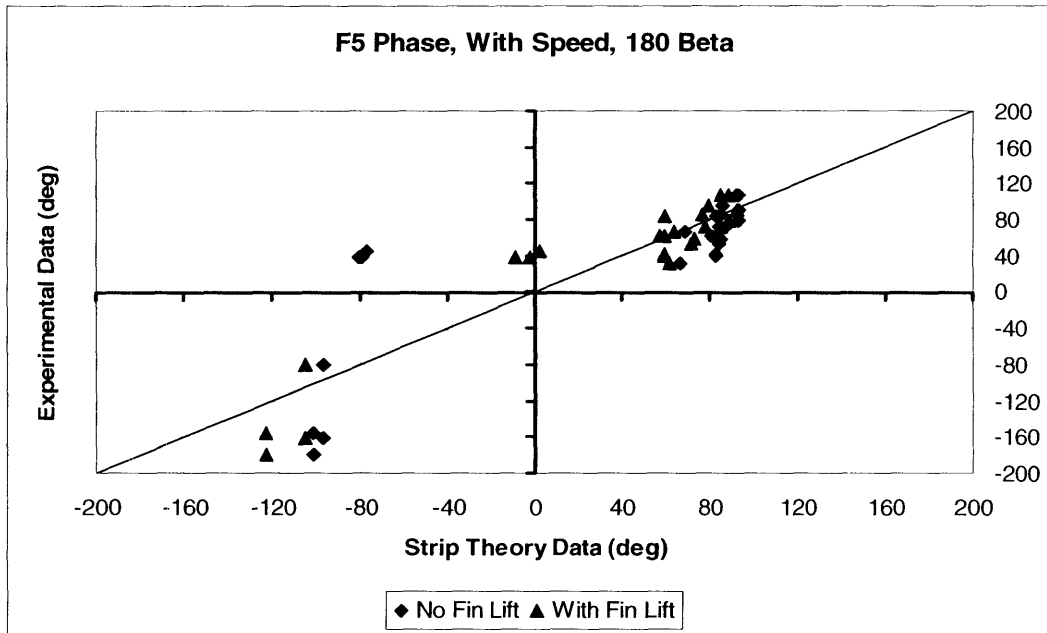


Figure 61 Experiment v STC F5 Phase with Speed, 180 Beta

As is the heave force representation the pitch data for experiments with speed are presented in larger format to better show the difference between STC data with and without fin lift effects. In general the trends for pitch moment in cases with speed show a strong trend of good comparison between experiment and STC. In all but one noticeable case the addition of fin lift effects creates a more accurate moment result in the STC.

The yaw data comparison is shown in Figures 62 through 65 and again, the data shows similar trends to the force and moment models above.

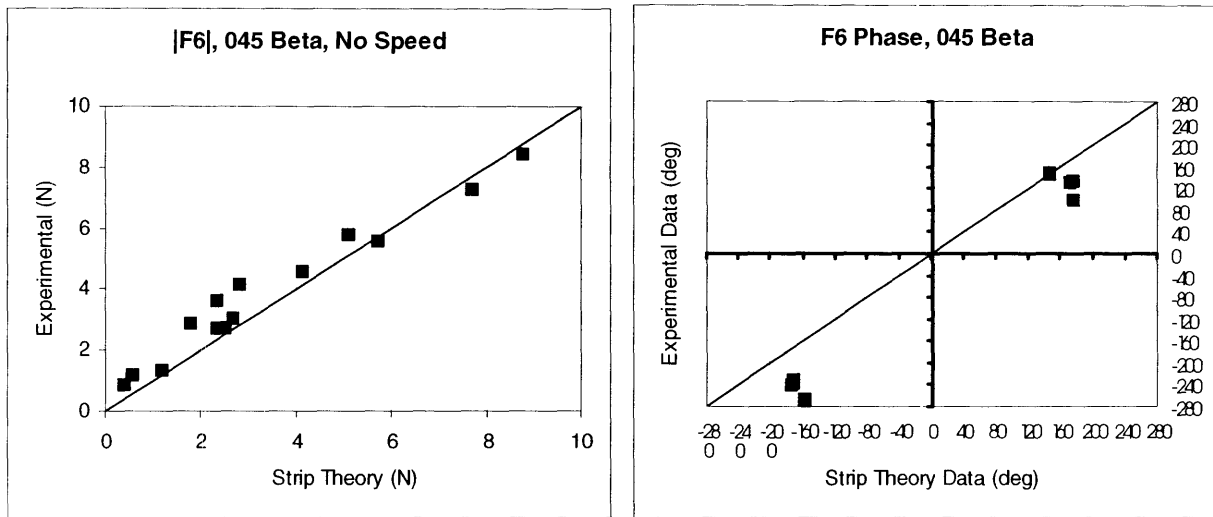


Figure 62 Experiment v STC F6 Data, 045 Beta

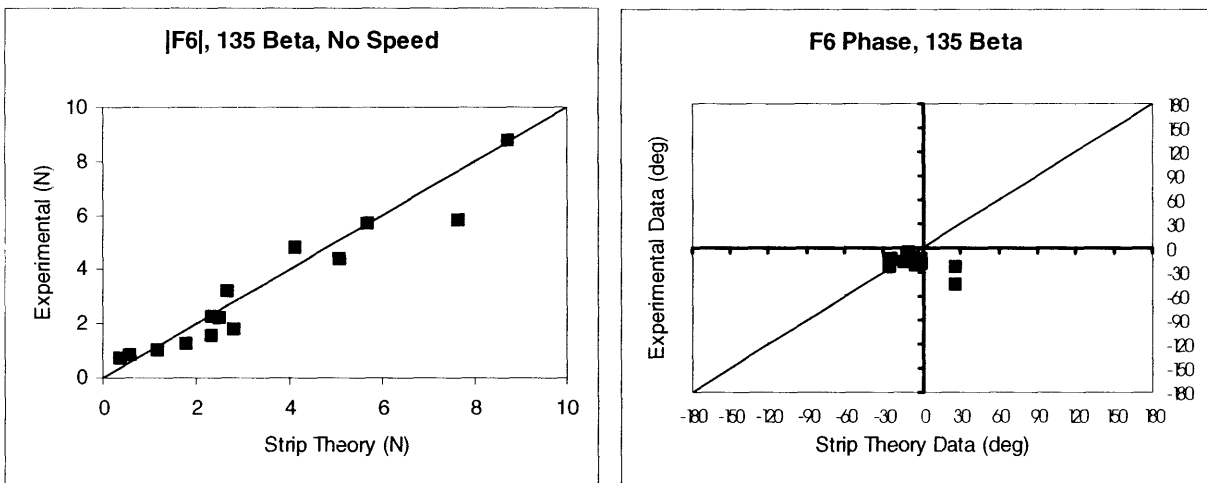


Figure 63 Experiment v STC F6 Data, 135 Beta

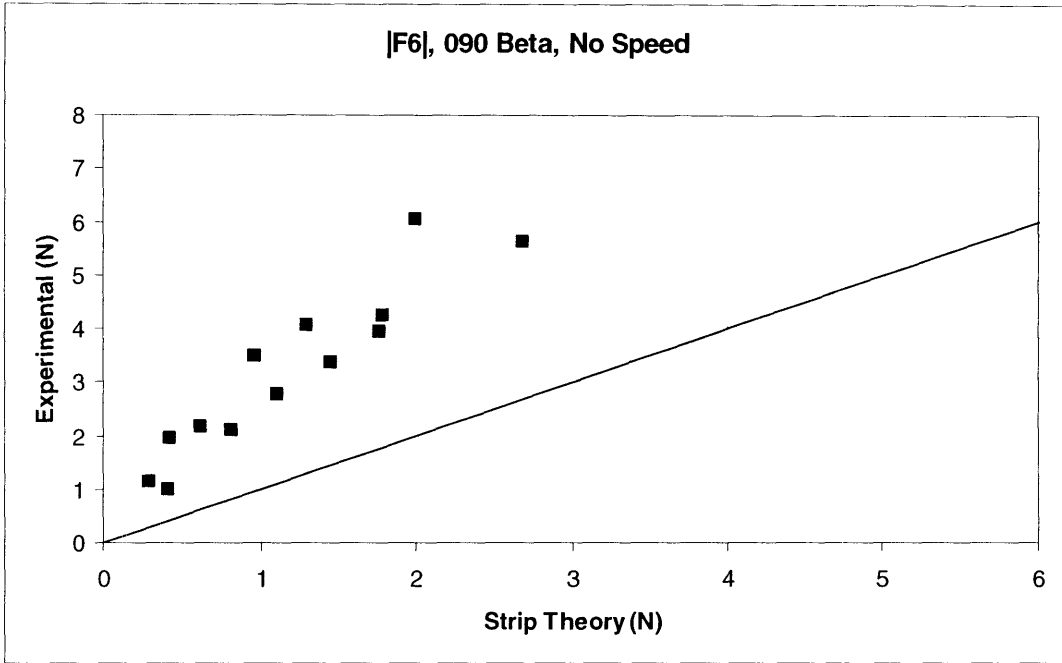


Figure 64 Experimental v STC, |F6], 090 Beta

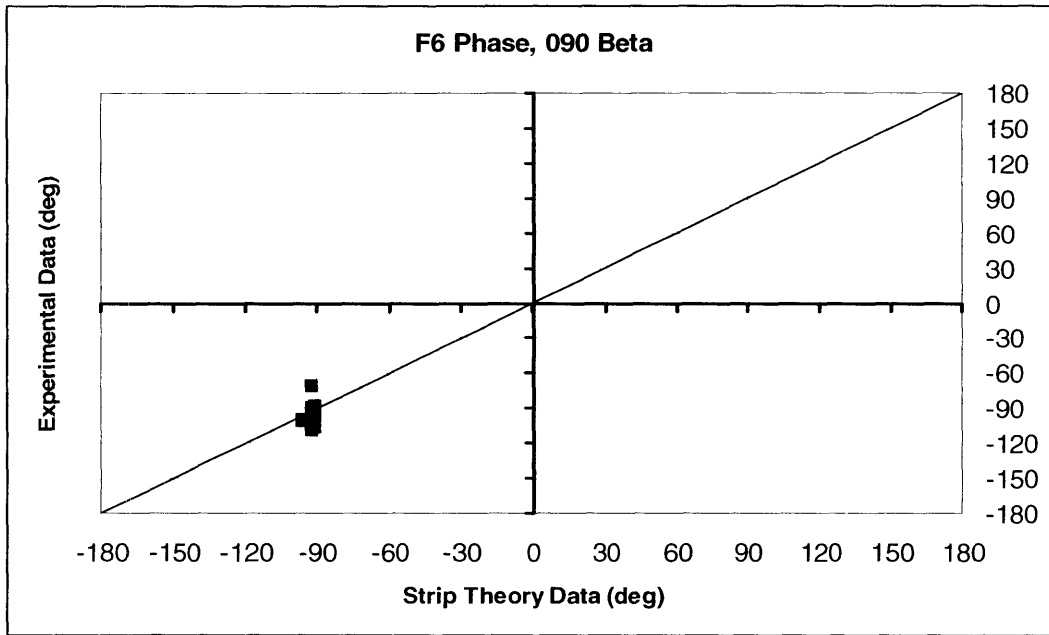


Figure 65 Experiment v STC F6 Phase, 090 Beta

The overall results of the comparison between the Naval Academy experiments and the Strip Theory Code show that the STC is a reasonable approximation of the force on the REMUS AUV. The inconsistency in modeling moments for cases with beam seas is of minor consequence in that the magnitude of the excitation moments on the body are relatively small and it is quite possible that the experimental data is not correct for these cases. The difficulty in modeling the phase data is explained by errors in the data acquisition for the experiments in question. Also, the close correlation between WAMIT and STC phase data lends a strong credibility to the accuracy of the Strip Theory Codes phase output.

Chapter 8: Conclusions

8.1 Summary and Conclusions

The completion time of this thesis was largely devoted to finding bugs in the Strip Theory Code and errors in the code, experimental, and WAMIT data. As discussed in Appendix A, there was a large portion of time dedicated to the determination of when and where to use base frequency as opposed to encounter frequency in the solution of the STC. Time sinks of this nature and do not make them selves apparent in this report as only the final version of the STC considered needs to be verified and checked versus other known solutions to the problem. As such, the largest conclusion to this project is the completed and reliable version of the code residing safely in Appendix B of this report.

The output of that code adequately models the wave forces and moments on a submerged vessel in shallow water. The reliability and accuracy of the STC is evident from the comparison of its outputs to known experimental data and WAMIT output. Additionally, the code can be used to determine the vehicles hydrodynamic characteristics which efficiently enable the user to determine vehicle motions in a wide range of sea conditions.

As part of the development of this code it was determined that the three dimensional fin effects, meaning the flow around the leading and trailing edges of the control fins, has little effect on added mass for the total vehicle. Meaning that the fin can be modeled as just part of the cross section of the AUV and the only additional force correction required is the calculation of fin lift force, which is created by circulation.

Also, it was determined that the domain sizing for the solution to Green's theorem for each cross section is not dependent on the wave conditions causing the flow around the body, but is dependent on submergence and presumably vehicle size. Also the panel size along the boundaries of the two dimensional domain only has impact on the solution in some circumstances and on average a panel size of less than 25cm's provides a predictable and stable solution.

There is some question as to the validity of the Strip Theory Code for determining pitch and yaw moments when the vehicle in question is in beam seas. Still, for almost every other test condition the STC outputs a reasonably accurate approximation for the forces and moments on the body. It is especially remarkable that the code provides such remarkably accurate results with such a simplistic set of input arguments for vehicle geometry. This reasonably accurate code is a large step in the development of AUV's which are highly capable in operating in shallow water.

8.2 Future Work

Due to time constraints in the completion of this thesis there are several areas of this subject which were not developed enough for complete satisfaction. The difficulties in determining conclusive and broadly applicable domain sizing for the Strip Theory Code was discussed in Chapter 5. As mentioned in that Chapter, further convergence studies should be conducted for different vehicles prior to using the STC to model those vehicles.

Additionally, the code should be amended to apply the output values of the code to determine the response amplitude operators for the system which it is being used to model. This was one of the intentions of this thesis but was not addressed due to time limitations. However, the general coupled linearized equations of motion were synthesized to determine the equations for sway, heave, pitch and yaw motion due to force and hydrodynamic input. The general linear equations of motion is equal to the real part of the following:

$$F_2 e^{i\omega t} = (M + A_{22}) \overset{\#}{\eta}_2 + A_{26} \overset{\#}{\eta}_6 + B_{22} \overset{g}{\eta}_2 + B_{26} \overset{g}{\eta}_6 + C_{26} \eta_6 \quad (5.3)$$

$$F_3 e^{i\omega t} = (M + A_{33}) \overset{\#}{\eta}_3 + A_{35} \overset{\#}{\eta}_5 + B_{33} \overset{g}{\eta}_3 + B_{35} \overset{g}{\eta}_5 + C_{35} \eta_5 \quad (5.4)$$

$$F_5 e^{i\omega t} = (I_5 + A_{55}) \overset{\#}{\eta}_5 + A_{53} \overset{\#}{\eta}_3 + B_{55} \overset{g}{\eta}_5 + B_{53} \overset{g}{\eta}_3 + C_{55} \eta_5 \quad (5.5)$$

$$F_6 e^{i\omega t} = (I_6 + A_{66}) \overset{\#}{\eta}_6 + A_{62} \overset{\#}{\eta}_2 + B_{62} \overset{g}{\eta}_2 + B_{66} \overset{g}{\eta}_6 + C_{66} \eta_6 \quad (5.6)$$

where $\eta_i = \eta_i e^{i\omega t}$. Solving for each η_i gives:

$$\eta_2 = \frac{F_2(-\omega^2(I_6 + A_{66}) + i\omega B_{66} + C_{66}) - F_6(-\omega^2 A_{26} + i\omega B_{26} + C_{26})}{(-\omega^2(M + A_{22}) + i\omega B_{22})(-\omega^2(I_6 + A_{66}) + i\omega B_{66} + C_{66}) - (-\omega^2 A_{26} + i\omega B_{26} + C_{26})(-\omega^2 A_{62} + i\omega B_{62})} \quad (5.7)$$

$$\eta_3 = \frac{F_3(-\omega^2(I_5 + A_{55}) + i\omega B_{55} + C_{55}) - F_5(-\omega^2 A_{35} + i\omega B_{35} + C_{35})}{(-\omega^2(M + A_{33}) + i\omega B_{33})(-\omega^2(I_5 + A_{55}) + i\omega B_{55} + C_{55}) - (-\omega^2 A_{35} + i\omega B_{35} + C_{35})(-\omega^2 A_{53} + i\omega B_{53})} \quad (5.8)$$

$$\eta_5 = \frac{F_5(-\omega^2(M + A_{33}) + i\omega B_{33}) - F_3(-\omega^2 A_{53} + i\omega B_{53})}{(-\omega^2(M + A_{33}) + i\omega B_{33})(-\omega^2(I_5 + A_{55}) + i\omega B_{55} + C_{55}) - (-\omega^2 A_{35} + i\omega B_{35} + C_{35})(-\omega^2 A_{53} + i\omega B_{53})} \quad (5.9)$$

$$\eta_6 = \frac{F_6(-\omega^2(M + A_{22}) + i\omega B_{22}) - F_2(-\omega^2 A_{62} + i\omega B_{62})}{(-\omega^2(M + A_{22}) + i\omega B_{22})(-\omega^2(I_6 + A_{66}) + i\omega B_{66} + C_{66}) - (-\omega^2 A_{26} + i\omega B_{26} + C_{26})(-\omega^2 A_{62} + i\omega B_{62})} \quad (5.10)$$

Using the output for the diffraction and radiation forms of the STC in equations 8.5 through 8.8 will give motion values for the AUV in the given wave conditions. Those motions can be studied to determine the operating limits of the vehicle. Future work in this area will complete the code and provide meaningful results which can later be incorporated into a control system design.

Appendix A: Development of the Strip Theory

STRIP THEORY FOR UNDERWATER VEHICLES IN WATER OF FINITE DEPTH by: JEROME H. MILGRAM

Introduction

Strip theory of ship motions, as it is normally used, is mathematically inconsistent approximation in the sense that some terms of various orders in beam/length are retained and others are absent. The principal justification for its use has been that it gives estimates for seakeeping motions and structural loads in ships of satisfactory engineering accuracy. Likewise, it is the comparison between theory and experiment that justifies use of strip theory for underwater vehicles, even in ranges of wavelength/vehicle length that are not fully justified mathematically. Furthermore, Ogilvie and Tuck (1969) have developed a strip theory including all terms of leading order in beam/length and found that the normally omitted terms are negligible. Descriptions of the background of Strip Theory are provided by Newman (1977- Chapter 7) and in the paper: "Ship Motions and Sea Loads" (Salvesen, Tuck and Faltinsen, 1970), who also developed a thorough formulation of the theory, hereinafter referred to as STF. For the past 35 years, STF has been one of the most widely used strip theories.

The theory is the modified form of STF. The modifications used here are:

1. The vehicle is submerged,
2. The water depth is finite,
3. The two-dimensional forces of a cross section are computed by an implementation of Green's Theorem,
4. The vehicle is presumed to end in a section having zero crosssectional area so there are no transom corrections,
5. The hydrostatic restoring coefficients are related only to the vertical distance between the center of gravity and the center of buoyancy, with no free surface hydrostatic effects,
6. The forces and moments due to hydrodynamic lift forces on the vehicle fins are included.

The sixth item will be found to be important for three reasons:

- a. The relative fin lift forces in comparison to the remaining forces are larger for a typical underwater vehicle than for a ship because the relative size of the underwater vehicle fins is larger,
- b. For a submerged vehicle, the damping forces due to radiated waves are comparatively smaller than for surface ships.
- c. Due to this fact and item (a) above, the damping of underwater vehicle motions is frequently dominated by fin lift forces and moments.

Since an underwater vehicle does not have the strong hydrostatic spring-like forces associated with a pierced free surface, spring-like forces due to fin lift can be the dominant spring-like forces in the presence of pitch and/or yaw motions which generate angles of attack on the fins.

The same notation for the sectional added mass, damping coefficients and (spring-like) restoring coefficients for the whole vehicle, added mass, damping and wave forces and moments as used

in STF are used here. Indices 1, 2, 3, 4, 5 and 6 refer to surge, sway, heave, roll, heave and yaw respectively, although surge and roll and their influences are neglected here on the presumptions that the vehicle is slender and roll is unimportant for the problems to be solved. a_{ij} and b_{ij} are the added mass and damping coefficients for any given section. i refers to the direction of the associated force and j refers to the direction of the associated motion. pA_{ij} and pB_{ij} are the complete vehicle set of added mass and damping coefficients due to the integrals of sectional effects (These are called A_{ij} and B_{ij} in STF, but the altered notation is used here so the final notations can be identical after the lift forces on the fins are included). Likewise, the total vehicle sectional wave forces resulting from an integral of the wave forces over all cross sections are called pF_i . The sectional added masses and damping coefficients in heave and sway are called a_{33} , b_{33} , a_{22} and b_{22} where the a's are two-dimensional added masses, b's are two dimensional damping coefficients, 2 refers to sway and 3 refers to heave. The complex amplitudes of the wave forces due to integrals of the potential flow sectional wave forces and moments in sway, heave, pitch and yaw are called pF_2 , pF_3 , pF_5 , and pF_6 . Likewise, the related two-dimensional forces on each section are called r_2+h_2 and r_3+h_3 . r refers to Froude-Krylov forces and h refers to diffraction (scattering) forces. The phases of wave forces and moments are with respect to the wave crest at the midship location with a time function $\exp(i\omega t)$. ω is the circular frequency of encounter of the waves on the vehicle moving at speed U . The circular frequency of waves in a fixed coordinate systems is called ω_0 .

Since the vehicle does not pierce the free surface, the only hydrostatic restoring forces are:

$${}_pF_{H4} = {}_pC_{44}\eta_4 \quad \text{and} \quad {}_pF_{H5} = {}_pC_{55}\eta_5, \quad \text{where} \quad {}_pC_{44} = {}_pC_{55} = \rho g V (GB)^2 \quad (\text{A-1})$$

${}_pF_{H4}$ is the hydrostatic roll moment, ${}_pF_{H5}$ is the hydrostatic pitch moment, η_4 is the roll angle, η_5 is the pitch angle, ρ is the water density, g is the acceleration of gravity, V is the vehicle volume, and GB is the vertical distance that the center of buoyancy is above the center of gravity. It is assumed that the weight of the vehicle equals the weight of displaced water.

The contributions to the complete vehicle added mass, damping, and "springlike" restoring coefficients from lift forces on the fins are called ${}_fA_{ij}$, ${}_fB_{ij}$, and, ${}_fC_{ij}$, and the contributions to the complex amplitudes of wave forces and moments due to lift on the fins are called ${}_fF_i$. Thus the total vehicle added masses, damping coefficients, spring constants and wave force complex amplitudes, called A_{ij} , B_{ij} , C_{ij} and F_i , respectively, are given by:

$$A_{ij} = {}_pA_{ij} + {}_fA_{ij}, \quad B_{ij} = {}_pB_{ij} + {}_fB_{ij}, \quad C_{ij} = {}_pC_{ij} + {}_fC_{ij}, \quad F_i = {}_pF_i + {}_fF_i \quad (\text{A-2})$$

Quantities with pre-subscript "p" are called non-lifting contributions. With exceptions a single constant in the ${}_pF_i$'s, they agree with the theory in STF for quantities given there without the pre-subscript, except there are no transom corrections here, and the two-dimensional added masses, damping coefficients and wave force of sections are calculated by a different method.

The quantities with pre-subscript "f" are the sum of contributions from the time-varying lift of all fins on the vehicle. With U being the forward speed of the vehicle, T being the period of vehicle motions and c being a typical fin chord length, the ratio $c/UT \ll 1$ for almost all operational

conditions so that quasi-steady lift calculations for each fin are expected to provide good estimates.

The coordinate system (x,y,z), the definition of unsteady vehicle motions, and the definitions of the submergence, s, and the water depth, h, are shown in Figure A-1. x is forward, y is to port and z is upward. The linear motions in the x, y and z directions are η_1 , η_2 , and η_3 , and the rotational motions about these axes are η_4 , η_5 , and η_6 . Here, only η_3 and η_5 in the vertical plane and η_2 and η_6 in the horizontal plane will be considered. It will be assumed that the vehicle has left-right symmetry leading to decoupling of horizontal plane motions from vertical plane motions and that coupling effects from η_1 and η_4 are negligible.

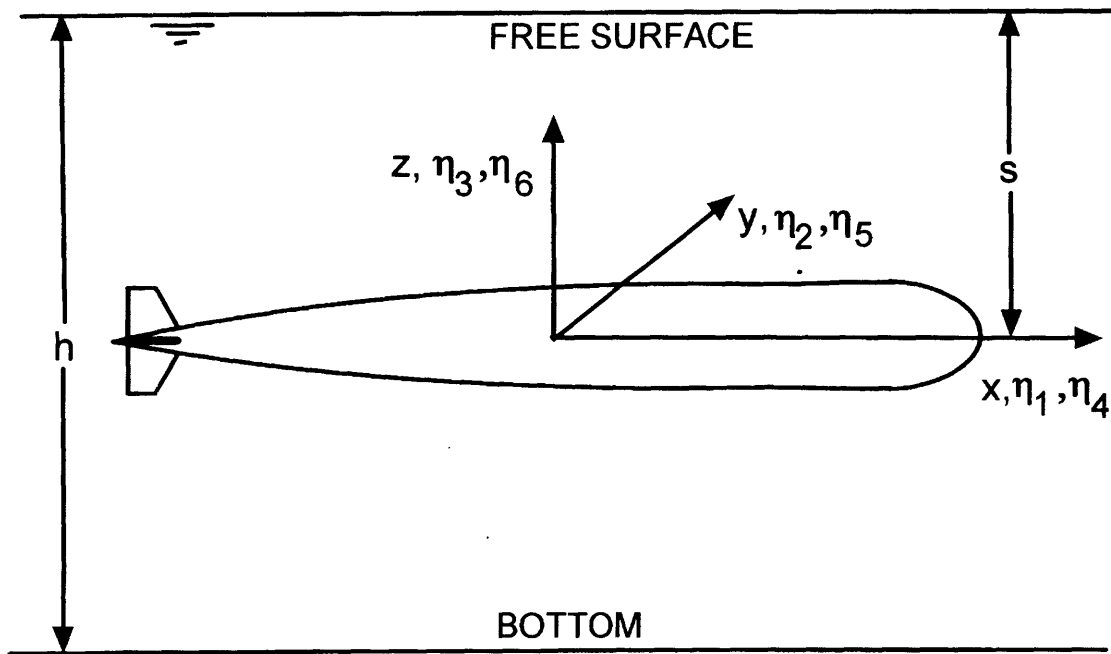


Figure 66 Coordinate and Motion Definitions

Seakeeping Equations of Motion

The forces on the vehicle, both from the sea waves and from the vehicle motions, will be linearized in the wave amplitude and the vehicle motions respectively. Therefore, the response in an arbitrary sea state can be expressed in terms of the response to sinusoidal waves, over ranges of frequency and propagation angles, through the use of Fourier Integrals. This allows the equation of motion to be developed for sinusoidal waves.

The amplitude of any wave is called α and the wave elevation following the propagation angle convention of STF is: $\alpha \cdot e^{(i\alpha x - kx \cos(\theta) + ky \sin(\theta))}$.

In water of depth h, the associated velocity potential is: $\beta \cdot e^{(i\alpha x - kx \cos(\theta) + ky \sin(\theta))} \cdot e^{kz}$

The complete linearized vehicle equations of motion in the presence of sinusoidal waves as given by STF are:

$$\sum_{k=1}^6 [(M_{jk} + A_{jk})\ddot{\eta}_k + B_{jk}\dot{\eta}_k + C_{jk}\eta_k] = F_j \exp(i\omega t) \quad (\text{A-3})$$

where M_{jk} is the 6 x 6 mass matrix of the vehicle, ω is the circular encounter frequency of the waves and t is time. The real part of the equation is the physical result. Since surge and roll motions are neglected in this analysis, and any terms having any subscript equal to 1 or 4 are assumed to be zero.

As in STF, the equations in the vertical and horizontal planes for a vehicle with port-starboard symmetry, and with the center of gravity at $(0,0,z_c)$, are decoupled from each other. The vertical plane equations, as given by STF are:

$$(M + A_{33})\ddot{\eta}_3 + B_{33}\dot{\eta}_3 + A_{35}\ddot{\eta}_5 + B_{35}\dot{\eta}_5 + C_{35}\eta_5 = F_3 \exp(i\omega t) \quad (\text{A-4})$$

$$A_{53}\ddot{\eta}_3 + B_{53}\dot{\eta}_3 + (I_5 + A_{55})\ddot{\eta}_5 + C_{55}\eta_5 = F_5 \exp(i\omega t) \quad (\text{A-5})$$

In equation (A-4), the term involving C_{33} has been omitted since it is zero for underwater vehicles. M is the mass of the vehicle and I_5 is its moment of inertia in pitch.

The horizontal plane equations given by STF, but with effects of surge and roll omitted, and addition of a "springlike" forces due to fin lift forces, are:

$$(A_{22} + M)\ddot{\eta}_2 + B_{22}\dot{\eta}_2 + A_{26}\ddot{\eta}_6 + B_{26}\dot{\eta}_6 + C_{26}\eta_6 = F_2 \exp(i\omega t) \quad (\text{A-6})$$

$$A_{62}\ddot{\eta}_2 + B_{62}\dot{\eta}_2 + (A_{66} + I_6)\ddot{\eta}_6 + B_{66}\dot{\eta}_6 + C_{66}\eta_6 = F_6 \exp(i\omega t) \quad (\text{A-7})$$

I_6 is the vehicle moment of inertia in yaw. To re-iterate, the terms involving C in the above two equations do not normally appear in the seakeeping equations of motion for ships. They appear here as a result of accounting for the lift forces on the fins when the vehicle has a yaw angle and these effects contribute to C_{35} and C_{55} as well. Transverse velocities on fins when the vehicle has forward speed contribute to the wave forces (F 's) and to the damping coefficients (B 's).

The fluid mechanics part of problem is determination of the A 's, B 's, C 's and F 's. This is done by finding the terms that are not due to fin lift forces, as formulated in STF, except the sectional strip forces are calculated differently, and then calculating the terms due to lift forces.

Added Mass , Damping , and Wave Force Coefficients due to non-Lifting Effects

As given in STF, and assuming the submerged vehicle ends in a section of zero area at the stern,

$${}_p A_{33} = \int a_{33} d\xi \quad (\text{A-8}) \quad {}_p B_{33} = \int b_{33} d\xi \quad (\text{A-9})$$

$${}_p A_{35} = -\int \xi a_{33} d\xi - \frac{U}{\omega^2} B_{33} \quad (\text{A-10}) \quad {}_p B_{35} = -\int \xi b_{33} d\xi + U A_{33} \quad (\text{A-11})$$

$${}_p A_{53} = -\int \xi a_{33} d\xi - \frac{U}{\omega^2} B_{33} \quad (\text{A-12})$$

$${}_p B_{53} = -\int \xi b_{33} d\xi - U A_{33} \quad (\text{A-13})$$

$${}_p A_{55} = \int \xi^2 a_{33} d\xi + \frac{U^2}{\omega^2} A_{33} \quad (\text{A-14})$$

$${}_p B_{55} = \int \xi^2 b_{33} d\xi + \frac{U^2}{\omega^2} B_{33} \quad (\text{A-15})$$

$${}_p A_{22} = \int a_{22} d\xi \quad (\text{A-16})$$

$${}_p B_{22} = \int b_{22} d\xi \quad (\text{A-17})$$

$${}_p A_{26} = \int \xi a_{22} d\xi + \frac{U}{\omega^2} B_{22} \quad (\text{A-18})$$

$${}_p B_{26} = \int \xi b_{22} d\xi - U A_{22} \quad (\text{A-19})$$

$${}_p A_{62} = \int \xi a_{22} d\xi + \frac{U}{\omega^2} B_{22} \quad (\text{A-20})$$

$${}_p B_{62} = \int \xi b_{22} d\xi + U A_{22} \quad (\text{A-21})$$

$${}_p A_{66} = \int \xi^2 a_{22} d\xi + \frac{U^2}{\omega^2} A_{22} \quad (\text{A-22})$$

$${}_p B_{66} = \int \xi^2 b_{22} d\xi + \frac{U^2}{\omega^2} B_{22} \quad (\text{A-23})$$

$${}_p F_3 = \rho \alpha \int (f_3 + h_3) d\xi \quad (\text{A-24})$$

$${}_p F_5 = -\rho \alpha \int \left[\xi (f_3 + h_3) + \frac{U}{i\omega} h_3 \right] d\xi \quad (\text{A-25})$$

$${}_p F_2 = \rho \alpha \int (f_2 + h_2) d\xi \quad (\text{A-26})$$

$${}_p F_6 = -\rho \alpha \int \left[\xi (f_2 + h_2) + \frac{U}{i\omega} h_2 \right] d\xi \quad (\text{A-27})$$

The integrals are over the length of the vehicle. The f-terms are Froude-Krylov wave forces, and the h-terms are wave forces due to the diffracted waves.

The wave excitation force (complex) amplitudes from non-lifting effects are derived by STF in terms of integrals over the length of the vehicle of the sectional Froude-Krylov forces, (f_2 and f_3 in sway and heave respectively), and integrals of the sectional diffraction forces, (h_2 and h_3 in sway and heave respectively). The Froude-Krylov forces are due to the pressure distributions in the incident wave and the diffraction forces are associated with the diffracted wave generated because the incident wave orbital velocities are not normal to the surface of the vehicle. The sectional forces are the two-dimensional forces, per unit length for a shape equal to the cross section of the vehicle at each longitudinal location. The way the Froude-Krylov sectional forces will be computed here are the same as done in STF, except that the finite depth wave pressures are used here whereas STF used the infinite depth pressures. Contrary to the methods used in STF, here a_{22} , b_{22} , a_{33} , b_{33} , h_2 , and h_3 are determined by solving two-dimensional Green's theorem formulations.

Boundary Conditions on the Sections

A typical section for which the two-dimensional velocity potential and subsequently the pressure forces is to be computed is shown in figure A-2. It is a cross section of an AUV with a circular section hull and a sonar transducer on each side. The computational domain surrounds the cross section by the free surface on which the free surface boundary condition applies, the bottom on which the boundary condition is zero normal velocity, and the two sides which are taken far enough from the vehicle for the vehicle-generated waves to be outgoing. The linearized boundary conditions for this situation are shown in the figure. The boundary conditions on the cross section depend on the problem to be solved.

For the heave radiation problem with unit velocity amplitude in heave, the normal derivative of the radiation potential on the surface of the cross section is:

$$d\phi/dn = \hat{k}\bar{g}\bar{n}, \text{ where } \hat{k} \text{ is the unit vector in the } z \text{ (upward) direction.}$$

For the sway radiation problem with unit velocity amplitude in sway,

$$d\phi/dn = \hat{j}\bar{g}\bar{n}, \text{ where } \hat{j} \text{ is the unit vector in the } y \text{ (to port) direction.}$$

For the diffraction problem in sinusoidal waves, $d\phi/dn$ on the cross section is the negative of the normal velocity distribution imposed by the wave field.

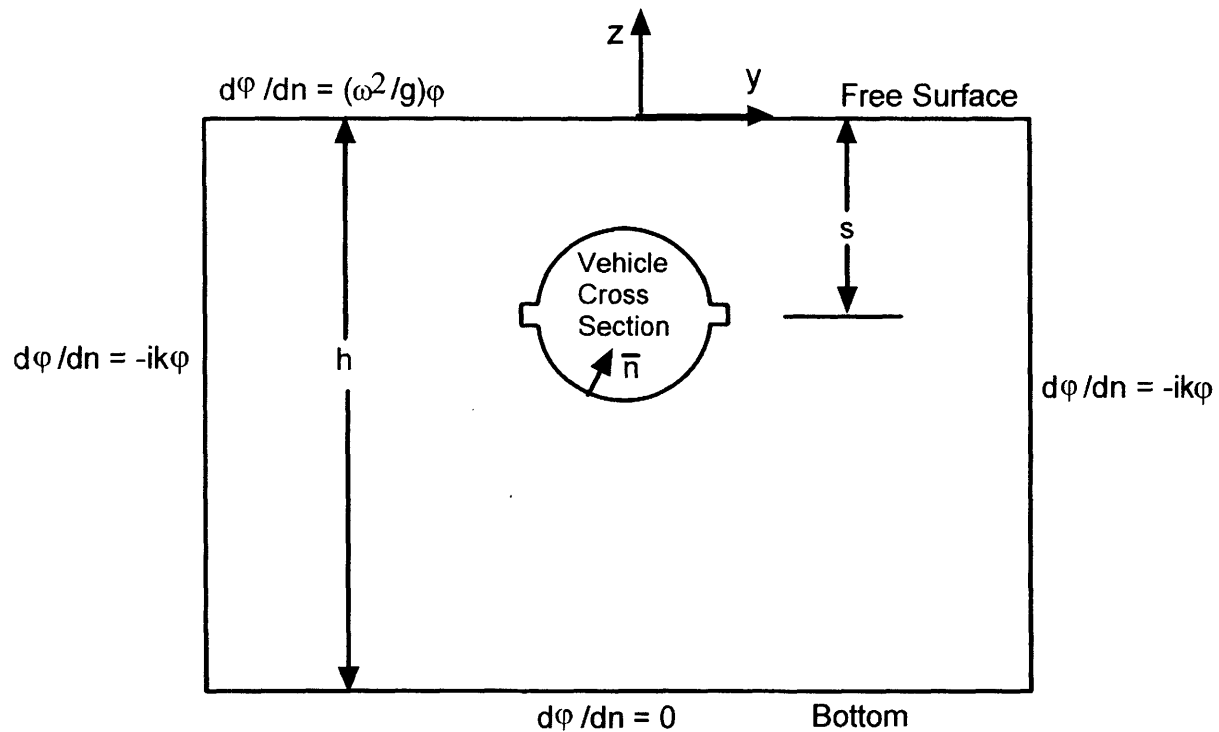


Figure 67 Cross Section of an Underwater Vehicle in a Two-Dimensional Computation Domain, Viewed from Forward, Looking aft

With reference to Figure 2, it has been shown by STF, Newman (1977) and others, that for the radiation problem, the circular frequency in the free surface boundary condition should be the encounter frequency of the vehicle in the waves. However, for the wave diffraction problem, the circular frequency used in solving the potential should be the base wave frequency, ω_0 . The wavenumber, k , that appears in the outgoing wave radiation conditions on the sides of the domain are related to the frequency used in the free surface boundary condition by the finite depth dispersion relation:

$$\omega^2 = gk \tanh kh \tag{A-28}$$

Calculation of Non-Lifting Two Dimensional Forces on The Sections

With the boundary conditions specified on a section and the rectangular boundary surrounding it, Green's theorem can be used to determine the two-dimensional velocity potential and the associated forces. The Green function $G(y,z,\eta,\zeta)$ depends on the field point (y,z) and the source point (η,ζ) through the distance between them, $r = [(y-\eta)^2 + (z-\zeta)^2]^{1/2}$ and G is the sink potential,

$$G = -\ln r \quad (\text{A-29})$$

The two-dimensional Green's theorem takes the form:

$$\left[\int_S \phi(\eta,\zeta) \frac{\partial G}{\partial n(\eta,\zeta)} - G \frac{\partial \phi(\eta,\zeta)}{\partial n(\eta,\zeta)} \right] ds = \begin{cases} 0, & (y,z) \text{ outside } S \\ -\pi\phi(y,z), & \text{on } S \\ -2\pi\phi(y,z), & \text{inside } S \end{cases} \quad (\text{A-30})$$

n is the normal vector drawn out of the fluid on all boundaries. S represents the surface area of all boundaries which is a set of lines in this two-dimensional problem and ds , the element of surface area is the element of arc length on the boundaries in the two-dimensional problem. In all cases, ϕ is appended by $\exp(i\omega t)$ which is omitted for clarity. In general, ϕ is complex and the real part of $\phi \exp(i\omega t)$ is the physical quantity.

As shown in Figure 2 and described in the text below it, $\partial\phi/\partial n$ is known on all boundaries for the radiation problems in heave and sway and in the diffraction problem of waves on the surface. Thus, the unknown becomes the values of ϕ over all boundaries; the cross section and the surrounding rectangle. Whereas the imposed heave or sway velocities are the same for all sections of the vehicle, the imposed wave velocities in the diffraction problem vary, not only around the section, but also between sections according too the wavelength and propagation angle of the wave. Zero phase of the wave is taken when the wave crest is over the center of the vehicle.

To solve equation (A-30) numerically, all the boundaries are divided into panels and in this work, flat panels (lines) with constant potential strength on each panel is used. In this form, the resulting two-dimensional panel method becomes a set of linear equations with the number of equations and number of unknown potential strengths equal to the number of panels.

Determination of the two-dimensional velocity potential by use of Green's theoerm is quite different than the procedure used by STF and described by Newman (1977) , but is far more general for any sectional shapes.

Forces on the Sections

To use equations (A-8) through (A-27) the zero forward speed forces on each section must be known. As described in STF, and using the slender body approximation, the required radiation forces on each section are determined by:

$$t_{jj} = -\rho i \omega \int_{C_x} n_j \phi_j dl \quad \text{where } j = 2 \text{ for sway and } j = 3 \text{ for heave} \quad (\text{A-31})$$

$$t_{jj} = \omega^2 a_{jj} - i\omega b_{jj}, \quad j = 2, 3$$

Cx is the contour around a section and ρ is the fluid density. (A-31) is simply the pressure force associated with the rate of change of the velocity potential integrated around the section. The component opposed to the acceleration is due to the added mass and the component opposed to the velocity is the damping related to the energy in the outgoing waves produced when the vehicle oscillates at the wave encounter frequency which drives the vehicle motion.. The total added mass and damping for the entire vehicle are given by the integrals of the sectional force over the vehicle length shown in equations (A-8) through (A-23). Those equations also include the leading order terms in the pressure due to the velocity as prescribed by Bernoulli's equation.

The excitation forces from the waves on each section are f_2 and f_3 for the Froude Krylov forces due to the pressure distribution in incident wave, and h_2 and h_3 due to the pressure distribution in the diffracted wave.

Equation (A-26) and (A-27) include the leading order velocity terms for the pressure in Bernoulli's equation.

The diffraction force on each section is called h_j , $j=1..6$. As shown in equations (A-24) and (A-25), $h_3(\xi)$ is required to determine ${}_pF_3$ and ${}_pF_5$. ξ is the longitudinal coordinate along the vehicle. Similarly, according to equations (A-26) and (A-27) $h_2(\xi)$ is needed to determine ${}_pF_2$ and ${}_pF_6$. ϕ_d is the diffraction potential needed to have zero normal flow through any crosssection in the presence of sea waves. The solution for the diffraction potential by use of the panel method resulting from the discretized form of Green's theorem is general and applicable to any submerged crosssectional shape. Although, as shown by Newman (1977) the appropriate free surface boundary condition is based on the wave frequency in a fixed coordinate system, and that has been used here, in a reference frame attached to the vehicle the frequency of the diffraction potential is the encounter frequency.

$$h_2 = \int_{Cx} \hat{j} \bar{g} p_d dl, \quad h_3 = \int_{Cx} \hat{k} \bar{g} p_d dl \quad (A-32 \text{ a,b})$$

\hat{j} and \hat{k} are unit vectors in the y and z directions respectively and p_d is the pressure distribution on the surface of the section due to the diffraction potential. Identical expressions apply for the sectional Froude Krylov Forces, f_2 and f_3 , when p_d is replaced by the incident wave pressure distribution.

Because the sectional diffraction potential has a time variation of $\exp(i\omega t)$, the correct two dimensional pressure distribution on a section is:

$$p_d \equiv p = -i\rho\omega\phi_d \quad (A-33)$$

However, since the diffraction potential is derived using a free surface boundary condition based on the fixed frame circular frequency, ω_o , one might conclude that the two dimensional section pressure should be:

$$p_d \equiv p_o = -i\rho\omega_o\phi_d \quad (A-34)$$

where ω_o is the fixed frame circular frequency

Figure 3 shows the magnitudes of the experimental heave force vs the theoretical heave force according to equations (A-24 and A-2) for the whole vehicle based on pressures using the encounter frequency, ω (eq. A-33) and Figure 4 shows the experimental vs theoretical heave force magnitudes based on pressures using the fixed coordinate frequency, ω_o (eq. A-34). Perfect correlation would have equal values of theory and experiment designated by the straight lines in the figures. The theoretical results include the lifting forces which are described subsequently.

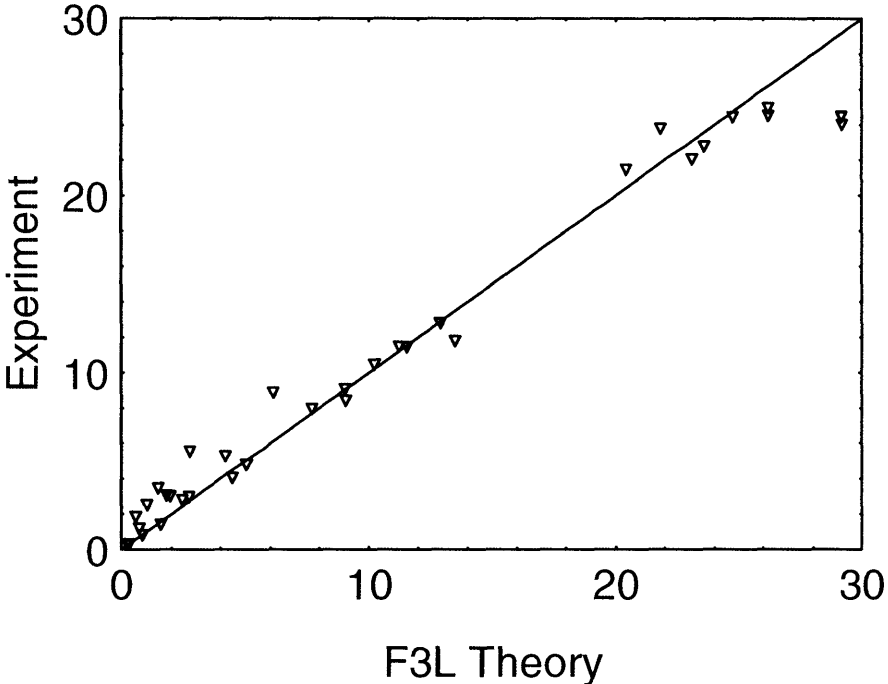


Figure 68 Experiment v Theory for Amplitude of Heave Force with Theoretical Section Pressure base on Encounter Frequency, ω , Equation (A-33).

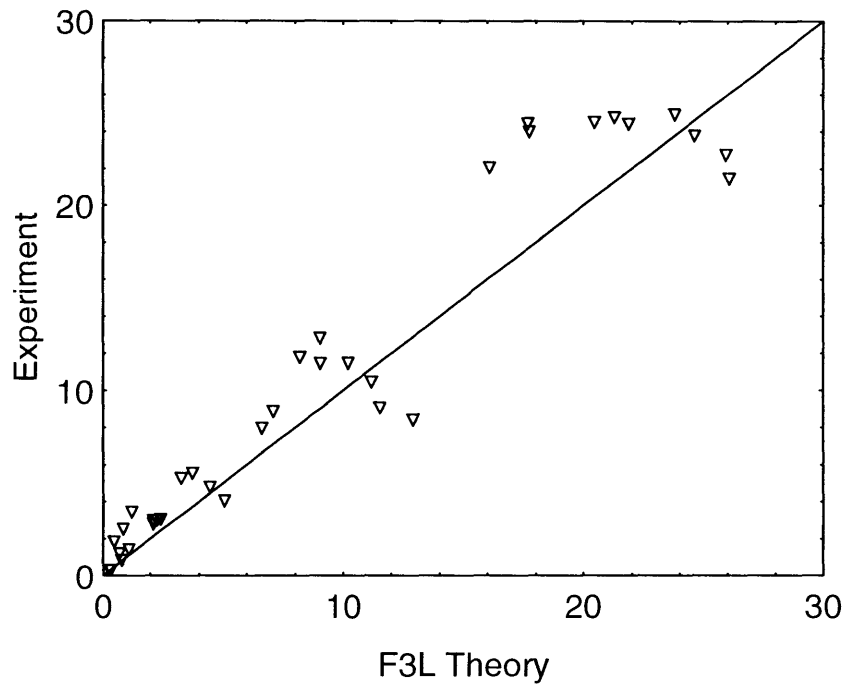


Figure 69 Experiment v Theory for Amplitude of Heave Force with Theoretical Section Pressure based on Fixed Frame Frequency, ω_0 , Equation (A-34).

Figures ### and ### show the comparisons between theory and experiment for the pitch moment according to equations (A-25 and A-2) using pressures bases on ω and ω_0 respectively.

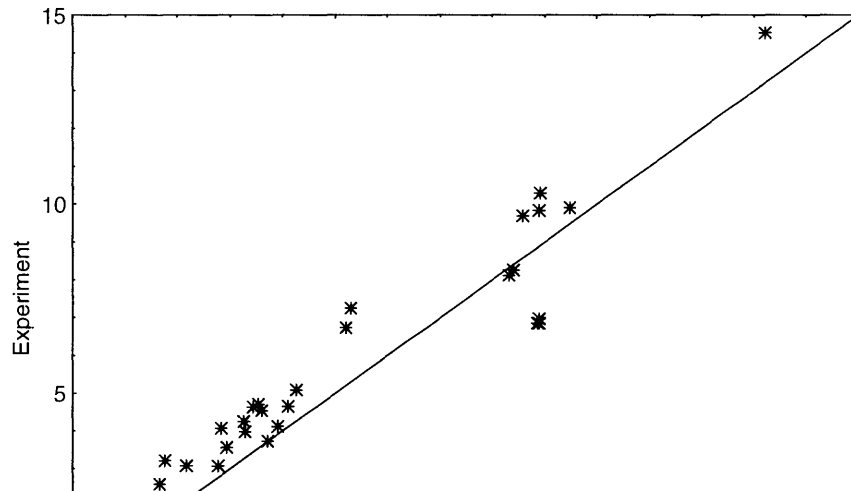


Figure 70 Experiment v Theory for Amplitude of Pitch Moment with Theoretical Section Pressure based on Fixed Frame Frequency, ω , Equation (A-33).

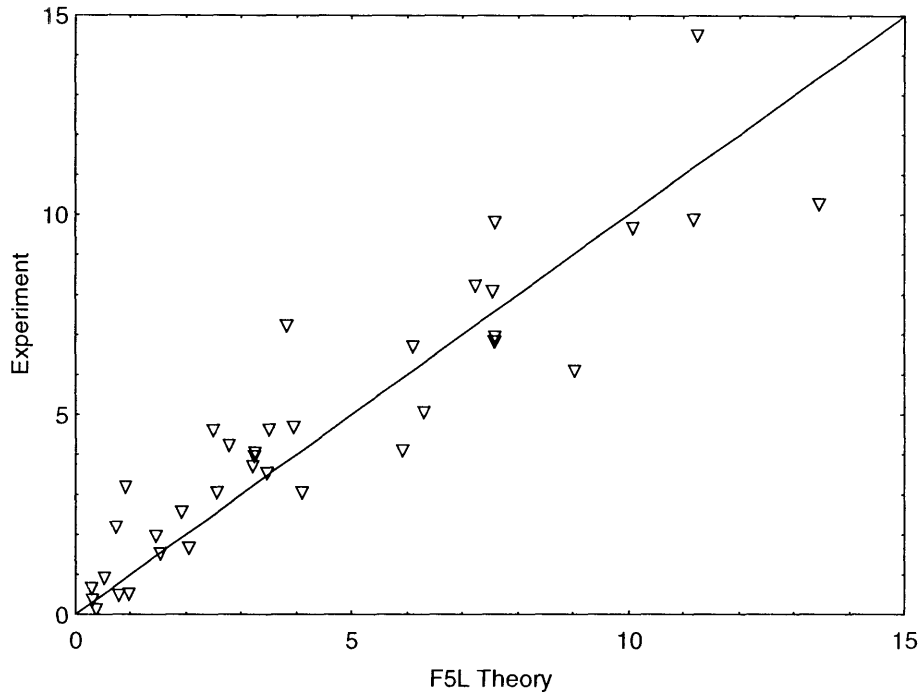


Figure 71 Experiment v Theory for Amplitude of Pitch Moment with Theoretical Section Pressure based on Fixed Frame Frequency, ω_o , Equation (A-34).

Forces and Moments Due to Lift Forces on the Fins

An approximate linearized theory for the lift force on the m 'th fin is:

$$f_m = \frac{1}{2} \rho U^2 A_m \beta_m C_{L\beta m} \quad (A-35)$$

where, A_m is the effective planform area of the fin, β_m is the angle of incidence and $C_{L\beta m}$ is the lift coefficient per unit angle of attack (in radians). The yaw moment from the fin is:

$$M_m = f_m x_m \quad (A-36)$$

x_m is the longitudinal location of the center of lift force of the fin, usually approximated at the quarter chord of the fin.

The linearized angle of incidence is the crossflow, V_m , generated by vehicle motions and sea waves, divided by the forward speed, U , plus the unsteady angle of the vehicle. Thus the equation for the lift force on a single fin becomes:

$$f_m = \frac{1}{2} \rho V_m U A_m C_{L\beta m} + \frac{1}{2} \rho U^2 A_m \beta_{mT} C_{L\beta m} \quad (A-37)$$

β_{mT} is the total vehicle angle, pitch or yaw, which imposes an angle of incidence on the m th fin. The first term in equation (A-37) is proportional to unsteady velocities so it contributes either to wave forces or damping forces, whereas the second term is proportional to unsteady vehicle angles so it contributes to spring constants in the equations of motion.

For any fin, or set of fins, it is necessary to estimate the effective area, A_m , and the center of fin lift force so that x_m can be calculated. The experiments associated with this project were done on a REMUS class vehicle (Von Alt, et al., 1994) which has four identical tail fins in a cruciform shape. Figure 5 shows the vertical planform of the tail fins, and the horizontal planform is identical.

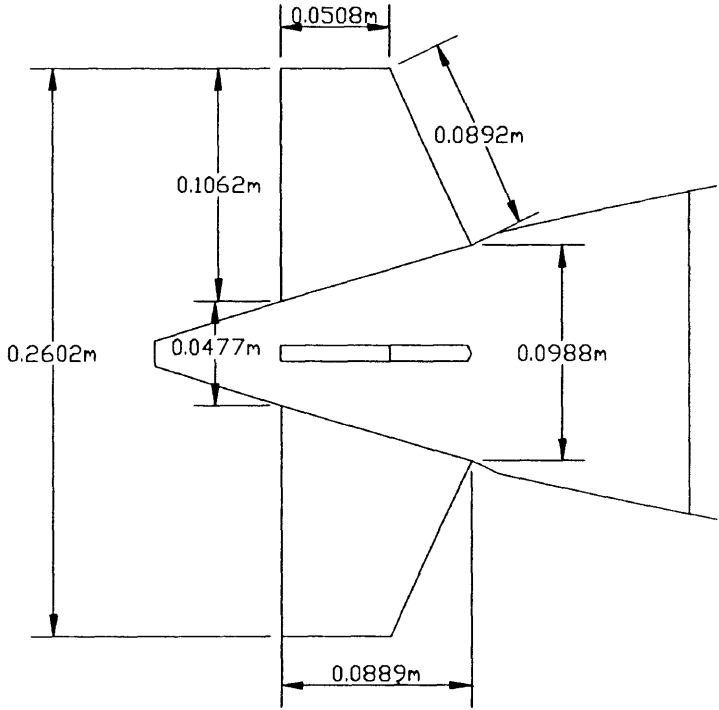


Figure 72 Vertical Profile of the Tail Section of the REMUS AUV

Experiments have shown that the effective vertical tail fin is comprised of the two vertical fins and the section of the vehicle centerplane formed by connecting the fin root leading edges and the fin root chord leading edges and the fin root trailing edges. This effective fin has an area of 0.02 m^2 , a mean longitudinal quarter chord location with respect to the vehicle midship of 0.7 meters an aspect ratio of 3.23, and an aspect ratio of 3.23. For aspect ratios (AR) between 3 and 5, Hoerner and Borst (1985) predict values of $C_{l\beta}$, with their formula converted from degrees to radians, as

$$C_{l\beta} = \left[0.175 + \frac{0.175}{(AR)^2} + \frac{0.454}{(AR)} \right]^{-1} \tag{A-38}$$

Wave Forces and Moments Due to Fin Lift

Crossflow velocities on horizontal and vertical fins will be considered here. In water of depth h , the linearized wave elevation, ζ for a propagation angle θ , measured clockwise from the positive x -axis, is:

$$\zeta = \alpha \exp[i(\omega t - kx \cos \theta + ky \sin \theta)] \quad (\text{A-39})$$

where: α is the complex amplitude of the waves, ω is the circular encounter frequency in the frame of reference of the moving vehicle and the wavenumber is $k = 2\pi / \lambda$, where λ is the wavelength. x and y are measured with respect to the origin of the coordinate system on the moving vehicle.

For this wave, at location $(x, y, -s)$ the vertical, positive upward, wave-induced fluid velocity, w , is:

$$w = \frac{i\omega_o \alpha}{\sinh kh} \exp[i(\omega_o t - kx \cos \theta + ky \sin \theta)] \sinh k(h - s) \quad (\text{A-40})$$

and the y -directed wave-induced horizontal fluid velocity, v , is:

$$v = \frac{-\omega_o \alpha \sin \theta}{\sinh kh} \exp[i(\omega_o t - kx \cos \theta + ky \sin \theta)] \cosh k(h - s) \quad (\text{A-41})$$

ω_o is the circular frequency of the wave in a fixed frame of reference.

Vehicles whose fins line in vertical and horizontal planes usually have their planes in symmetrical pairs. For example, if a vehicle has a vertical fin above its centerline, it will usually have a mirror image vertical fin below the centerline as shown in Figure 5. The vertical center of lift of the combination of fins and the lifting portion of the vehicle between them is at the centerline submergence for a vehicle with up-down hell symmetry. Furthermore, the length scales of the fins are generally much smaller than the wavelengths of sea waves. As a result, the value of s in equations (A-40) and (A-41) can be taken as the centerline submergence of the vehicle.

Similarly, horizontal planes generally exist in symmetrical pairs so the value of y in equations (A-40) and (A-41) can be taken as zero.

The fin lift forces due to sea waves are due only to the wave induced angles of attack on the fins whose linearized form is given by the first term of equation (A-37). Thus linearized wave forces and moments due for lift forces on the fins are:

$${}_f F_2 = \sum_{m\text{-Vertical}} \frac{1}{2} \rho U A_m C_{L\beta m} \frac{-\omega_o \alpha \sin \theta_m}{\sinh kh} \exp[i(\omega_o t - kx_m \cos \theta_m)] \cosh k(h - s) \quad (\text{A-43})$$

$${}_f F_3 = \sum_{m\text{-Horizontal}} \frac{1}{2} \rho U A_m C_{L\beta m} \frac{-\omega_o \alpha \sin \theta_m}{\sinh kh} \exp[i(\omega_o t - kx_m \cos \theta_m)] \cosh k(h - s) \quad (\text{A-44})$$

$${}_f F_5 = \sum_{m\text{-Horizontal}} -\frac{1}{2} \rho U A_m C_{L\beta m} x_m \frac{-\omega_o \alpha \sin \theta_m}{\sinh kh} \exp[i(\omega_o t - kx_m \cos \theta_m)] \cosh k(h - s) \quad (\text{A-45})$$

$${}_f F_6 = \sum_{m\text{-Vertical}} \frac{1}{2} \rho U A_m C_{L\beta m} x_m \frac{-\omega_o \alpha \sin \theta_m}{\sinh kh} \exp[i(\omega_o t - kx_m \cos \theta_m)] \cosh k(h - s) \quad (\text{A-46})$$

m -Vertical is the group of fins with vertical planforms and m -Horizontal is the group of fins with horizontal planforms.

Damping Coefficients Due to Fin Lift

When the vehicle with forward speed U experiences an upward motion $\eta_3 = N_3 e^{i\omega t}$, it has an upward velocity $\dot{\eta}_3 = i\omega N_3 e^{i\omega t}$ so that the linearized angle of incidence on horizontal fins is $-i\omega \eta_3 / U$. Using equation (A-35) for the fin lift and defining the contribution to the damping coefficient through, fin lift = $-\delta_f B_{33} \dot{\eta}_3$, the total fin lift damping coefficient, B_{33} , and the damping coefficient for pitch moment due to heave force, B_{53} , are:

$${}_f B_{33} = \sum_{m\text{-Horizontal}} \frac{1}{2} \rho U A_m C_{L\beta m}, \quad {}_f B_{53} = \sum_{m\text{-Horizontal}} -\frac{1}{2} \rho U A_m C_{L\beta m} x_m \quad (\text{A-47 a,b})$$

Similarly the sway damping coefficient due to sway motion, B_{22} , and the Yaw damping coefficient due to sway motion due to sway motion, B_{62} , are:

$${}_f B_{22} = \sum_{m\text{-Vertical}} \frac{1}{2} \rho U A_m C_{L\beta m}, \quad {}_f B_{62} = \sum_{m\text{-Vertical}} \frac{1}{2} \rho U A_m C_{L\beta m} x_m \quad (\text{A-48 a,b})$$

For pitch motion, $\eta_5 = N_5 e^{i\omega t}$, the vertical velocity of a fin at longitudinal position x_m is: $-i\omega x_m N_5 e^{i\omega t}$. This leads to:

$${}_f B_{55} = \sum_{m\text{-Horizontal}} \frac{1}{2} \rho U x_m^2 A_m C_{L\beta m}, \quad {}_f B_{35} = \sum_{m\text{-Horizontal}} -\frac{1}{2} \rho U x_m A_m C_{L\beta m} \quad (\text{A-49 a,b})$$

and the damping coefficients due to yaw are:

$${}_f B_{66} = \sum_{m\text{-Vertical}} \frac{1}{2} \rho U x_m^2 A_m C_{L\beta m}, \quad {}_f B_{26} = \sum_{m\text{-Vertical}} \frac{1}{2} \rho U x_m A_m C_{L\beta m} \quad (\text{A-50 a,b})$$

Spring Constants Due to Fin Lift

When the vehicle has a non-zero yaw angle, η_6 fins with vertical planforms have an associated angle of incidence, and when there is a non-zero pitch angle, η_5 , fins with a horizontal planforms have an associated angle of attack. These angles of attack lead to the spring constants, C_{26} , C_{66} , C_{35} , and C_{55} . They are given by:

$$C_{35} = \sum_{m\text{-Horizontal}} \frac{1}{2} \rho U^2 A_m C_{L\beta m}, \quad C_{55} = \sum_{m\text{-Horizontal}} -\frac{1}{2} \rho U^2 A_m x_m C_{L\beta m} \quad (\text{A51 a,b})$$

$$C_{26} = \sum_{m\text{-Vertical}} -\frac{1}{2} \rho U^2 A_m C_{L\beta m}, \quad C_{66} = \sum_{m\text{-Vertical}} -\frac{1}{2} \rho U^2 A_m x_m C_{L\beta m} \quad (\text{A-52 a,b})$$

Appendix B: MATLAB form of the Diffraction Strip Theory Code

The following code contains modifications to Professor Milgram's code made by the author to facilitate obtaining the results presented in this thesis report. Each subroutine is headed by the name of the m file in bold text.

DiffPblm.m, Base file for the diffraction problem

```
% Thesis Version of STC, Diffraction Base File
clear;
dpr = 180.0/pi;
fbase = input('Enter base file first name: ','s');
filo = strcat(fbase,'.out');
fido = fopen(filo,'w');
filout = strcat(fbase,'v.arc');
filouthor = strcat(fbase,'h.arc');
das = '-----';
fili = input('Type name of input parameter file: ','s');
fidi = fopen(fili,'r');
ncon = fscanf(fidi,'%d',1);
rho = 1000.0 ;
gr = 9.81;
for m=1:ncon;
    fprintf(1,'%d',m);
    if (10*floor(m/10) == m);
        fprintf(1,'\n');
    end;
    fprintf(fido,'\n');
    fprintf(fido,'%s\n',das);
    rn(m) = fscanf(fidi,'%d',1);    % Run Number
    betawd(m)= fscanf(fidi,'%f',1);    % Beta Degrees
    beta = betawd(m)/(180./pi);
    betar(m) = beta;
    U=fscanf(fidi,'%f',1);    % Speed
    u(m) = U;
    s=fscanf(fidi,'%f',1);    % Submergence
    sb(m) =s;
    h = fscanf(fidi,'%f',1);    % Depth
    ht(m) = fscanf(fidi,'%f',1);    % Wave Height
    AW = ht(m)/200.0;
    aw(m) = AW;

% w = fscanf(fidi,'%f',1); % Uncomment if want to use wn vice Lambda in input code
% wn = wnf(h,w);
% lambda=2*pi/wn;

lambda = fscanf(fidi,'%f',1);    % Wavelength
wn = 2*pi/lambda;
w = sqrt(wn*gr*tanh(wn*h));

we = w-wn*U*cos(beta);
```

```

wne = wnf(h,we);
lambdae = 2*pi/wne;
om(m) = w;
lam(m) = lambda;
lame(m) = lambdae;
BW=(i*w/wn)*AW/sinh(wn*h);

hw = 3;
dha(m) = 0.0325;
nph = 40;
npv = 10;
% hw = fscanf(fid,'%f',1);      % Half Width
% dha(m) = fscanf(fid,'%f',1);  % dhs
% nph = fscanf(fid,'%f',1);    % Horiz Panels
% npv = fscanf(fid,'%f',1);    % Vert Panels
hwa(m) = hw;
dhs = dha(m);

A=1.0; % Heave Amplitude
B=1.0; % Sway Amplitude
fil = 'remallL.dat';
fid = fopen(fil,'r');
fil2 = 'finremus.dat';
fprintf(fid,'Input file is: %s\n',fil);
fprintf(fid,'Input geometry and fin files are: %s and %s\n',fil,fil2);
fprintf(fid,'circular frequency = %7.3f, encounter circ. freq. = %7.3f\n',w,we);
fprintf(fid,'Wave amplitude = %8.3f, Wave angle = %4.0f\n',AW,betawd(m));
fprintf(fid,'Water Depth = %7.3f, Vehicle Speed = %5.2f\n',h,U);
fprintf(fid,'Lambda = %8.3f, Lambdae = %8.3f\n',lambda,lambdae);
fprintf(fid,'Submergence = %7.3\n',s);
fprintf(fid,'hw = %4.2f, dhs = %5.3f\n',hw,dhs);

nsec = fscanf(fid,'%d',1);
for sc=1:nsec;

[x(sc),a22(sc),a23(sc),a32(sc),a33(sc),b22(sc),b23(sc),b32(sc),b33(sc),h2(sc),h3(sc),f2(sc),f3(sc)]=...
    strippart(A,B,AW,beta,rho,w,we,wn,h,s,nph,npv,fid,sc,hw,dhs);
end;
fclose(fid);
%A33 = -trapz(x,a33);
%B33 = -trapz(x,b33);
%A35 = trapz(x,(x.*a33)) - (U/we^2)*B33;
%B35 = trapz(x,(x.*b33)) - U*A33;
%A53 = trapz(x,(x.*a33)) +(U/we^2)*B33;
%B53 = trapz(x,(x.*b33)) - U*A33;
%A55 = -trapz(x,(x.^2.*a33)) - (U/we)^2 * A33;
%B55 = -trapz(x,(x.^2.*b33)) - (U/we^2) * B33;
F3(m) = -rho*AW*trapz(x,(f3 + h3));
F5(m) = rho*AW*trapz(x,(x.*(f3 + h3) + U*h3/(i*we)));
%A22 = -trapz(x,a22);
%B22 = -trapz(x,b22);
%A26 = -trapz(x,(x.*a22)) - (U/we^2)*B22;
%B26 = -trapz(x,(x.*b22)) - U*A22;
%A62 = -trapz(x,(x.*a22))-(U/(we^2)) * B22;
%B62 = -trapz(x,(x.*b22)) - U*A22;

```

```

%A66 = -trapz(x,(x.^2 .*a22)) + (U/we)^2 * A22;
%B66 = -trapz(x,(x.^2 .*b22)) + (U/we)^2 * B22;
F2(m) = -rho*AW*trapz(x,(f2 + h2));
F6(m) = -rho*AW*trapz(x, (x.*(f2 + h2)+U*h2/(i*we)));
F3L(m) = F3(m);
F5L(m) = F5(m);
F2L(m) = F2(m);
F6L(m) = F6(m);
fprintf(fido,'Results Without fin lift\n');
fprintf(fido,'|F3| = %g, arg(F3) = %4.0f, |F5| = %g, arg(F5) = %4.0f \n',...
    abs(F3(m)), dpr*angle(F3(m)), abs(F5(m)),dpr*angle(F5(m)));
fprintf(fido,'|F2| = %g, arg(F2) = %4.0f, |F6| = %g, arg(F6) = %4.0f \n',...
    abs(F2(m)),dpr*angle(F2(m)),abs(F6(m)),dpr*angle(F6(m)));
fprintf(fido,' \n');
fprintf(fido,'Results With Fin Lift\n');
fid2 = fopen(fil2,'r');
nf = fscanf(fid2,'%d',1);
if ((nf == 0) || (abs(U) < 0.01));
    F3L(m) = F3(m);
    F5L(m) = F5(m);
    F2L(m) = F2(m);
    F6L(m) = F6(m);
    fprintf(fido,'|F3| = %g, arg(F3) = %4.0f, |F5| = %g, arg(F5) = %4.0f \n',...
        abs(F3(m)), dpr*angle(F3(m)), abs(F5(m)),dpr*angle(F5(m)));
    fprintf(fido,'|F2| = %g, arg(F2) = %4.0f, |F6| = %g, arg(F6) = %4.0f \n',...
        abs(F2(m)),dpr*angle(F2(m)),abs(F6(m)),dpr*angle(F6(m)));
    fprintf(fido,' \n');
else;
    for k=1:nf;
        xf=fscanf(fid2,' %f',1);
        areaf=fscanf(fid2,' %f',1);
        afd=fscanf(fid2,' %f',1);
        af=afd/dpr;
        lsfd=fscanf(fid2,' %f',1);
        lsf=dpr*lsfd;
        wv=wn*BW*(exp(-i*wn*xf*cos(beta)))*sinh(wn*(h-s));
        vv=i*wn*(sin(beta))*BW*(exp(-i*wn*xf*cos(beta)))*cosh(wn*(h-s));
        vn=wv*cos(af) - vv*sin(af);
        finforce = 0.5*rho*U*areaf*lsf*vn;
        fvert = finforce*cos(af);
        fhor = -finforce*sin(af);
        F3L(m) = F3L(m) + fvert;
        F2L(m) = F2L(m) + fhor;
        F5L(m) = F5L(m) - fvert*xf;
        F6L(m) = F6L(m) + fhor*xf;
    end;
    fprintf(fido,'|F3| = %g, arg(F3) = %4.0f, |F5| = %g, arg(F5) = %4.0f \n',...
        abs(F3L(m)), dpr*angle(F3L(m)), abs(F5L(m)),dpr*angle(F5L(m)));
    fprintf(fido,'|F2| = %g, arg(F2) = %4.0f, |F6| = %g, arg(F6) = %4.0f \n',...
        abs(F2L(m)),dpr*angle(F2L(m)),abs(F6L(m)),dpr*angle(F6L(m)));
    fprintf(fido,' \n');
end;
fclose(fid2);
fprintf(fido,' \n');

```

```

end;
fclose(fid);
fclose(fido);
fidout = fopen(filout,'w');
fidouthor = fopen(filouthor,'w');
fprintf(fidout,'Inputfile:\t%s \t%s\n',fili,filout);
fprintf(fidouthor,'Inputfile:\t%s \t%s\n',fili,filouthor);
fprintf(fidout,' |F3|\t a(F3)\t |F5|\t a(F5)\t |F3L|\t a(F3L)\t |F5L|\t a(F5L)\t hw\t dha\n' );
fprintf(fidouthor,' |F2|\t a(F2)\t |F6|\t a(F6)\t |F2L|\t a(F2L)\t |F6L|\t a(F6L)\t hw\t dha\n');
for m=1:ncon;
    fprintf(fidout,'%5.2ft%5.0ft%5.2ft%5.0ft%5.2ft%5.0ft%5.2ft%5.0ft%5.2ft%5.0ft%4.2ft%5.3fn',...
        abs(F3(m)),dpr*angle(F3(m)),abs(F5(m)),dpr*angle(F5(m)),abs(F3L(m)),dpr*angle(F3L(m)),...
        abs(F5L(m)),dpr*angle(F5L(m)),hwa(m),dha(m));
    fprintf(fidouthor,'%5.2ft%5.0ft%5.2ft%5.0ft%5.2ft%5.0ft%5.2ft%5.0ft%5.2ft%5.0ft%4.2ft%5.3fn',...
        abs(F2(m)),dpr*angle(F2(m)),abs(F6(m)),dpr*angle(F6(m)),abs(F2L(m)),dpr*angle(F2L(m)),...
        abs(F6L(m)),dpr*angle(F6L(m)),hwa(m),dha(m));
end;
fclose(fidout);
fclose(fidouthor);

```

StripPart.m

```

function[x,a22,a23,a32,a33,b22,b23,b32,b33,h2,h3,f2,f3]=...
    strippart(A,B,AW,beta,rho,w,we,wn,h,s,nph,npv,fid,sc,hw,dhs);
gr = 9.81;
lambda=2*pi/wn;
[npanels,xvert,yvert,xbv,ybv,xcontrol,ycontrol,length,nx,ny,x] = setpan(fid,h,s,lambda,nph,npv,hw,dhs,sc);
fkf = rho*gr*AW*exp(-i*wn*x*cos(beta))/cosh(wn*h);
npantot = npanels+2*nph+2*npv;
[g, dgdn] = infcograf(npantot,npanels,xvert,yvert,xbv,ybv,xcontrol,ycontrol,length);
[lhs, rhs] =
matrix(npanels,npantot,A,B,AW,nph,npv,nx,ny,w,we,wn,g,dgdn,length,h,beta,x,xcontrol,ycontrol);
phi = lhs\rhs;
p(:,1) = -rho*i*w*phi(:,1);
p(:,2) = -rho*i*w*phi(:,2);
p(:,3) = -rho*i*w*phi(:,3);
forcey1 = 0.0;
forcex1 = 0.0;
forcey2 = 0.0;
forcex2 = 0.0;
forceyd = 0.0;
forcexd = 0.0;
forceyk = 0.0;
forceyd = 0.0;
for m = 1:npanels;
    pfk(m) = fkf*cosh(wn*(ycontrol(m)+h))*exp(i*wn*xcontrol(m)*sin(beta));
    forcex1 = forcex1 + nx(m) * length(m) * p(m,1);
    forcey1 = forcey1 + ny(m) * length(m) * p(m,1);
    forcex2 = forcex2 + nx(m) * length(m) * p(m,2);
    forcey2 = forcey2 + ny(m) * length(m) * p(m,2);
    forcexd = forcexd + nx(m) * length(m) * p(m,3);
    forceyd = forceyd + ny(m) * length(m) * p(m,3);
end;

```

```

forcek = forcek + nx(m) * length(m) * pfk(m);
forceyk = forceyk + ny(m) * length(m) * pfk(m);
pb1(m) = p(m,1);
pb2(m) = p(m,2);
pbd(m) = p(m,3);
end;
a33 = real(forcey1)/(A * we * we);
a23 = real(forcex1)/(A * we * we);
b33 = -imag(forcey1)/(A * we);
b23 = -imag(forcex1)/(A * we);
a22 = real(forcex2)/(B * we * we);
a32 = real(forcey2)/(B * we * we);
b22 = -imag(forcex2)/(B * we);
b32 = -imag(forcey2)/(B * we);
h2 = forcexd/(rho*AW); %fxd/rho
h3 = forceyd/(rho*AW); %fyd/rho
f2 = forcek/(rho*AW); %fxk/rho
f3 = forceyk/(rho*AW); %fyk/rho

```

matrix.m

```

function[a,b] = matrix(npantot,A,B,AW,nph,npv,nx,ny,w,we,wn,g,dgdn,length,h,beta,xs,xc,yc);
% calculates the a matrix and the b vector for heave motion, sway motion (nx is to side,
% ny is vertical) and diffraction
gr=9.81;
fac = w * w/gr; % this is for using base freq in free surface boundary condition
fb = w*AW/sinh(wn*h);
fc = xs*cos(beta);
fs = sin(beta);
for m=1:npantot;
    b(m,1) = 0.0;
    b(m,2) = 0.0;
    b(m,3) = 0.0;
end;
for m= 1:npantot;
    for n = 1:npantot;
        a(m,n) = dgdn(m,n) ;
        b(m,1) = b(m,1) + g(m,n) * i*we*A*ny(n);
        b(m,2) = b(m,2) + g(m,n) * i*we*B*nx(n);
        b(m,3) = b(m,3) + g(m,n) * fb*exp(-i*wn*(fc-xc(n)*fs))*(nx(n)*fs*cosh(wn*(yc(n)+h))-
i*ny(n)*sinh(wn*(yc(n)+h)));
    end;
    for nn = 1:nph;
        n = npantot+nn;
        a(m,n) = dgdn(m,n) - fac*g(m,n);
    end;
    for nn = 1:npv;
        n = npantot+nph+nn;
        a(m,n) = dgdn(m,n) + i * wn * g(m,n);
        n =npantot + 2*nph + 2*npv-(nn-1);
        a(m,n) = dgdn(m,n) + i * wn * g(m,n);
    end;
    for nn=1:nph;

```

```

n = npanels +nph + npv + nn;
a(m,n) = dgdn(m,n);
end;
a(m,m) = a(m,m) + pi;
end;

```

setpans.m

```

function [a,xvert,yvert,xbv,ybv,xcontrol,ycontrol,length,nx,ny,x] =
setpans(fid,h,s,lambda,nph,npv,hw,dhs,sc)
a = fscanf(fid,'%d',1);
x = fscanf(fid,'%f',1);
for k = 1:(a+1);
xvert(k) =fscanf(fid,' %f',1);
yvert(k) = fscanf(fid,' %f',1);
end;
yvert=yvert - s;
for k=2 :(a+1);
xcontrol(k-1) = 0.5*(xvert(k-1)+xvert(k));
ycontrol(k-1) = 0.5*(yvert(k-1)+yvert(k));
length(k-1)=sqrt((xvert(k)-xvert(k-1))^2 ...
+(yvert(k)-yvert(k-1))^2);
nx(k-1)= -(yvert(k)-yvert(k-1))/length(k-1);
ny(k-1) = (xvert(k)-xvert(k-1))/length(k-1);
end;
dhl = (2.0*hw-12.0*dhs)/(nph-12);
dv = h/npv;
for k=1:((nph-12)/2 + 1);
xbv(k) = hw - (k-1)*dhl;
xbv(nph+npv+k) = -hw+ (k-1)*dhl;
end;
for k = 1:12;
j = (nph-12)/2 +1 +k;
xbv(j) = xbv(j-1) - dhs;
xbv(nph+npv+j)= xbv(nph+npv+j-1) + dhs;
end;
for k=1:((nph-12)/2 - 1);
j = (((nph-12)/2)+1 + 12 ) + k;
xbv(j) = xbv(j-1) -dhl;
xbv(nph+npv+j) = xbv(nph+npv+j-1) +dhl;
end;
for k = 1:nph;
ybv(k) =0.0;
% xbv(k) = hw - (k-1)*dh;
ybv(nph+npv+k) = -h;
% xbv(nph+npv+k) = -hw + (k-1)*dh;
end;
for k=1:npv ;
xbv(nph+k)= -hw;
ybv(nph+k) = -(k-1)*dv;
xbv(2*nph+npv+k) = hw;
ybv(2*nph+npv+k) = -h +(k-1)*dv;

```



```

end ;
kk = 2*npv+2*nph + 1;
xbv(kk) = xbv(1);
ybv(kk) = ybv(1);
for k=2:kk;
    xcontrol(a+k-1) = 0.5*(xbv(k-1)+xbv(k));
    ycontrol(a+k-1) = 0.5*(ybv(k-1)+ybv(k));
    length(a+k-1)=sqrt((xbv(k)-xbv(k-1))^2 ...
        +(ybv(k)-ybv(k-1))^2);
    nx(a+k-1)= (ybv(k)-ybv(k-1))/length(k-1);
    ny(a+k-1) = -(xbv(k)-xbv(k-1))/length(k-1);
end;
% if sc == 18
% dv
% xbv
% ybv
% plot(xbv,ybv)
% end

```

inflcofauv.m

```

function [g, dgdn] = inflcofauv(npantot,npanel,xvert,yvert,xbv,ybv,xc,yc,length);
npanbox = npantot-npanel;
for i = 1:npantot; % Loops on the panels with output for each control point
    for j = 1:npanel; %Finds effect of each panel
        %transformation to local coordinates
        xt = [ xvert(j) xvert(j+1) ];
        yt = [ yvert(j) yvert(j+1) ];
        [xlocal, ylocal] = localize(xt,yt,xc(i),yc(i));
        % Calculate the influence Coeffieient (integrated Green Ftn)
        [g(i,j), dgdn(i,j),ier] = rank2d(xlocal, ylocal, length(j));
    end;
    for j = 1:npanbox;
        xt = [ xbv(j+1) xbv(j) ];
        yt = [ ybv(j+1) ybv(j) ];
        [xlocal ylocal] = localize(xt,yt,xc(i),yc(i));
        jj = npanel+j;
        [g(i,jj), dgdn(i,jj),ier] =rank2d(xlocal, ylocal, length(jj));
    end;
end;
end;

```

localize.m

```

function [xlocal, ylocal] =localize(xpan,ypan,xglob,yglob);
% This function gives the local coordinates of (xglob,yglob) with respect
% to a panel where the panel is trhe local x axis and the y axis is to the
%left when going from the first point to the second of the panel.
alpha = atan2(-ypan(2)+ ypan(1), xpan(2)-xpan(1));
xlocal=(xglob-0.5 * (xpan(2)+xpan(1))) * cos(alpha)- ...
    (yglob-0.5*(ypan(1) + ypan(2)))*sin(alpha);

```

```
ylocal = (xglob - 0.5*(xpan(1)+xpan(2)))*sin(alpha)+ ...
          (yglob- 0.5 * (ypan(1) + ypan(2)))*cos(alpha);
```

rank2d.m

```
function[sour,dipl, ier] = rank2d(x,y,dl);
% This gives velocity potentials at(x,y), called sour and dipl.
% sour is from a unit strength source on dl
% dipl is from a unit dipole on dl
tol = 0.5e-6;
tol1 = 1.0e20;
sour = 0.0;
dipl = 0.0;
x2 = x*x;
y2 = y*y;
r2 = x2 + y2;
d2 = dl * dl;
rc = r2/d2;
dl2 = 0.5*dl;
% Test Input Values x, y, dl for overflow
if ( (x2 > tol1) | (y2 > tol1) | (d2 > tol1));
    ier=1;
elseif (dl < tol);
    ier = 0;
elseif (rc > 25);
% Far Field Expansions
    ier = 0;
    d12 = 1.0/12.0;
    r2i = 1.0/r2;
    dr2 = d2 * r2i;
    xr2 = x2 * r2i;
    yr2 = y2 * r2i;
    sour = -dl2*(log(r2) + d12 * dr2 *(yr2 -xr2));
    dipl = y*dl*r2i*(1. +d12*dr2*(4.0*xr2 - 1.0));
else
% Near Field Closed Form Expressions
    ier = 0;
    xx1 = x + dl2;
    xx2 = x - dl2;
    r1 = sqrt(xx1*xx1 + y2);
    r2 = sqrt(xx2*xx2 + y2);
    if (y2 > 0.25e-12);
        dipl = -sign(y)*(acos(xx1/r1) - acos(xx2/r2));
    end
    axx1 = abs(xx1);
    axx2 = abs(xx2);
    if (axx1 < tol);
        dl1 = 0.0;
    else
        dl1 = xx1*log(r1);
    end
    if (axx2 < tol);
        dl2 = 0.0;
```

```

else
    dl2 = -xx2*log(r2);
end
sour = -(y*dipl + dl1 + dl2 -dl);
end

```

wnf.m

```

function [wn] = wnf(h,w)
g=9.81;
wno = w.*w./g;
for j = 1:100;
    A= wno*g*tanh(wno*h) - w*w;
    dAdk=g*(tanh(wno*h) + h*wno/cosh(wno*h)^2);
    wnn = wno-A/dAdk;
    if ( abs (wnn-wno) < 0.0001*abs(wnn));
        break;
    end;
    wno = wnn;
end;
wn = wnn ;

```

Bibliography

- [1] J. N. Newman, "Marine Hydrodynamics," MIT Press, Cambridge, MA 1977
- [2] Nils Salvesen, Tuck, E.O., Faltinsen, O., "Ship Motions and Sea Loads," Society of Naval Architects and Marine Engineers Transactions, pp 250-287, 1970.
- [3] Jerome Milgram, "Numerical Marine Hydrodynamics," Lecture Notes for MIT Ocean Engineering Course 13.024, 2005.
- [4] Alex Techet. "Design Principles for Ocean Vehicles," Lecture Notes for MIT Ocean Engineering Course 13.42, 2003.
- [5] Michael S. Triantafyllou. "Maneuvering and Control of Surface and Underwater Vehicles," Lecture Notes for MIT Ocean Engineering Course 13.49, 1996. 25, 26
- [6] WAMIT Inc, "WAMIT User Manual, Versions 6.1." Chesternut Hill, MA.
- [7] Gregory Sabra, "Wave Effects on Underwater Vehicles in Shallow Water," Master of Science in Ocean Engineering thesis, Massachusetts Institute of Technology, Department of Ocean Engineering, June 2003.
- [8] Erik D. Oller, "Forces and Moments Due to Unsteady Motion of and Underwater Vehicle," Naval Engineer's thesis, Massachusetts Institute of Technology, Department of Ocean Engineering, June 2003.
- [9] Sighard F. Hoerner, "Fluid-Dynamic Lift," 2nd ed. Liselotte A. Hoerner Press, 1985.